



MONASH UNIVERSITY

DOCTORAL THESIS

**Assimilating remotely sensed
evapotranspiration data into
next-generation hydrogeological models**

Author:
Simone GELSINARI

Supervisors:
A. Prof. Valentijn PAUWELS
A. Prof. Edoardo DALY
Dr. Rebecca DOBLE

*A thesis submitted in fulfillment of the requirements
for the degree of Doctor of Philosophy*

in the

Department of Civil Engineering

August 18, 2020

Copyright notice

Notice 1

© Simone Gelsinari (2020).

Under the Copyright Act 1968, this thesis must be used only under the normal conditions of scholarly fair dealing. In particular no results or conclusions should be extracted from it, nor should it be copied or closely paraphrased in whole or in part without the written consent of the author. Proper written acknowledgement should be made for any assistance obtained from this thesis.

Declaration of Authorship

I, Simone GELSINARI, declare that this thesis titled, “Assimilating remotely sensed evapotranspiration data into next-generation hydrogeological models” and the work presented in it are my own. I confirm that:

- contains no material which has been accepted for the award of any other degree or diploma at any university or equivalent institution. and that,
- to the best of my knowledge and belief, this thesis contains no material previously published or written by another person, except where due reference is made in the text of the thesis.
- Where I have consulted the published work of others, this is always clearly attributed.
- Where I have quoted from the work of others, the source is always given. With the exception of such quotations, this thesis is entirely my own work.
- I have acknowledged all main sources of help.
- Where the thesis is based on work done by myself jointly with others, I have made clear exactly what was done by others and what I have contributed myself.

This thesis includes 1 original paper published in peer reviewed journal, and corresponds to chapter 4.

TABLE 1: Author contribution to the journal articles. A = Analysis. C = Conceptualization. E = Editing. M = Numerical Modeling. W = Writing

Chapt.	Publication	Status	Author	Contribution	Co-authors Monash student
4	Feasibility of improving groundwater modeling by assimilating evapotranspiration rates	Published	Simone Gelsinari Edoardo Daly Rebecca Doble Valentijn Pauwels	A,C,M,W (80%) C,E (5%) C,E (5%) A,C,E (10%)	- No No No

Candidate:

Supervisor:

Date:

*“Luogo è là giù da Belzebù remoto
tanto quanto la tomba si distende,
che non per vista, ma per suono è noto*

*d’un ruscelletto che quivi discende
per la buca d’un sasso, ch’elli ha roso,
col corso ch’elli avvolge, e poco pende.*

*Lo duca e io per quel cammino ascoso
intrammo a ritornar nel chiaro mondo;
e senza cura aver d’alcun riposo,*

*salimmo sù, el primo e io secondo,
tanto ch’i’ vidi de le cose belle
che porta ’l ciel, per un pertugio tondo.*

E quindi uscimmo a riveder le stelle.”

(Dante - Cfr. Inferno XXXIV vv. 127-139)

MONASH UNIVERSITY

*Abstract*Faculty of Engineering
Department of Civil Engineering

Doctor of Philosophy

Assimilating remotely sensed evapotranspiration data into next-generation hydrogeological models

by Simone GELSINARI

In the underground, the invisible groundwater resource is the largest and most reliable source of water for arid and semi-arid regions. In these regions around the world, depletion of groundwater resources has been recorded due to anthropogenic and natural causes, such as the effects of climate change, the increasing freshwater demand as a result of the growing population, or the contamination of aquifers. Guaranteeing the sustainable management of this vital resource is one of the most important hydrogeological challenges.

The biophysical processes occurring in the unsaturated zone have a direct impact on water table dynamics and groundwater budgets. The numerical modeling of these soil water-vegetation interactions in the unsaturated zone can be performed with models of different complexity. These are able to estimate recharge rates which can become inputs when unsaturated zone models are coupled to groundwater models. Because recharge estimates are always affected by uncertainty, model-data fusion methods, such as data assimilation, can be used to constrain and quantify the uncertainty in the model results.

This work presents a method for assimilating evapotranspiration data into coupled unsaturated zone-groundwater models of different complexity using the Ensemble Kalman Filter. Evapotranspiration fluxes are assimilated because of the soil-water information they can hold and because they have been shown to be related to the groundwater table dynamics, representing the link between remote sensing data and the deeper parts of the soil profile. Thus, assimilating observed evapotranspiration values has the potential to constrain groundwater model results. The method is firstly tested on a synthetically generated losing stream system for climatic conditions common in South Australia. In a second phase, the required complexity (i.e. conceptual versus physically-based) of the unsaturated zone model to update groundwater models through the assimilation of evapotranspiration rates is assessed for a water-limited site in South Australia. Lastly,

the conceptually based configuration is applied to four silvicultural sites with different soil profiles, average water table depths, and vegetation types. This variety of conditions allows for an assessment to prioritize the regions for which the assimilation of evapotranspiration yields the largest improvements to groundwater models.

The data assimilation algorithm consistently improved water table levels and soil moisture state variables when the ensemble spread was adequate. Improvements were also obtained in the calculation of fluxes of net-recharge and modeled actual evapotranspiration for which the Ensemble Kalman filter is not specifically designed. Under the test site conditions, a conceptual unsaturated zone model was sufficient to improve groundwater model results through the assimilation of evapotranspiration rates. The results also showed that the condition which most influenced the assimilation performance was the depth to the water table, with a positive impact recorded for water table depths up to 6.5 m. Finally, the opportunity for the operational application of this methodology in groundwater management is discussed.

Acknowledgements

My sincere gratitude goes, in an equal manner, to my main supervisor A.Prof. Valentijn Pauwels, and the co-supervisors A.Prof. Edoardo Daly and Dr Rebecca Doble. I am very grateful for the opportunity I had to be supervised by a team of scientists who were not only experienced and dedicated but very supportive and patient in each phase of this project. Their guidance drove me throughout all the research components of this thesis, and greatly contributed to developing my critical thinking and shaping my scientific skills.

The primary funding for this research was a Co-funded Monash Graduate Scholarship with the CSIRO contribution from the Land and Water Effective Floodplain Management Project. A stipend top-up from the main supervisor VP was also provided. I also like to acknowledge the financial support by the Faculty of Engineering at Monash University through the Graduate Research International Travel Award.

Besides my supervisors, I would like to thank the colleagues and people I have met during my visit at the group of Hydrology and Quantitative Water Management at Wageningen University & Research. I would also like to thank CSIRO Staff members Tanya Doody, Russell Crosbie and Luk Peeters for their precise suggestions in ecohydrology, groundwater modeling and data assimilation. I would also like to extend my thank to the CSIRO members Chris Li, Trine, and Chris Turnage.

A special thank goes to my Adelaidian friends and colleagues Karina, Enrique, Zack, Carlos, Martim, Diego, Margherita, Maria, Michele, Francesca, & Camille for their closeness and support throughout the entire length of the project. At Monash, I especially thank Stefania, Filomena, Jaya, Jihane, Nora, Antara, and Homa.

There are very few ways to express gratitude to all my close friends; from the "Gruppo Gonfi" to Lorenzo, Ni'ò, and Anna.

Most importantly, a big GRAZIE to my parents Ronaldo and Patrizia, my brother Stefano, aunts and uncles Michela, Daniela, Pasquale and Alberto, my cousin Arianna and my beautiful nonna, Franca. Their love and support over the years have meant a lot to me while living far away from my nest.

Contents

Declaration of Authorship	iii
Abstract	vii
Acknowledgements	ix
1 Introduction	1
1.1 Background	1
1.2 Motivations for the Research	4
1.3 Aim and Outline of the Research	5
1.4 Thesis Structure	6
2 Literature Review and Research Questions	9
2.1 Hydrogeological Modeling	9
2.2 Use of Remotely Sensed Data	11
2.3 Data Assimilation in Hydrological Studies	13
2.4 Research Gaps and Statement of the Questions	18
3 Material and Methods	19
3.1 Site Description	19
3.2 Data	22
3.2.1 Climatic Data	22
3.2.2 The CMRSET	22
3.3 UnSAT - UZM	24
3.3.1 Conceptualization	24
3.3.2 Time Step Evaluation	27
3.3.3 Root Distribution	28
3.3.4 Decay of the Hydraulic Conductivity	28
3.4 SWAP	30
3.5 MODFLOW - Groundwater Model	31
3.6 Model Coupling	32
3.7 Data Assimilation	37
3.8 Model Performances Evaluation	40
3.8.1 Assimilation Skills Verification	40
3.8.2 Additional Metric - CRPS	41

4	Feasibility of improving groundwater modeling by assimilating evapotranspiration rates	43
4.1	Abstract	43
4.2	Introduction	43
4.3	Experiment Description	44
4.3.1	Data Assimilation	44
4.3.2	Synthetic Experiment Domain	45
4.3.3	Forcing Inputs Perturbation and Observations	47
4.3.4	Experiment Description	48
4.3.5	Ensemble Performance Verification	49
4.4	Results and Discussion	50
4.4.1	Ensembles Verification	50
4.4.2	Assimilation Performance	51
	States	51
	Fluxes	53
	Group Comparison	58
4.5	Conclusion	58
5	Unsaturated zone models complexity for the assimilation of evapotranspiration rates in groundwater modeling	63
5.1	Abstract	63
5.2	Introduction	64
5.3	Experiment Set-up	64
5.3.1	Model Description	65
5.3.2	Model Domain and Calibration	65
	Ensemble Generation	67
5.4	Results and Discussion	67
5.4.1	Deterministic Runs	67
5.4.2	Ensemble Simulations	71
5.5	Conclusions	79
6	Prioritizing regions for the assimilation of evapotranspiration rates into hydrogeological models	81
6.1	Introduction	81
6.2	Experiment Description	82
6.2.1	Site Description	82
6.2.2	Site Location and Model Conceptualization	84
6.2.3	Model Calibration	88
6.3	Results and Discussion	89
6.3.1	WT Levels	89
6.3.2	Evapotranspiration	93
6.4	Conclusions	95

7 Overall Discussion and Conclusions	99
7.1 Overview	99
7.2 Summary of the Finding	99
7.2.1 Feasibility Study	99
7.2.2 Model Complexity Assessment	101
7.2.3 Area Prioritization	103
7.3 Contribution	104
7.4 Limitations & Future Developments	105
A UnSAT - Sensitivity Analysis	107
B UnSAT - Calibration	109
B.1 Inputs and Calibration	109
B.1.1 Calibration Algorithm	109
B.1.2 Calibration	110
Hydraulic Conductivity Decay	111
C Domain Sensitivity Analysis	115
Bibliography	117

List of Figures

1.1	Regional dependence of surface water and groundwater (Harrington and Cook, 2014).	2
1.2	Rainfall deficiencies for the period Apr 18 - Jan 20 [a]. Relative root zone soil moisture for 2019 [b]. Courtesy: Boureau of Meterology.	3
2.1	Maps of diffuse recharge estimated (large) and the upper and lower 95% percentiles estimates from (Crosbie et al., 2015)	10
2.2	Representation of the difference of EKF vs. EnKF	16
2.3	The sequence of the EnKF	16
3.1	Location of the study area within Australia [a], and whitin the south-east of South Australia [b]. Major towns of the study area used throughout this thesis [c].	20
3.2	Digital elevation model of the area [a]. Depth to WT map [b].	21
3.3	Conceptualization and flowchart for the unsaturated zone model	24
3.4	Schematic of the UnSAT model.	25
3.5	Water stress reduction function. the various θ values in the Figure are taken from the calibration in Appendix B.	26
3.6	Accuracy of two time-steps chosen compared with the analytical solution of eq. 3.11	27
3.7	Different distribution shapes due to variation of p_z	29
3.8	Configuration-1 coupling between UnSAT and MODFLOW. The two cases on the left represent different WT depths and corresponding number and saturation of modeled layers. On the right hand side, the coupling flowchart s represented. The UZM internal time step represented refers to the simulation of Chapter 4.	34
3.9	Representaion of the two coupling configurations. Configuration - 1 involves UnSAT and MODFLOW. Configuration - 2 is between SWAP and MODFLOW	36
3.10	Schematic of the sequential data assimilation experiment for the first two assimilation time steps.	38

- 4.1 Representation of the losing stream-groundwater system interaction in a densely vegetated area. The unconfined aquifer overlies an impervious layer, the WT is declining moving away from the river interface. The model domain and boundary conditions are shown in the two insets. The right inset shows the top view of the domain formed by 18×5 cells. The blue cells indicate the constant head boundary, while grey cells indicate the no-flow boundary (inactive cell). In the left inset, the red line is the root depth, the light blue dotted-line is the initial water table distribution. These two lines divide the domain into three areas (Recharge, Transition and Extraction). 46
- 4.2 Schematic of the synthetic experiment set-up. The left panel illustrates the deterministic run of the coupled model. On the right, the flow path of a single ensemble member is represented. This run uses the synthetic actual ET from the deterministic run as observation to be assimilated. 48
- 4.3 Results of simulation DD1 with $A = 0.25$ and $OE = 0.1$ for the extraction area. Top panel: rainfall input data. Middle panel: modeled SM values for ensemble member 21 (layer numbers increase with depth). Bottom panel: modeled AET and the assimilated observation for the same ensemble member. The grey boxes numbered 1, 2, and 3 are further explained in Section 4.4.2. 52
- 4.4 WT levels for the entire simulation period in the Extraction Area. The blue line is the deterministic truth, the green line is the Open-loop mean and the red is the mean of the assimilations runs. The individual ensemble runs are shown as gray lines. Panels [a] and [b] show results for the datasets with sufficient spread, i.e. DD1-I and DD2-I. Panel [c] shows results of DD2-III with insufficient spread. 54
- 4.5 WT levels for the entire simulation period in the Recharge Area. Colors of lines as in figure 4.4. Panels [a] and [b] show results for the datasets with sufficient spread, i.e. DD1-I and DD2-I. Panel [c] shows results of DD1-III with insufficient spread. 55
- 4.6 SM content at depth 900 [mm] for simulation period 2004-10-28 to 2007-12-11. Colors of lines as in figure 4.4. Panels [a] and [b] show results for the datasets with sufficient spread, i.e. DD1-I and DD2-I. Panel [c] shows SM profiles for the simulations of DD2-II with insufficient spread. 56
- 4.7 Comparison of the WT levels ubRMSE for the Extraction area across all the simulation groups. The red bar is the assimilation ubRMSE and the green bar is the associated open loop ubRMSE. The colored area highlights the adequately generated ensemble. 59

4.8	Comparison of the SM ubRMSE for the Extraction area across all the simulation groups. The red bar is the assimilation ubRMSE and the green bar is the associated open loop ubRMSE. The colored area highlights the adequately generated ensemble.	59
5.1	Localization of the study area within the South East of South Australia [a] and detail of the forest plantation [b]. The red square indicates the CMRSET tile.	65
5.2	Schematic of the simulation domain. Configuration-1 models the unsaturated zone as a homogeneous profile with UnSAT. Configuration-2 models the soil heterogeneity by accounting for the change in soil properties with SWAP. The WT is represented at initial conditions on the left-hand side, and at a generic simulation time, showing the depression caused by the root water extraction, on the right-hand side.	66
5.3	Combined WT fluctuations [a] and AET [b] for both configurations.	69
5.4	Temporal evolution of the soil moisture contents. Panels [a] and [d] show the entire modeled column, including the fluctuation of the WT (i.e. the dark blue area). Panel [b] and [e] represent the modeled and observed water content for the upper soil (averaged over 0-300 mm depth). Panel [c] and [f] show these results for the lower soil (averaged of the interval 1500-1800 mm depth).	72
5.5	WT levels and AET and spread of the Open Loop ensembles for Configuration-1 [a,c] and Configuration-2[b,d]	73
5.6	WT levels and AET and spread of the assimilation run for Configuration-1 [a,c] and Configuration-2[b,d]	75
5.7	Observations, open loop and assimilation means for Configuration-1. In the insets, green and red surfaces represent the violin plots of the open loop (Prior) and the assimilation runs (Posterior) distributions, for two dates indicated by the boxes.	76
5.8	Observations, open loop and assimilation means for Configuration-2. In the insets, green and red surfaces represent the violin plots of the open loop (Prior) and the assimilation runs (Posterior) distributions, for two dates indicated by the boxes.	76
5.9	Scatter plots of the upper [a,b,e,f] and lower [c,d,g,h] soil water content. Configuration 1 Open-Loop [a,c], Assimilation [b,d]. Configuration 2 Open-Loop [e,g], Assimilation [f,h]. N.B. Observations are reported on the x axes.	78
6.1	Satellite images of the 4 locations. Piney [a], Woakwine [b], Jack and Jill [c]. Note: [c] refers to a time beyond the simulation period, taken after the harvesting of the plantation.	84

6.2	Bias correction of ET. [a] Regression analysis. [b] Comparison of the three AET as per legend.	85
6.3	Conceptual representation of the four locations.	86
6.4	Conceptual representation of the local depth to WT. AET from the CMRSET averaged over 1 km ² and field data of Jack and Jill].	87
6.5	Bore observations at Piney, at the neighbour bore, for the extended corrected dataset.	88
6.6	Depth to WT and AET at Jack, Jill, Woakwine and Piney.	91
6.7	CRPS values are computed for the assimilation, open-loop and bias corrected runs each time an observation is available.	92
6.8	Residuals of the AET volumes calculated over 6 months. NB. the mark indicates a partial year.	96
A.1	Results of the sensitivity analysis.	108
(a)	Sensitivity to Ks	108
(b)	Sensitivity to the drainage value	108
(c)	Sensitivity to the root depth	108
(d)	Sensitivity to p_z	108
(e)	Sensitivity to Wang decay	108
B.1	Results of calibrated soil moisture values for the 50 mm depth observation and first model layer.	111
B.2	Results of calibrated soil moisture values for the 150 mm depth observation and the second model layer.	112
B.3	Results of calibrated soil moisture values for the 290 mm depth observation and the third model layer.	112
B.4	Results of calibrated soil moisture values for the 470 mm depth observation and the fifth model layer.	112
C.1	Water table fluctuation at the cell in the centre of the domain for Configuration-1 after calibration. The simulation is based on real forcing inputs. The "Coarse" resolution is a 5 X 1 cell domain, the same as the one used for the experiment in this paper. The "Fine" resolution is a 20 X 1 cell domain.	115

List of Tables

1	Author contribution to the journal articles. A = Analysis. C = Conceptualization. E = Editing. M = Numerical Modeling. W = Writing	iv
3.1	Name and coordinates of the meteorological stations	22
4.1	Parameters used for the simulations. Columns two to four report the parameters used for the Truth, the Disturbed Dataset 1 and the Disturbed Dataset 2	49
4.2	Simulations classification and ensembles verification. The table is divided in two parts according to the parametric dataset used, reported in column 1. <i>A</i> is the input perturbation fraction which was used to generate the ensemble. <i>OE</i> is the observation error. Column 4 and 5 are the ensemble skills calculated on AET values averaged over the three areas, column 6 is the spread classification as described in Section 4.4.1.	51
4.3	State variables (i.e. WT levels and SM) results for the Adequate spread simulations (DD1-I and DD2-I). Column 1 and 2 report the area of the domain and the dataset considered. Columns 3 through 5 report the <i>ubRMSE</i> and <i>r</i> of the WT levels between the assimilation run and the deterministic truth. The $\Delta ubRMSE$ % is the percentage of improvements (if positive) or worsening (if negative) of the <i>ubRMSE</i> of assimilation and OL. R is the correlation, the sign in parenthesis is positive in case of the assimilation improving the correlation, negative otherwise. Columns 6 to 8 refer to SM.	57
4.4	Fluxes results for the Adequate spread simulations (DD1-I and DD2-I). Column 1 and 2 report the area of the domain and the dataset considered. Columns 3 through 5 report RMSE and <i>r</i> of the AET between the assimilation run and the deterministic truth. The $\Delta RMSE$ % is the percentage of improvements (if positive) or worsening (if negative) of the RMSE of assimilation and OL. R is the correlation, the sign in parenthesis is positive in case of the assimilation improving the correlation, negative otherwise. Columns 6 to 8 refer to net-recharge.	57

5.1	Calibrated parameter values used for the simulations and their perturbation fraction.	68
5.2	Results for the calibrated runs.	70
5.3	RMSE and correlation for three variables between the open loop and the assimilation.	74
6.1	Name, coordinates and characteristics of the silviculture sites	83
6.2	Parameters, perturbation fractions, and forcing input generation fractions used for the simulations.	85
6.3	Results for the WT dynamics. In green the values where the assimilation is improving the WT levels compared to the open loop. In red the cases when the open loop performs better than the assimilation.	89
6.4	Results for the AET. In green the values where the assimilation is improving the AET compared to the open loop. In red the cases when the open loop performs better than the assimilation.	94
6.5	RMSE values calculated for the integral of the ET ratios.	95
B.1	Parameter, range, calibrated values and RMSE	111
B.2	Parameters and normalized error for the different decay profiles.	113

List of Abbreviations

AET	Actual EvapoTranspiration
CRPS	Continuous Ranked Probability Score
CSIRO	Commonwealth Scientific and Industrial Research Organisation
DD1	Disturbed Dataset 1
DD2	Disturbed Dataset 2
EnKF	Ensemble Kalman Filter
ET	EvapoTranspiration
LAI	Leaf Area Index
MODIS	MODerate resolution Imaging Spectroradiometer
PSO	Particle Swarm Optimization
PET	Potential EvapoTranspiration
RMSE	Root Mean Squared Error
RS	Remote Sensing
SD	Standard Deviation
SM	Soil Moisture
SWAP	Soil Water Atmosphere Plant
UZM	Unsaturated Zone Model
WT	Water Table

Dedicated to:

*my Family, my Friends,
and my Livorno*

Chapter 1

Introduction

In Australia, the importance of groundwater is often brought to the attention of the public by cyclically, long dry periods, which emphasize how much the country relies on its groundwater resources. To manage and better characterize these resources, scientists, engineers and policymakers seek the support of numerical models. A model is always a simplified representation of reality and comes with a certain level of associated uncertainty. Reducing these uncertainties and thus reinforcing the confidence in model outputs is an active and challenging topic for the scientific community. One part of this involves applying the concept of data assimilation. Data assimilation is a model-data fusion technique that aims to find the best results from the combination of observations and modeled state variables. Some of the data assimilation algorithms can positively use the information associated with the models and measurements errors to reduce uncertainties. A considerable number of the most recent achievements with the application of data assimilation have been performed using data sets of remote sensing (RS) observations. More specifically, a subset of these RS data is based on satellite observations and has shown great potential, particularly for data-scarce regions. This project pursues multiple objectives: a) assimilating satellite RS evapotranspiration (ET) into hydrogeological models, b) assessing the potential improvements of the ET assimilation on the model outputs using models of different complexity, and c) prioritizing the regions with the highest uncertainty reduction.

1.1 Background

Groundwater can be identified as the predominant and most reliable source of water, specifically for arid and semi-arid regions (Carroll et al., 2015; Orellana et al., 2012). In these regions around the world, the availability of groundwater is under pressure due to anthropogenic and natural causes (Shrestha, Sada, and Melsen, 2014). Examples are the effects of climate change, the increasing freshwater demand as a result of growing population, and the contamination of aquifers. The possible combination of these factors is further threatening groundwater resources and posing more complex problems to policy makers (Usman, Liedl, and Kavousi,

2015; Glenn et al., 2011).

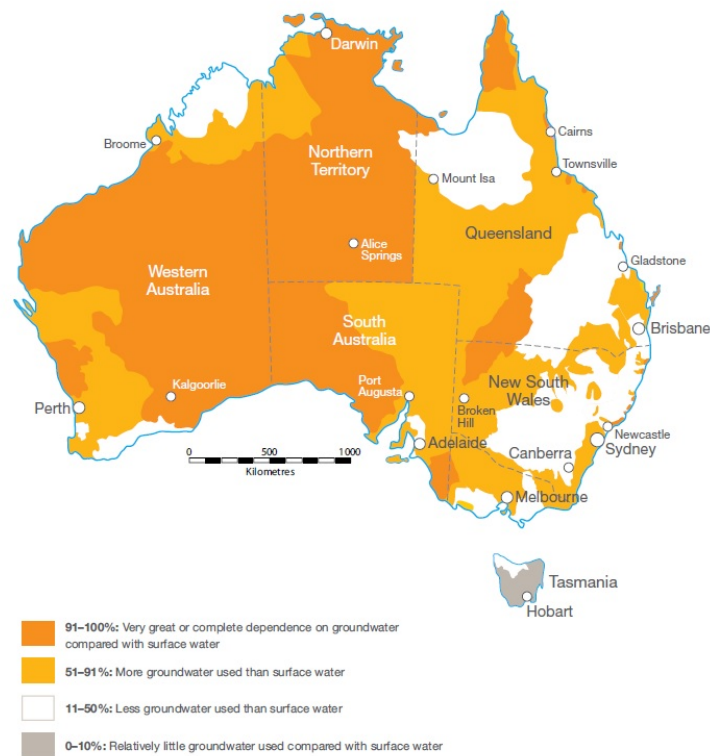


FIGURE 1.1: Regional dependence of surface water and groundwater (Harrington and Cook, 2014).

During the period known as Millennium Drought, defined as "arguably the worst dry period since the European settlement" (van Dijk et al., 2013), the effects of drought in Australia have been particularly prominent in the most populated part of the country. The reduction of groundwater resources availability caused ecological, social and economic problems increasing the awareness of the population and politicians to undertake a proactive approach towards an improved management of water resources (Leblanc et al., 2012). However, the period between 2010 and 2012 saw the important effects of the "La Niña" climate phenomenon (van Dijk et al., 2013), which brought extreme rainfall and flood events and reversed the public perception about droughts by generating a perception of water abundance. Throughout the recent history of Australia, this alternation of perceptions in the people's memory is well documented in the book of Miller (2019). On the other hand, the scientific community has been continuously investigating the Australian water resources for decades. Numerous reports (e.g. the Australian Water Resource Council reports - AWRC and the Australian Water Resources Assessment reports AWRA) have confirmed that Australia heavily relies on its groundwater resources. In certain regions, this dependence is above 90 %, where groundwater

represents almost the only source of water, especially for agriculture as shown in Figure 1.1.

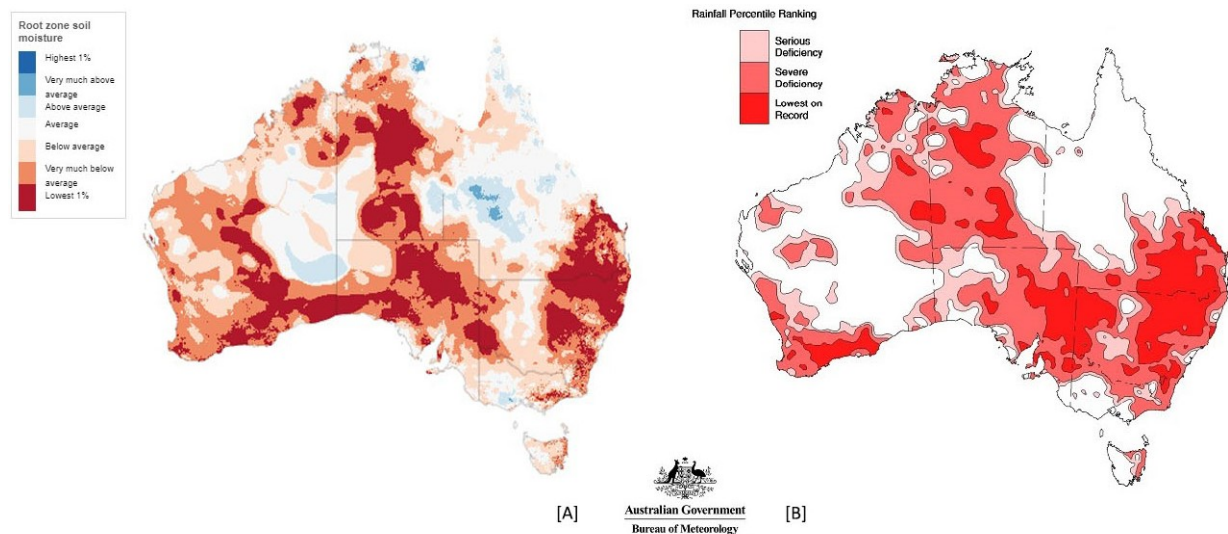


FIGURE 1.2: Rainfall deficiencies for the period Apr 18 - Jan 20 [a]. Relative root zone soil moisture for 2019 [b]. Courtesy: Bureau of Meteorology.

Recently, several environmental scientists have warned that the long-term trend is pointing again towards a "below the average" level of rainfall and soil moisture (SM) values across Australia (See Figure 1.2), the year 2019 being the warmest and driest on the Australian records according to the Bureau of Meteorology (BOM) Annual Climate statement (2019). These conditions were, in part, the genesis of the tragic bushfire events of the 2019/20 summer, as reported in the Commonwealth Scientific and Industrial Research Organisation (CSIRO) white paper produced from attendees of the "Bushfire Science Roundtable" held in January 2020. It is thus important to encourage researchers in continuing to develop the science behind water resources management and creating new tools to support decision-makers.

Some of these tools are satellite RS observations (McCabe, Kalma, and Franks, 2005; Houborg et al., 2012), new methods for data analysis (Pipunic, Walker, and Western, 2008; Montzka et al., 2012), and/or improved computing capabilities (Vrugt and Sadegh, 2013). In particular, the potential for satellite RS to provide spatio-temporal distributed data sets has been investigated by the hydrological modeling community for different purposes. Sensors ranging from optical, infra-red, and active/passive microwaves are now able to provide land surface temperature data (McCabe, Kalma, and Franks, 2005), SM content estimates (Walker, Willgoose, and Kalma, 2001), LAI (Lu, Steele-Dunne, and De Lannoy, 2020), and ET rates (Mohanty et al., 2013). These observations are used for validating existing

models, quantifying and reducing model uncertainties (Lucas et al., 2015), events forecasting (Bindlish, Crow, and Jackson, 2009) or investigating the impact of possible future climates scenarios (Múnch et al., 2013).

The great majority of environmental studies rely on numerical models. Modeling always requires a certain degree of simplification and assumptions, which reflect into a level of uncertainty affecting model outputs. The source of these uncertainties may come from the model conceptualization (Oreskes, Shrader-Frechette, and Belitz, 1994; Melsen et al., 2018), parameterization (Beven and Binley, 1992; Vrugt and Beven, 2018) and model inputs (Peterson and Western, 2014). Quantifying, and ultimately, reducing these uncertainties is one of the most challenging fields of the hydrogeological research (Brunner et al., 2007).

1.2 Motivations for the Research

About two decades ago, in the context of a symposium of the International Association of Hydrological Sciences, Schumann and Antl (2001) pointed out the need in hydrological modeling for a probabilistic approach to account for climate change and specifically stressed the importance of quantifying the uncertainty. One technique for evaluating and reducing uncertainty, by combining the products of models with observations, is data assimilation (e.g. Nearing et al., 2018). A vast number of papers shows that RS data assimilation has been applied to many branches of geoscience including hydrology, but only to a lesser extent to groundwater or hydrogeological modeling (Liu et al., 2012; Li et al., 2016). From the literature review in Chapter 2 of this thesis, it appears that more aspects need to be investigated in the assimilation of RS data into hydrogeological models.

The two components of the water balance, ET and recharge to the water table (WT), are intertwined. Performing a proper calculation of ET by means of a detailed representation of the water transport in the unsaturated zone can lead to improved estimates of recharge and better simulation of the WT dynamics. This concept becomes crucial when root extraction is occurring from the groundwater, as it is common in Australian semi-arid catchments (Banks, Brunner, and Simmons, 2011), where the direct transpiration from the WT is a major contribution to the total ET (Mensforth et al., 1994; Vervoort and van der Zee, 2012; Orellana et al., 2012). ET is also a function of the soil water content within the root zone, as the root water uptake is distributed along the entire root system (Grinevskii, 2011; Neumann and Cardon, 2012). Thus, this thesis hypothesized that assimilating ET into groundwater models may provide useful information of the water content to the deep part of the soil column. This, eventually, can lead to better simulations of recharge and WT dynamics.

1.3 Aim and Outline of the Research

The main aim of the project is to

**improve hydrogeological models through
the assimilation of remotely sensed ET.**

The project outcome is to assess the potential of the ET assimilation in reducing the uncertainties linked to the groundwater model products. Specifically, this research is structured into four main tasks as follow.

Task 1 This step consists in creating a model for the unsaturated zone and coupling it to the hydrogeological model MODFLOW-2005. The unsaturated zone model (UZM) accounts for the variation of the thickness of the unsaturated zone determined by the fluctuation of the WT, and considers possible root water uptake from groundwater. In doing so, the recharge variable can become negative and it is therefore defined as net-recharge.

Task 2 This step focuses on developing a framework for the assimilation of ET observations. The proposed method was tested within a synthetic experiment, on a domain presenting different groundwater-vegetation interactions. The sequential assimilation procedure, through the EnKF, allows for the ET diagnostic variable to update the prognostic variables of the coupled model. The uncertainty reduction of the hydrogeological variable is assessed.

Task 3 This step focuses on the required level of detail of two coupled UZM + MODFLOW configurations. This task is divided into two phases:

I. - Two UZMs of different complexity were independently coupled to MODFLOW-2005, through the net-recharge and the WT depth, creating two configurations. Configuration-1 applied the UZM developed in Task 1. Configuration-2 applied the Soil-Water-Atmosphere-Plant (SWAP) model, based on the Richards equation. Both configurations were deterministically applied and calibrated for a semi-arid environment. A multi-objective calibration function was applied in order to reproduce the correlation between ET and WT dynamics.

II. - The two configurations were tested for the assimilation of ET data from the CSIRO Modis Reflectance Scaling ET (CMRSET). The framework proposed in Task-2 was validated against real data in a pine plantation in the south-east of South Australia. Results of the assimilation for the two model configurations were evaluated in terms of performances of the WT dynamics, SM and modeled actual ET (AET).

Task 4 This step explores the effects of different parameterizations on the assimilation of ET, by applying Configuration-1 to locations with different vegetation, soil and WT depth conditions. Four suitable locations were identified to conduct this analysis. The depth to WT was seen to be able to positively impact ET assimilation performances.

1.4 Thesis Structure

This document is organised into 7 chapters including the present "Introduction" chapter. The other 6 chapters are:

Chapter 2:

This chapter presents the literature review, divided into three areas: hydrogeological modeling, use of RS data and an analysis of the data assimilation in the field of hydrology. Then, the research gap is identified and the scientific questions are stated.

Chapter 3:

This chapter groups the material and the methods developed and used for the study. Here, Task 1, 2 and 3a are introduced.

The chapter presents the site and data description, the Unsaturated zone model descriptions (i.e. UnSAT and SWAP), the groundwater model (i.e. MODFLOW-2005), the coupling of the models (Task 1 & Task 3a), and the assimilation framework (Task 2).

Chapter 4:

This chapter introduces the data assimilation algorithm used to assimilate ET observations. Then, it assesses the results of the assimilation, through a synthetically generated experiment, into different conditions of WT and vegetation interaction. This is based on Task 1 and Task 2.

Chapter 5:

This chapter describes the level of details of the UZMs required to perform the ET assimilation. It performs a comparative analysis using two UZM applied to a water-limited region in the south-east of South Australia. This is based on Task 3a and Task 3b.

Chapter 6:

This chapter aims at identifying the conditions in which the ET data assimilation has the greatest impact. The method is applied to three locations with different vegetation, soil and WT depth conditions. The effect of soil heterogeneity, vegetative species, and forcing inputs are investigated. This is based on Task 4.

Chapter 7:

This chapter provides an overview of the findings of this thesis. It is divided into a section presenting the summary of the finding about the "Feasibility Study", the "Model Complexity Assessment" the "Area Prioritization", and the "Overall Contribution". Finally, the "Limitations & Future Developments" are presented.

Chapter 2

Literature Review and Research Questions

2.1 Hydrogeological Modeling

Recharge to the WT and ET are two major components of the water cycle. The first is also one of the most important variables for groundwater management because it drives the hydrogeological system (Szilagyi et al., 2011). Recharge and ET are linked through the bio-physical processes that take place in the unsaturated zone. When the estimation of recharge includes the calculation of fluxes due to the transpiration from the groundwater, the variable is defined as net-recharge and accounts for plant water extraction (Szilagyi, Zlotnik, and Jozsa, 2013; Doble and Crosbie, 2017).

Generally, net-recharge cannot be evaluated directly by sensing technologies (Múnch et al., 2013). Thus, implicit methods, based on physical or chemical measurements, are used for the estimation of net-recharge from other measurements. Some examples are, WT fluctuation (Usman, Liedl, and Kavousi, 2015), hydrograph separation (Batelaan and De Smedt, 2007), recharge estimation based on Darcy's equation (Scanlon, Healy, and Cook, 2002), or environmental tracers (Crosbie et al., 2017). Some of these methods involve the calculation of ET, such as long-term series of precipitation minus ET (Crosbie et al., 2015), or numerical modeling of the unsaturated zone (Doble et al., 2015). All the methods listed previously are associated with a degree of uncertainty, an example is shown in figure 2.1 (Crosbie et al., 2015), which reports the best estimates and the 95% prediction intervals for a specific empirical method. The upper and lower values in the interval may often vary by up to two orders of magnitude, particularly when applied to water-limited environments where ET is close to precipitation.

Therefore, performing a proper calculation of ET, by means of a detailed representation of the water transport in the unsaturated zone, can lead to improved estimates of net-recharge and better simulation of the WT dynamics. One way of performing this calculation is through numerical models that reproduce the soil

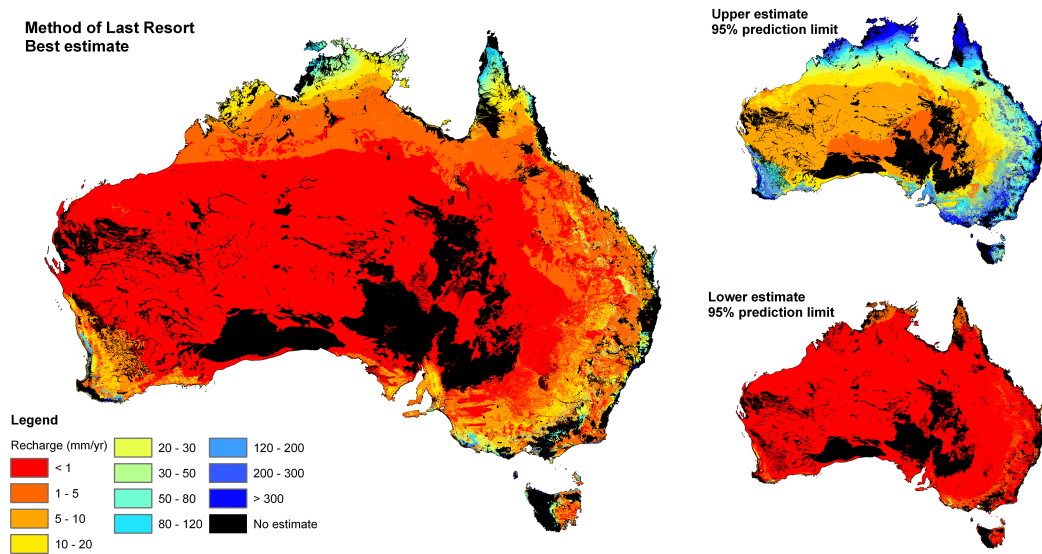


FIGURE 2.1: Maps of diffuse recharge estimated (large) and the upper and lower 95% percentiles estimates from (Crosbie et al., 2015)

water - vegetation - atmosphere interaction. This can lead to better estimates of the other hydrological components (Hendrickx et al., 2016). In general, two main approaches are used for the representation of the unsaturated zone, simple conceptual water balance models or detailed physically-based models. Conceptual soil water balance UZMs may over-simplify the biophysical process of transpiration but are widely used for spatially distributed simulation of the hydrological components (Batelaan and De Smedt, 2007; Doble et al., 2017). These models present a wide variety of complexity, but they are fundamentally based on equations expressing the evolution in time of the SM content in a control volume, which generally, is a layer of a certain thickness. Studies such as Dripps and Bradbury (2007) or the single-layer model presented in Walker and Zhang (2002) are examples of very simple soil water balance models. In other cases, conceptual models are coupled to groundwater models used for integrated simulations or to represent specific processes. Two of these examples are Batelaan and De Smedt (2007), who successfully applied a coupled water balance model at a regional scale focusing on the assessment of recharge, and Facchi et al. (2004) who coupled a conceptual UZM to MODFLOW to reproduce the hydrological processes for crop water consumption in an alluvial plain. Conceptual water balance models have been found to be flexible as they usually require shorter run times and fewer parameters, and are suitable when stochastic simulations based on Monte-Carlo techniques are applied (Kim and Stricker, 1996; Fatichi et al., 2016). These models may be less parametrized, nonetheless, they require continuous and accurate forcing input datasets to perform the simulations.

For more detailed simulations, such as in ecohydrology or agricultural modeling, simple UZMs may fail to accurately simulate important processes (i.e. water stress, root growth, capillary fringe) (Krysanova and Arnold, 2008), and physically-based models are preferred (e.g. Hydrogeosphere, Therrien et al., 2006, CATHY, Camporese et al., 2010, PARFLOW, Jones and Woodward, 2001, & SWAP, van Dam et al., 2008). These models commonly solve the Richards equation (which is a combination of Darcy's law and the conservation equations for soil water) for water flow in porous media, relying on the relationship between volumetric water content, hydraulic conductivity and soil water pressure head (van Dam et al., 2008; Scheerlinck et al., 2009). Therefore, physically-based models have the ability to account for specific effects (e.g. capillary rise) that affect the calculation of ET, thus impacting recharge estimates. These models can either implicitly or explicitly be coupled to saturated models (PRAMS Silberstein et al. (2009), GSFLOW Markstrom et al. (2008), MIKE SHE (Hughes and Liu, 2008)). In this configuration, it is possible to account for the direct groundwater-vegetation interaction (Facchi et al., 2004; Zhu et al., 2012; van Walsum and Veldhuizen, 2011).

However, because of the number and spatial variability of parameters (e.g. the water retention curve, detailed vegetation characteristics) required by physically-based models, their application, particularly in data-scarce areas, can be challenging (Simmons and Meyer, 2000). On the other hand, conceptual models may require fewer input data, but their recharge estimates may be less reliable. This is because they are affected by both structural uncertainty, induced by the simplification of the model (Renard et al., 2010), and more sensitive to the epistemic and aleatory uncertainty of the forcing inputs (Khatami et al., 2019). Accurate model parameters and meteorological inputs are far from always available, especially at large spatial scales. Therefore, the use of RS data can provide vital information for these models (Entekhabi and Moghaddam, 2007; Carroll et al., 2015; Lu, Steele-Dunne, and De Lannoy, 2020).

2.2 Use of Remotely Sensed Data

One of the advantages of satellite RS is the ability to provide continuous spatio-temporally distributed data sets of observations, overcoming the limitations posed to field-based campaigns. Thus, data products from RS are a set of valid management tools for Earth observation research (Lucas et al., 2015). In the last decades, RS data have been extensively used, processed, and integrated with traditional surveying techniques (Madry, Pelton, and Bukley, 2010). In fact, since the inception of satellite RS for military purposes, during the fifties, the data availability has increased dramatically (McCabe et al., 2017; Girotto et al., 2019). Satellite data collection for civil use started with the Landsat mission in 1972 run by the United

States Geological Service (USGS) and the National Aeronautics and Space Administration (NASA). Since then, Landsat has become the longest continuous coverage of RS data observations of Earth.

Most of the spacecraft in the atmosphere use two orbits, of which the Sun-synchronized polar orbit (around 500-800 km) provides coverage to a high to moderate resolution. This improves the robustness of the observations because it permits to obtain periodic data at the same time of the day and same sun-light angle (Madry, Pelton, and Bukley, 2010). Two of the spacecrafts using this orbit are Terra (1999) and Aqua (2002). These vehicles are part of the Moderate Resolution Imaging Spectroradiometer (MODIS) mission, which produced some of the most used RS data for research purposes. The instruments on board of these two spacecrafts, use 36 spectral bands (ranging from 0.4 to 14.4 μm), at three nominal spatial resolutions of 250 m (2 bands), 500 m (5 bands) and 1 km (29 bands). A scanning pattern of $\pm 55^\circ$ at an orbital height of 705 km, taking 99 min for each revolution, produces a swath width of 2330 km cross-track by 10 km along a track at nadir. This covers the entire globe in one to two days (Barnes, Pagano, and Salomonson, 1998).

Raw data from MODIS are either sent to stations for preprocessing, in order to be used for research, or directly broadcasted in a continuous stream which a 3 m or larger x-band antenna is able to receive (Barnes, Pagano, and Salomonson, 1998). Most products used for analysis are processed and available from the Land Process Distributed Active Archive Center (LPDAAC). The center provides free access to data sets such as numerous ocean and land products ranging from surface temperature, land cover, reflectance, albedo, LAI or incident solar radiation, to mention some. These products are amongst the most used sources of hydrologic observations (e.g. Houser, De Lannoy, and Walker, 2012). The combination of some of these products is used for the calculation of ET as these estimates are not directly retrievable from observations (Guerschman et al., 2009; Szilagyi et al., 2011; Hendrickx et al., 2016). The Guerschman et al. (2009) product is one of the most interesting for Australia, as it is locally generated and accounts for all sources of ET including canopy and soil evaporation. The detailed procedure of this algorithm is presented in section 3.2.2

Entekhabi and Moghaddam (2007) and Doble and Crosbie (2017) stated that the use of RS observations would be beneficial for those remote areas that are chronically lacking data and in particular for the reduction of the uncertainty related to recharge and ET. Some of these satellite observations have been used for constraining the water balance approach (Szilagyi et al., 2011). An example is Lucas et al. (2015), who successfully estimated recharge from a RS water balance compared to WT fluctuation and a field-based water budget. Similarly, Coelho et al. (2017) compared different methods to infer recharge values using RS precipitation

and ET data. However, all these studies recognized a certain degree of uncertainty related to the different methods of calculating recharge. For instance, Lucas et al. (2015), found a variation of over 57% in 3 different methods of recharge estimation, suggesting that the use of RS data alone may not be sufficiently accurate for the estimation of recharge and thus be used at an operational level. Thus, using techniques for model data fusion, such as data assimilation, RS observation can be proficiently merged with groundwater model outputs with the aim to produce more reliable model results.

2.3 Data Assimilation in Hydrological Studies

Data assimilation dates back to the study of Charney, Halem, and Jastrow (1969) who, in the field of meteorology, introduced the concept of assimilating temperature observations to predict wind and pressure values. In general terms, data assimilation seeks for the best results by combining observations and model forecasts of state variables. It also assumes that these variables come with errors and information that can be positively used to reduce uncertainties (Houser, De Lannoy, and Walker, 2012). This process has been used for more than two decades in weather forecasting (Daley, 1991) and climate prediction modelling (Reichle, McLaughlin, and Entekhabi, 2002) with some of the most recent and positive achievements by using data derived from RS (Glenn, Nagler, and Huete, 2010; Pipunic, Ryu, and Walker, 2014; Hartanto et al., 2017; Nearing et al., 2018).

The work on the assimilation of RS data in hydrologic forecasting is well reviewed in several studies of Liu et al., 2012, Rajabi, Ataie-Ashtiani, and Simmons, 2018 and Abbaszadeh, Moradkhani, and Daescu, 2019, who stated the positive impact of data assimilation to identify and reduce the uncertainty associated with various sources (i.e. model conceptualization, observations, boundary conditions). The first study on assimilation in hydrology was Entekhabi, Nakamura, and Njoku (1994) where the extended Kalman filter was used. The work of Li et al. (2016) provides an overview of RS products being currently used for hydrological purposes with a focus on satellite-based observations. According to this study, precipitation, SM, temperature and reflectance are the most extensively used satellite products, some of them in correlation with ground-based measurements. SM is perhaps the most available product with several spacecrafts carrying microwave sensors (e.g. Aqua, SMOS, SMAP). This availability supported SM assimilation studies of which a few examples are Pauwels et al. (2001), Reichle (2008), and Montzka et al. (2011). According to both Li et al. (2016) and Liu et al. (2012), other RS observations like LAI or ET have not received interest to the same extent of SM. Thus, more effort should be concentrated on ET, which is the second most important component of the water balance after precipitation (Glenn, Nagler, and Huete, 2010).

The study of Kustas and Norman (1996) defined the advantages and the drawbacks of the early use of RS ET. It pointed out the general efficiency and cost-effectiveness of RS ET at a regional scale. However, the advantages mentioned may be reduced because of the complexity of the parameters required by numerical models based on the estimation of the soil heat flux. Another recognized major inefficiency was the limitation of optical observations due to cloud cover. To overcome these limitations, they suggested the use of simplified models for the energy balance and investigated the benefits of microwave observations (e.g. cloud penetration) over optical data. More recently, other authors have used RS ET to improve hydrological models (Schuermans et al., 2003; Münch et al., 2013), for regional assessments (Gokmen et al., 2013; Hartanto et al., 2017), in modeling plant transpiration (Carroll et al., 2015), and for estimating recharge (Crosbie et al., 2015; Lucas et al., 2015). Hartanto et al. (2017) used the particle filter to assimilate AET data focusing on the improvement of the discharge.

Some of the ET assimilation studies used physically-based UZM for specific agro-hydrological simulations. For instance, Chemin, Honda, and Ines (2004) theorised the use of a genetic algorithm for assimilating ET from the Surface Energy Balance Algorithm for Land (SEBAL) into the SWAP model. This was applied a few years after by Irmak and Kamble (2009) who combined MODIS ET retrieval and SWAP modeled ET to inversely estimate crop and irrigation parameters, obtaining moderate success in the synthetical experiment application. Droogers, Immerzeel, and Lorite (2010) applied an inverse modeling approach (forward-backwards optimization) using SWAP and satellite ET products. They stated that improvements were obtained when the interval between the ET observations was shorter than 15-days and the associated observation error was below 10%. Better results were obtained by Vazifedoust et al. (2009) who explored the assimilation of the leaf area index and ET estimates on a quasi-distributed SWAP application by using simplified version of the Kalman filter (i.e. constant gain). They showed that the combined assimilation of both LAI and ET produced significant improvements, with LAI retrievals being the most effective. Because of the nature of the constant gain Kalman filter, their predictions were deteriorating quickly when the model was used for forecasting without the assimilation. This effect can be avoided by applying the EnKF, which sequentially recalculates the covariance matrices, thus the Kalman gain, every time an observation is available.

Only a few studies that specifically consider the assimilation of data into groundwater models have been found. One of the first papers on data assimilation in groundwater is Paniconi et al. (2003) who applies a nudging algorithm, assimilating SM, to a three-dimensional surface-subsurface model (i.e. CATHY) obtaining promising results in error reduction. Camporese et al. (2009), using the same model, tested a sequential data assimilation of synthetically generated pressure

head and streamflow through the EnKF. They showed that the combined assimilation increased the confidence of the state variable. In the same period, Ng et al. (2009) used a combined assimilation of SM and chloride concentration to identify recharge processes in semiarid environments; the combination of modelled and observed data allowed them to define singular events causing recharge. In the field of groundwater management, Cheng et al. (2011), through a nudging algorithm, assimilated the unknown value of private pumping to provide a more robust model.

Even though satellite observations present a trade-off among accuracy, temporal frequency and spatial coverage, the use of these products has been proven to be beneficial for the reduction of the recharge and ET uncertainty especially for data-scarce areas (Entekhabi and Moghaddam, 2007; Doble and Crosbie, 2017). It should also be noticed that the ET values obtained from satellites are not free from errors. Long, Longuevergne, and Scanlon (2014) analyzed and compared the uncertainty in the ET retrieval from three different sources including RS MODIS and the Gravity Recovery and Climate Experiment (GRACE), which provides observations of the Earth's gravity field to detect total water storage (Güntner, 2008; Giroto and Rodell, 2019). They showed as ET estimates derived from land surface (unsaturated zone, vadose zone) models had lower uncertainty than the MODIS based ET, which in turn was lower than the GRACE derived ET uncertainty. Finally, Long, Longuevergne, and Scanlon (2014) suggested a 'hybrid' approach taking advantage of the integration of land surface models and RS products to reduce uncertainty. Therefore an assimilation algorithm that proficiently accounts for the observation errors when assimilating RS ET observation into unsaturated zone models should be used for this purpose.

Introduction to the Kalman Filters Class

Kalman filters have the potential to sequentially assimilate observations of state variables in time and account for observation errors. The original Kalman Filter (Kalman, 1960) relies on assumptions, such as the linearity of the model and the error covariances matrix, which can be important drawbacks. The first attempt to improve the filter was the development of the Extended Kalman filter (Welch and Bishop, 2006).

The Extended Kalman filter propagates a non-linear evolution of the states mean (See Figure 2.2 - upper), but it still requires parameters that are computationally intensive to calculate (e.g. Jacobian), and has been found particularly unstable if the system is highly non-linear (Miller, Ghil, and Gauthiez, 1994). To overcome these limitations, the EnKF (Evensen, 1994) was developed. This method has no need for the linearization of the model as the probability density function of the error is represented not by a single parameter (e.g. as in the case of the EKF),

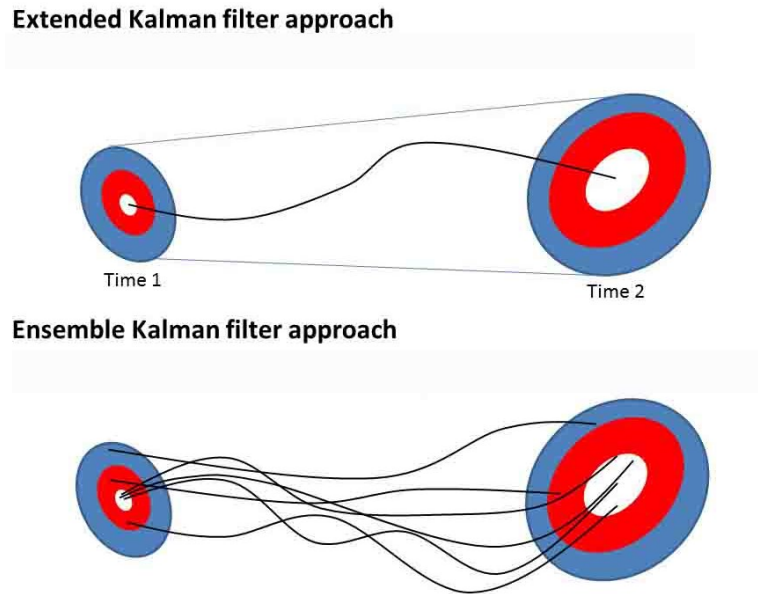


FIGURE 2.2: Representation of the difference of EKF vs. EnKF

but through an ensemble that evolves in time. This makes the filter suitable for the application to non-linear systems, as it can define an updating matrix (called the Kalman Gain) that permits non-linearity. This can be more computationally flexible, as the prior error covariance matrices only depend on the size of the ensemble (Figure 2.2 - lower panel), and they do not need to be calculated and stored.

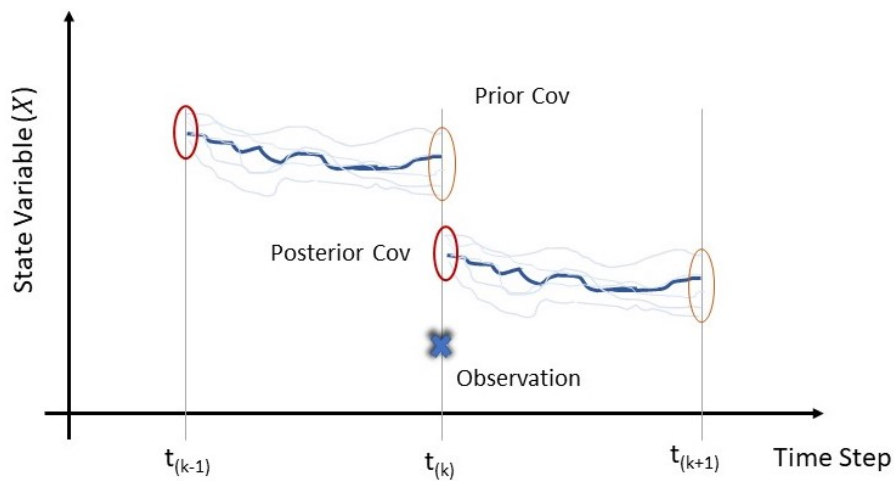


FIGURE 2.3: The sequence of the EnKF

Figure 2.3 represents the evolution the sequential assimilation performed with the standard version of the EnKF (i.e. the observation is part of the state variable space). At the time step before the assimilation ($t_{(k-1)}$), an ensemble of model runs is propagated in time to the time step ($t_{(k)}$), when the observation is available. Such a forecasted ensemble has an associated error covariance, called the prior.

The observation is affected by an error (e.g. instrument resolution, position errors, etc...), represented by the shadow around the cross. The error is itself a piece of information that can be used by the filter. After the EnKF is applied, a new error covariance, called the posterior, which is closer to the observation and reduced in amplitude, is calculated. This serves as the initial state for the propagation of the model to the next time step. The process is sequentially applied every time an observation is available.

However, the computational costs highly depend on the size of the ensemble, as the model has to be applied as many times as the members of the population. The EnKF has been chosen as the assimilation algorithm for this study because of the vast example of applications and its proven robustness in dealing with non-linear problems in hydrology (Liu et al., 2012).

Further examples of studies applying the EnKF, relevant for the assimilation of ET into groundwater models, are here listed. Notable is the study of Zou et al., 2017, who investigated the assimilation of ET data from the MODIS global ET project (MOD16) into a conceptual water balance model using the Ensemble Kalman Filter (EnKF). The study showed promising results by linking ET to the model state variables allowing the direct assimilation of the diagnostic variable ET. This feedback problem was already encountered by Schuurmans et al., 2003 who bypassed it by using a constant Kalman Gain that was not designed to provide feedback to the model states. However, Zou et al., 2017 focused on the effects of assimilation mostly on the superficial component of the hydrological cycle (i.e. SM and streamflow) and did not investigate the impact of data assimilation on recharge. Data assimilation for operational purposes was investigated by Hendricks Franssen et al. (2011), who used the EnKF to assimilate pressure head into a variably saturated groundwater flow model in an urbanized area. They found that the assimilation outperformed the results of the model calibrated with historical data, and the benefits of the assimilation were propagated for a period of up to 10 days. Xue (2015) applied an EnKF to a groundwater model using synthetic piezometric head observations. Similarly to the hydrological study discussed above, Xue (2015) did not thoroughly explore the feedback of the assimilation into the groundwater model. Recently, He et al., 2019 performed an assimilation study into MIKE-SHE using an evolution of the EnKF. In their study they found how the joint assimilation of streamflow and groundwater heads can reduce model bias; however, it does not necessarily reflect in improvements on the simulation of the coupled groundwater-surface water environments as the groundwater simulation was improved mostly because of the data assimilation ability to correct the initial groundwater heads. This study is also of particular interest because it applies performance metrics that allow ensemble skills verification as in De Lannoy et al. (2006).

2.4 Research Gaps and Statement of the Questions

The contents of section 2.1, 2.2 and 2.3, show the *state-of-the-art* of the scientific knowledge. This review suggested that more research needs to be conducted in the field of data assimilation into hydrogeological models. In particular, research gaps are identified in the representation of the intricate soil water-groundwater-vegetation system through models of different complexity. In addition, the use of the EnKF to assimilate ET fluxes into such a system has not been used yet to constrain coupled saturated - unsaturated models.

This thesis aims to tackle the research needs by investigating three main research questions. For each question, the motivations, hypothesis and expected findings are briefly explained.

1. *Is it possible to assimilate remotely sensed ET to improve UZM-groundwater model outputs?*

This question looks at the interaction between a coupled saturated - unsaturated zone model, particularly regarding the dynamics between ET and WT levels. It analyzes if the updated state variables are in turn improving the values of modeled ET and recharge. As part of this, the study explore the importance of carefully generating ensembles in order to obtain meaningful results.

2. *What level of complexity of the unsaturated zone model is needed for the assimilation of ET into groundwater models?*

This part investigates the level of model detail required for the simulation of the unsaturated zone and its coupling to a groundwater model. Complex physical models with many parameters may reduce the benefit of the assimilation; it is thus important to define a trade-off between complexity and accuracy of the outputs. The study explored the key aspect of calibrating coupled models on WT levels and actual ET.

3. *Under which soil, vegetation, and depth to WT condition does the assimilation improve model performance?*

We hypothesize that the approach has a greater impact on uncertainty reduction where the WT is shallow and the interaction with vegetated areas is more prominent. The effect of depth to WT, soil heterogeneity, type of vegetation, and the bias correction of the assimilated ET values are objects of the investigation.

Chapter 3

Material and Methods

This chapter first introduces the study area and the climatic data. Then, it describes the models, their coupling and the assimilation algorithm. A large part of this chapter are based on the article "**Feasibility of improving groundwater modeling by assimilating evapotranspiration rates**"¹ published in *Water Resources Research* (i.e the UnSAT model and the assimilation framework). The coupling of the physically-based model and the ET assimilation configuration are based on the article "**Required complexity of unsaturated zone models for the assimilation of evapotranspiration rates**" submitted to *Hydrology and Earth System Sciences*.

3.1 Site Description

The area selected for the application and validation of this study is located in the south-east of South Australia within the Otway and Murray Basins (See Fig. 3.1). The climate in the area is Mediterranean, with winter dominant rainfall and hot dry summers. The historical data, observed over the last 70 years, report an annual rainfall range between 640 mm and 747 mm year⁻¹ and PET ranges between 960 and 1400 mm year⁻¹. The Morton equation (Donohue, McVicar, and Roderick, 2010), and the Budyko-curve (Donohue, Roderick, and McVicar, 2007) thus classify the area as dominated by ET, or water-limited (Jackson, Jobbágy, and Noretto, 2009; Benyon, Theiveyanathan, and Doody, 2006).

The region is generally flat, decreasing from the highest elevation of the east-north-east towards the south-west coast. Undulations are present in the south-west of the region with two main peaks, Mount Gambier and Mount Burr (190 m). From a hydrogeological point, the area is the lower part of a tertiary confined sand aquifer named Dilwyn Formation. This confined aquifer is separated by an aquitard from the overlain unconfined quaternary/upper-mid Tertiary Gambier/Murray Group limestone aquifer. The study of Benyon, Theiveyanathan, and Doody (2006) described the groundwater resources of the area for a 95% in an unconfined aquifer that is generally shallow (i.e. < 20 m depth to WT), and presents

¹<https://doi.org/10.1029/2019WR025983>

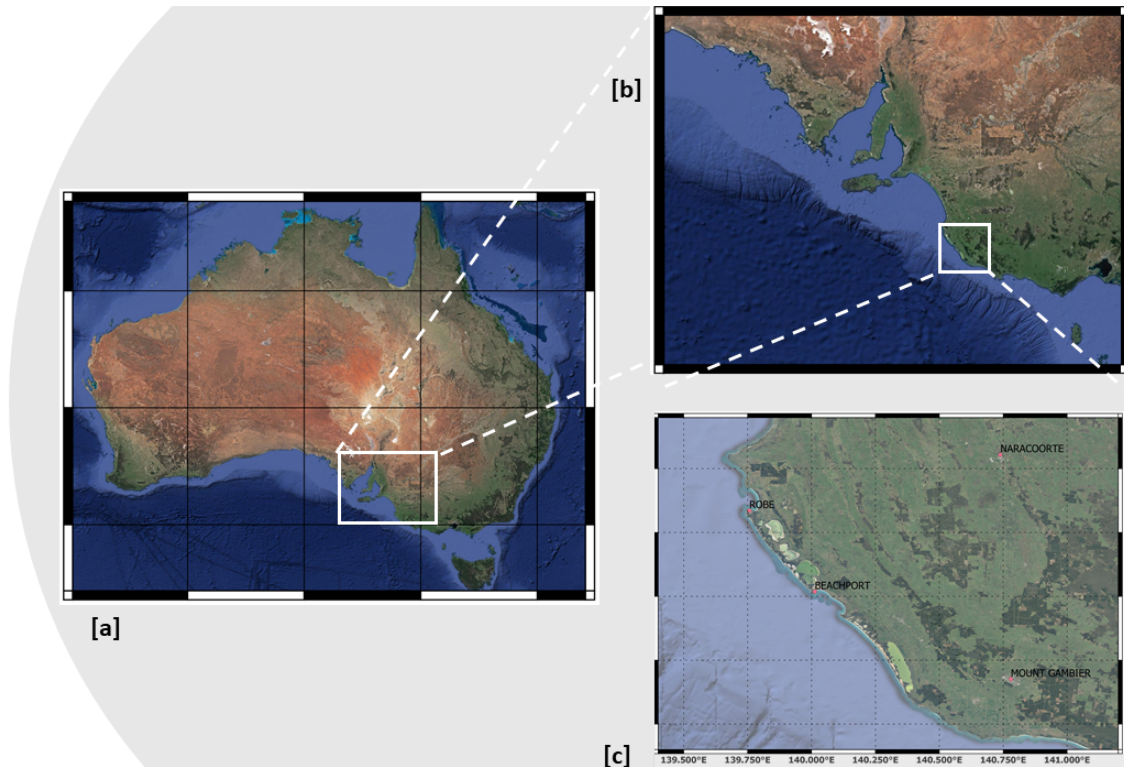


FIGURE 3.1: Location of the study area within Australia [a], and within the south-east of South Australia [b]. Major towns of the study area used throughout this thesis [c].

areas where the water table is within 2 m from the surface, especially towards the south-west part of the region. For the unconfined aquifer, the depth to WT is largely depending on surface topography as the region presents sandy ridges rising up to 20 m interspersed by inter-dunal flats (See Figure 3.2[a] for the topography and Figure 3.2[b] for the depth to WT).

Land use includes pasture and annual cropping, with areas of forestry and native vegetation. Irrigation of vineyards and pasture also occurs. Softwood and hardwood forests, used for timber production, have been planted for more than a century and are mostly dominated by radiata pine *Pinus radiata* and bluegum *Eucalyptus globulus* (Benyon, Theiveyanathan, and Doody, 2006). Eco-hydrological studies, carried out at different sites during the first decade of the millennium (Benyon and Doody, 2004; Benyon et al., 2008; Benyon and Doody, 2015), have shown that these forests have been planted in areas with mostly shallow WT, thus they have direct access to groundwater (Benyon and Doody, 2004). For each specific location, more details from these studies are presented in Chapters 5, and 6

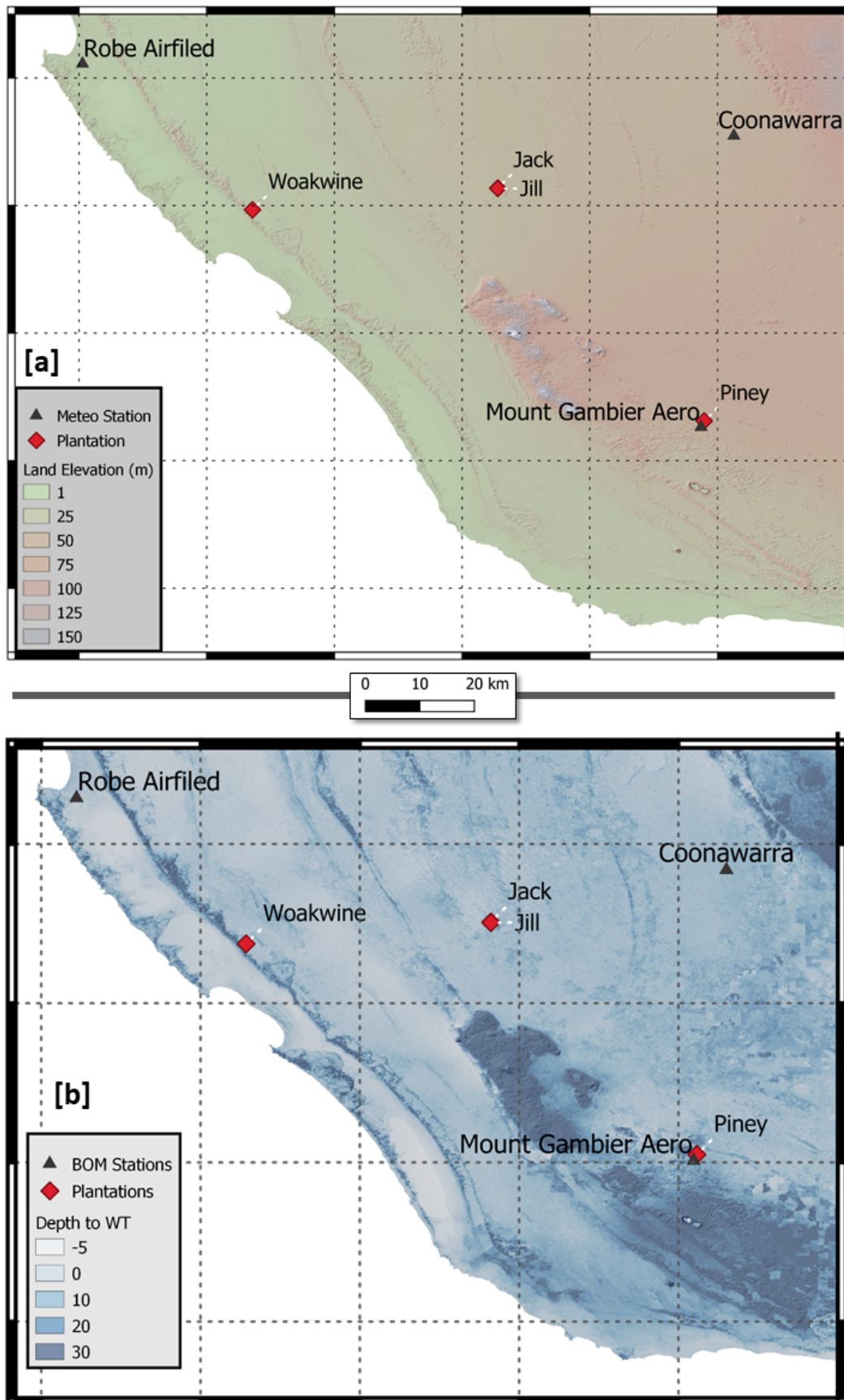


FIGURE 3.2: Digital elevation model of the area [a]. Depth to WT map [b].

TABLE 3.1: Name and coordinates of the meteorological stations

Station Name	Latitude	Longitude
Mount Gambier Aero	-37.747	140.773
Coonawarra	-37.290	140.825
Robe Airfield	-37.177	139.805

3.2 Data

3.2.1 Climatic Data

Rainfall and PET are the forcing inputs needed by the UZMs in order to estimate the net-recharge. These data are obtained from three stations of the Bureau of Meteorology (BoM). Rainfall is provided with a frequency of 30 minutes, and is accumulated to an hourly time step and a daily time step, depending on the UZM used. ET values are provided as daily values, these are also readjusted in time to the frequency by the UZMs should required (e.g. hourly).

The coordinates of the three stations used within this study site are shown in Table 3.1 and Figure 3.1 [c]. The synthetic simulation in Chapter 4 uses climatic input from the Coonawarra station, the simulations presented in Chapter 5 are based on the data from the Mount Gambier Aero station, while the simulations of 6 use inputs from all the three stations.

3.2.2 The CMRSET

AET is not a direct product of RS observations. It is calculated through algorithms which transform for example reflectance to ET, or PET to AET. Examples are SEBAL (Bastiaanssen et al., 1998) and METRIC (Allen, Tasumi, and Trezza, 2007), which are surface energy balance techniques that require several parameters proceeding from RS and/or ground observations. Another example is the fairly simple CREMAP technique proposed by Szilagyi et al., 2011 which linearly links the MODIS daytime surface temperature to the ET rate.

The empirical CSIRO MODIS reflectance-based scaling evapotranspiration (CMRSET) (Guerschman et al., 2009) estimates AET based on surface reflectance from MODIS-Terra and interpolated climate data. It uses the MODIS nadir bidirectional reflectance distribution function - adjusted product (MCD43A4) to rescale the Priestley-Taylor PET and calculate the AET through the global vegetation moisture index (GVMI) and the enhanced vegetation index (EVI). In this formulation, the EVI is associated with ET through the LAI. The GVMI accounts for the separation between surface water and bare soil when the EVI is low, while it provides information on vegetation water content when the EVI is high.

The model was calibrated using observed AET, from eddy covariance measurements at seven sites in Australia, including forests, savannas, and floodplain. The model was able to reproduce the main spatial and temporal patterns in AET across Australia. A clear advantage of this model is that it does not need land cover classification, thus avoiding the possible wrong categorization of land tiles and that it is able to estimate AET in open areas with direct evaporation from water bodies.

The CSIRO report (King et al., 2011) provides a detailed explanation of this model, including a comparison with other products. Here, only a brief explanation of the method is given. The model calculates AET as follow:

$$AET[mm/day] = k_c \cdot PET + K_{Ei} \cdot P \quad (3.1)$$

where k_c is the crop factor, an indicator of the ratio of AET/PET, PET [L T⁻¹] is obtained from climatic data, K_{Ei} quantifies evaporation from interception and P [L T⁻¹] is the precipitation.

The crop factor K_c is calculated as:

$$K_c = K_{c_{max}} \cdot [1 \exp -a \cdot EVI_r^\alpha - b \cdot RMI^\beta] \quad (3.2)$$

where $K_{c_{max}}$ is the maximum value for the crop factor, EVI_r is a rescaled EVI derived from MODIS data and RMI is a residual moisture index from MODIS data.

The rainfall interception factor K_{Ei} was linearly related to EVI_r following:

$$K_{Ei} = K_{Ei_{max}} \cdot EVI_r \quad (3.3)$$

In the equations above, $K_{c_{max}}$, $K_{Ei_{max}}$, a , α , b and β are parameters fitted empirically.

In its origin, the algorithm was devised to produce monthly values of ET, using the 16-day reflectance values, upscaled in time to a monthly value at a 1 km resolution. Recently, a finer temporal and spatial resolution data-set has been made available, with a 250 m grid at a 8-day composite time step. This is the version of the data used in this study. The CMRSET algorithm was found to produce reliable estimates across Australia compared to various other ET algorithms (Glenn et al., 2011).

3.3 UnSAT - UZM

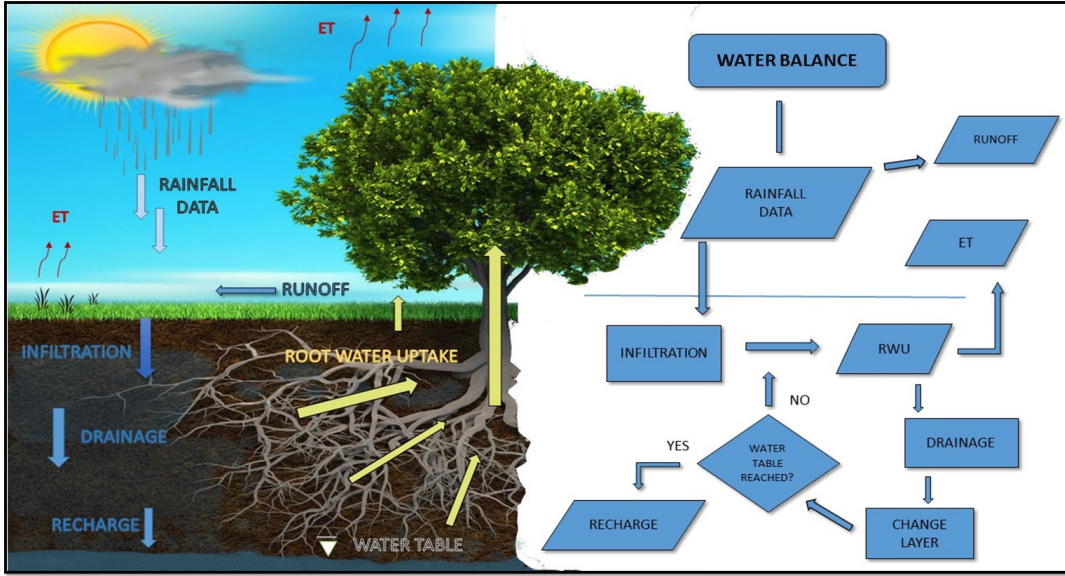


FIGURE 3.3: Conceptualization and flowchart for the unsaturated zone model

3.3.1 Conceptualization

This thesis present a model for water flow in the unsaturated zone, named **Un**saturated zone & **SAT**ellite (UnSAT), which we devised with the specific intent to account for the dynamics of evapotranspiration. The model conceptualization is depicted in Figure 3.3.

This model is developed as a one-dimensional UZM, where the vertical soil profile is simulated as a sequence of layers in which water flows downward from the first to the last, and the latter delivers recharge to the WT (See Figure 3.4). The size of the buckets remains constant while their number changes according to the depth to WT.

Using an explicit finite difference approximation for the water balance of the layer at the soil surface the model calculates

$$\theta_1^{t+1} = \theta_1^t + \frac{P^t - AET_1^t - Q^t - D_1^t}{\Delta z_1} \cdot \Delta t, \quad (3.4)$$

where θ [$L^3 L^{-3}$] is soil volumetric water content, P [$L T^{-1}$] is precipitation, AET [$L T^{-1}$] is AET, D [$L T^{-1}$] is drainage and Q [$L T^{-1}$] is runoff. In Eq. 3.4, the subscripts refer to the progressive position of the layer (e.g. 1 is the soil layer at the

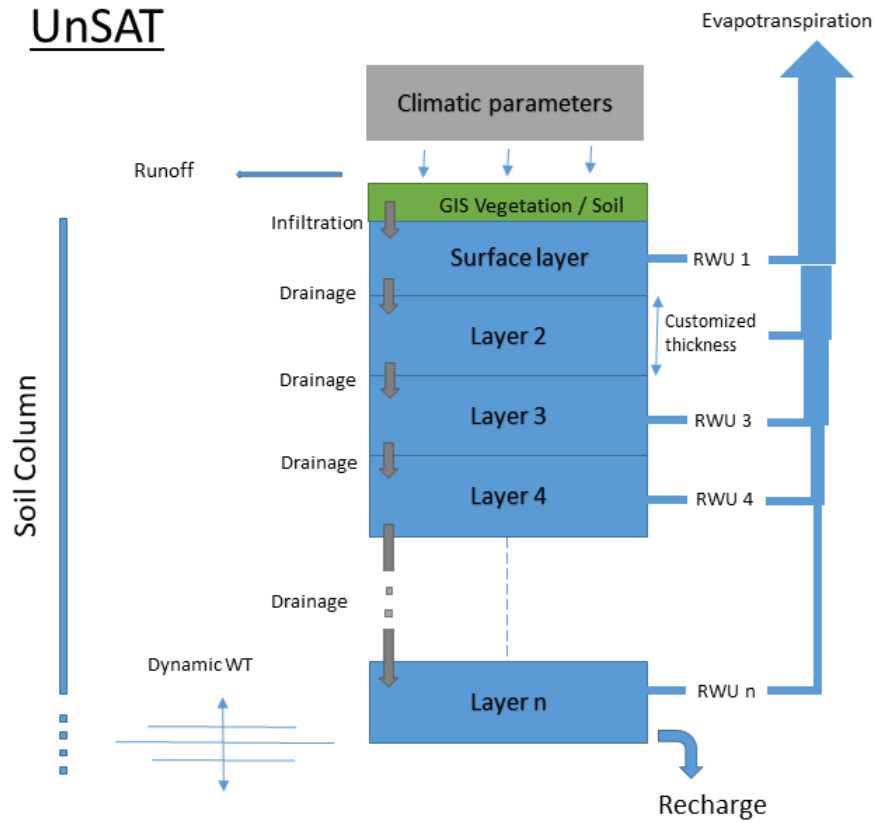


FIGURE 3.4: Schematic of the UnSAT model.

surface) and the superscripts refer to the time step.

Following the definition of Campbell (1974), the drainage D [$L T^{-1}$] that percolates to the lower layer reads

$$D = K_s \left(\frac{\theta}{\phi} \right)^c, \quad (3.5)$$

where K_s [$L T^{-1}$] is saturated hydraulic conductivity, ϕ is porosity [$L^3 L^{-3}$], and $c = 2b + 2.5$ is the exponent where b is an empirical value as explained in Clapp and Hornberger (1978). As part of this study, b was set as one of the parameters for calibration.

Actual Evaporation and Transpiration are modelled together in the water balance equation as a function of the SM and the vegetation using

$$AET = AET_{max} \cdot \beta(z) \cdot \alpha(\theta), \quad (3.6)$$

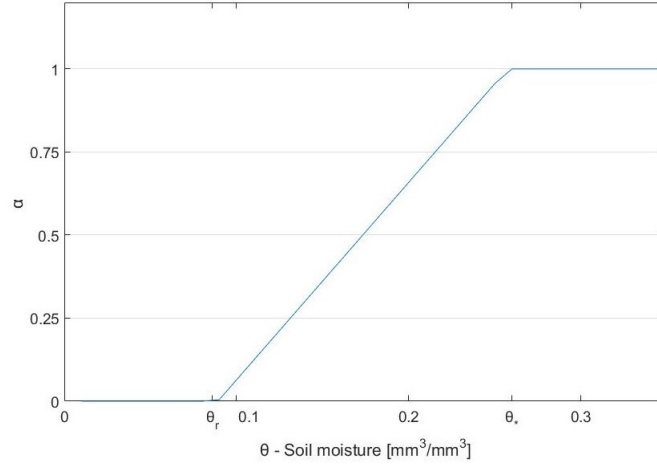


FIGURE 3.5: Water stress reduction function. the various θ values in the Figure are taken from the calibration in Appendix B.

where $\beta(z)$ is the root distribution function explained in section 3.3.3, and α is a water stress reduction function (See figure 3.5), which reads

$$\alpha(\theta) = \begin{cases} 0, & \theta < \theta_r \\ \frac{\theta - \theta_r}{\theta_* - \theta_r}, & \theta_r \leq \theta \leq \theta_* \\ 1, & \theta > \theta_* . \end{cases} \quad (3.7)$$

θ_r [$L^3 L^{-3}$] is the residual soil volumetric water content and θ_* [$L^3 L^{-3}$] is the volumetric water content, dependent on both the vegetation and soil type. When the water content drops below θ_* , vegetation starts to come under water stress, consequently a reduction of root water uptake is modelled similarly to Feddes et al. (1976).

The value of AET^t at each time step is distributed along the root depth; therefore, it is partitioned among the n-layers (AET_n^t) according to the root density (β).

Any of the n-layers underneath the first solves its respective water balance equation, which reads

$$\theta_n^{t+1} = \theta_n^t + \frac{D_{n-1}^t - (AET_n^t + D_n^t)}{\Delta z_n} \cdot \Delta t . \quad (3.8)$$

We tested and calibrated the model in a stand-alone configuration, results are presented in the Appendix B.

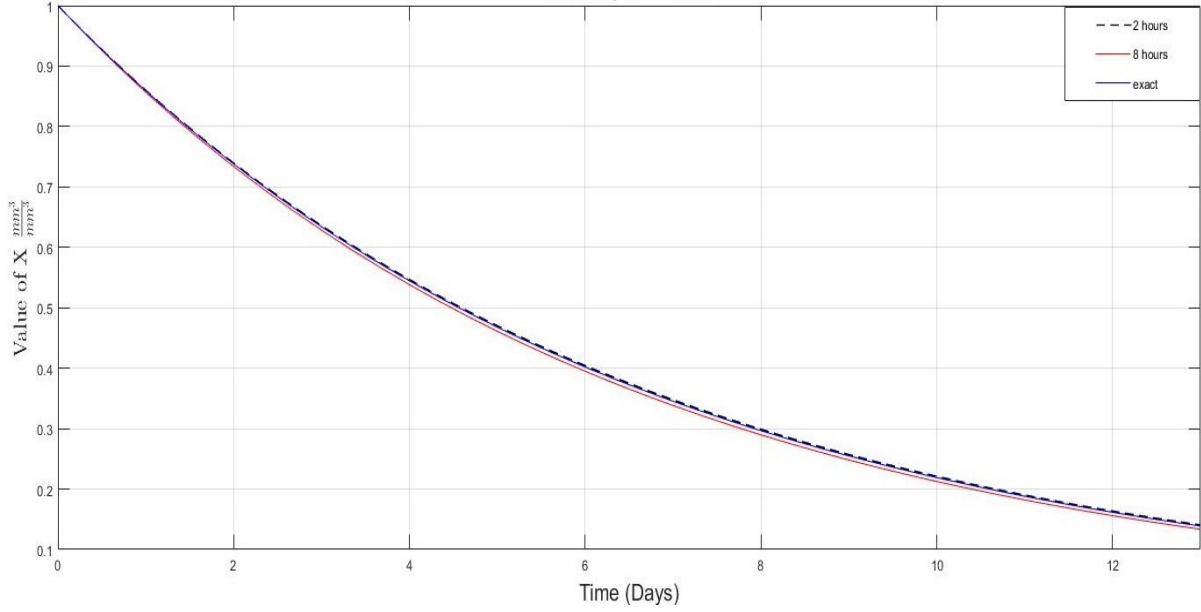


FIGURE 3.6: Accuracy of two time-steps chosen compared with the analytical solution of eq. 3.11

3.3.2 Time Step Evaluation

The correct definition of the time step applied to the numerical solution is decisive for the accuracy of the results. We define an exact solution, assuming a simplified version of the water balance for a single soil layer, with the intent to assess the time step size leading to numerically accurate results. In this model, $\beta(z)$ is assumed to be uniformly distributed over a depth ΔZ [L] and α is assumed to decrease linearly from θ_s [$L^3 L^{-3}$] (i.e. water content at saturation) to θ_r . Eq. 3.4, in which only the ET effect is accounted for, becomes

$$\Delta\theta = \frac{AET^t}{\Delta Z} \cdot \Delta t \quad (3.9)$$

where $AET^t = AET_{max} \cdot \alpha(\theta)$.

Calculating eq. 3.9 between a generic θ and θ_r , then dividing both term $\theta_s - \theta_r$ and substituting $\frac{\theta - \theta_r}{\theta_s - \theta_r} = x$, one obtains

$$\frac{\Delta x}{\Delta t} = \frac{-AET_{max}}{(\theta_s - \theta_r) \cdot \Delta Z} \cdot x \quad (3.10)$$

Assuming $k = \frac{AET_{max}}{(\theta_s - \theta_r) \cdot \Delta Z}$, eq. 3.10 becomes

$$\frac{dx}{dt} = -k \cdot x, \quad (3.11)$$

which can be solved exactly as

$$x = x_0 \cdot e^{-kt}, \quad (3.12)$$

where x_0 is the initial value of effective saturation; starting from a fully saturated soil, $x_0 = 1$ (i.e. $\theta = \theta_s$).

Eq. 3.12 can be solved numerically as

$$x^t = x^{t-1} - (kx^{t-1} \cdot \Delta t). \quad (3.13)$$

Several numerical solutions for different time-steps have been compared, assuming Δt varying from 1 hour to 1 day. The solution using a 1-hour step matches the exact solution, while the 1-day time step solution has considerable discrepancies of up to 20%. Fig. 3.6 shows how accuracy increases when the time step is reduced. For this thesis, a solution of an 8-hour time step is adopted for the synthetic case presented in Chapter 4 and its precision (i.e error < 1%) is considered satisfactory. The simulations of Chapter 5 and 6 use an hourly time step.

3.3.3 Root Distribution

A simple linear shape of the distribution for the root density $\beta_{(z)}$, is given by the equation

$$\beta_{(z)} = \frac{2}{Z_m} \cdot \left(1 - \frac{z}{Z_m}\right), \quad (3.14)$$

where Z_m [L] is the maximum depth of the root system and z [L] is the depth (positive downward). Because the linear distribution often results in SM values systematically low for the deeper layers, alternative distributions of the root extraction are implemented.

A possible alternative distribution follows Vrugt et al. (2001)

$$\beta_{(z)} = \left[1 - \frac{z}{Z_m}\right] \cdot e^{\frac{p_z}{Z_m} |z^* - z|}, \quad (3.15)$$

In this study, z^* has been set to 0 and the empirical value p_z is part of the calibration. The distribution $\beta_{(z)}$ is then normalized to have area = 1 and the root water uptake function (S_z) reads

$$S_z = \frac{\beta_{(z)} \cdot AET_{max}}{\int_0^{Z_m} \beta_{(z)} \cdot dz} \cdot . \quad (3.16)$$

The different solutions of the p_z investigation are illustrated in fig. 3.7. When $p_z = 0$, equation 3.15 normalized to have area 1 coincides with equation 3.14.

3.3.4 Decay of the Hydraulic Conductivity

A range of functions accounts for the heterogeneity of the saturated hydraulic conductivity parameter $K_s(z)$. Some studies treat the K_s as a constant value, as in

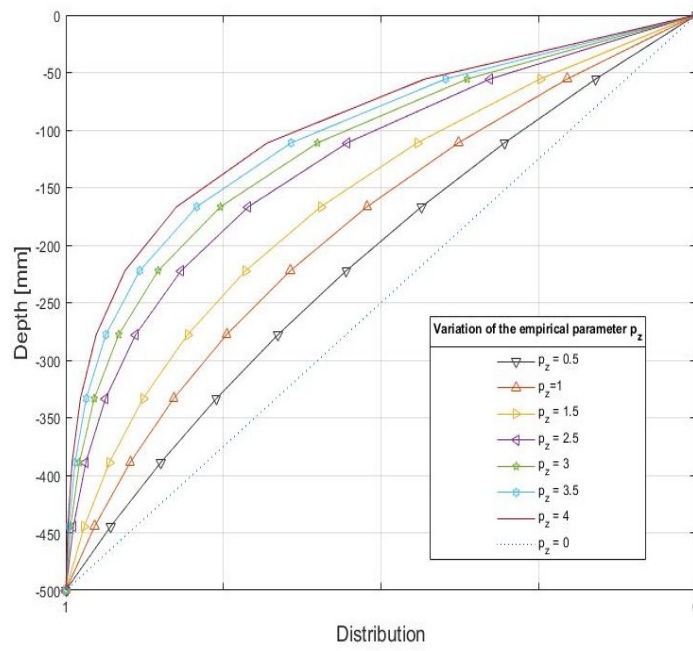


FIGURE 3.7: Different distribution shapes due to variation of p_z .

Gleeson and Manning (2008). Others consider the reduction of $K_s(z)$ with depth (Wang, Endreny, and Hassett, 2006; Jiang et al., 2009), and have been implemented into UnSAT.

Wang, Endreny, and Hassett (2006) proposed a power function decay of the hydraulic conductivity as

$$K_s(z) = K_0(1 - fz)^d, \quad (3.17)$$

where K_0 [$L T^{-1}$] is the value of hydraulic conductivity at the surface layer, and

$$f = \frac{\theta_s - \theta_n^1}{m}, \quad (3.18)$$

with m an empirical factor (see B.2 for values) and θ_n^1 the initial volumetric SM value for the $n - th$ bucket. The exponent d in eq. 3.17 produces a linear decay of K_s if $d=1$ and or parabolic decay if $d=2$.

The exponential decay was simulated through a modification of the method proposed by Beven and Kirkby (1979) and Jiang et al. (2009). Accordingly, K_s is written as

$$K_s(z) = K_0 \cdot e^{-B \cdot z}, \quad (3.19)$$

where $B = \frac{1}{Z_{max}}$ [L^{-1}] is the parameter that accounts for the decrease of conductivity and Z_{max} is the maximum modelled depth.

The results of the sensitivity analysis conducted on the model are reported in Appendix A. Note that this analysis was conducted on the stand-alone model (i.e. no coupling with the saturated model). Hence, parameters recognized to be important for the coupling, such as the root distribution and root length, here show a different sensitivity. The results of the model calibrations, including the effect of the possible decay of the hydraulic conductivity with depth, is treated in detail in Appendix B

3.4 SWAP

The Soil Water Atmosphere Plant (SWAP) model, developed by Alterra (van Dam et al., 2008), is one of the most used physically based UZMs. This agro-hydrological model applies the Richards equation to simulate the water, heat and solute flow in variably saturated soil (Kroes et al., 2017). This equation is derived from the Darcy equation, describing the water movement in the soil, which reads

$$q = K(h) \cdot \frac{\delta(h+z)}{\delta z} \quad (3.20)$$

and the continuity equation, which reads

$$\frac{\delta\theta}{\delta t} = -\frac{\delta q}{\delta z} - S_a(h), \quad (3.21)$$

where q [L day^{-1}] is the water flux moving through the soil, K [L day^{-1}] is the hydraulic conductivity, h [L] is the soil water pressure head, z [L] is the vertical coordinate, positive upward, θ [$\text{L}^3 \text{L}^{-3}$] is the volumetric soil content, t [T] is time, and S_a [$\text{L}^3 \text{L}^{-3} \text{T}^{-1}$] is a term that accounts for root water extraction.

Combining equation 3.20 and 3.21 gives the Richards equation:

$$C(h) \frac{\delta h}{\delta t} = \frac{\delta}{\delta t} \left[K(h) \left(\frac{\delta(h)}{\delta z} + 1 \right) \right] - S_a(h), \quad (3.22)$$

where $C(h)$ is differential soil water capacity $\frac{\delta\theta}{\delta h}$ [L^{-1}].

In addition, SWAP has the potential to account for a detailed soil water-vegetation interaction as it specifically simulates the dynamics of the crop growth cycle. Process-based models, like SWAP, are preferred when natural and anthropogenic modification of the hydrological cycle are assessed. The reason for this is the explicit mathematical formulation of the mass, energy and momentum conservation as a fundamental requirement for these problems (Fatichi et al., 2016). SWAP has a long history of application for this class of simulations, such as climate change (Droogers, van Loon, and Immerzeel, 2008; Farkas et al., 2014), fire hazard evaluation (Taufik, Setiawan, and van Lanen, 2019), impact of land-use change (Bennett, Bishop, and Vervoort, 2013), water use management (Droogers et al., 2000),

groundwater management (Li and Ren, 2019), and holistic assessment of the soil hydraulic properties (Pinheiro, de Jong van Lier, and Šimůnek, 2019).

In SWAP the Richards equation is solved for the pressure head using finite differences. The soil hydraulic retention functions are based on the analytical formulations proposed by van Genuchten (1980), reading

$$\theta = \theta_r + \frac{\theta_s - \theta_r}{(1 + |\alpha h|^n)^m}, \quad (3.23)$$

and Mualem (1976),

$$K(\theta) = K_s S_e^\lambda \left[1 - \left(1 - S_e^{\frac{1}{m}} \right)^m \right]^2 \quad (3.24)$$

where θ , θ_s and θ_r have been previously defined in section 3.3 and α , n and m are the van Genuchten empirical factors, with $m = 1 - 1/n$. λ is a shape parameter and S_e is the relative saturation which read,

$$S_e = \frac{\theta - \theta_r}{\theta_s - \theta_r}. \quad (3.25)$$

Finally, the model also requires a number of vegetation specific parameters (Feddes et al., 1976), including root depth, root distribution and oxygen stress.

SWAP has the ability to represent an internal saturated part of the soil column that is controlled by a specified head (simulating drains in the original conceptualization) at the boundary of the domain. In this study, the SWAP saturated function is neglected and replaced by the MODFLOW model.

3.5 MODFLOW - Groundwater Model

The groundwater model used for this study is MODFLOW-2005 (Harbaugh, Arlen, 2005), the three-dimensional (3D) finite-difference groundwater flow code developed by the U.S. Geological Service (USGS). The model solves the groundwater equation

$$\frac{\delta}{\delta x} (HK_{xx} \frac{\delta h}{\delta x}) + \frac{\delta}{\delta y} (HK_{yy} \frac{\delta h}{\delta y}) + \frac{\delta}{\delta z} (HK_{zz} \frac{\delta h}{\delta z}) - W = S_s \frac{\delta h}{\delta t} \quad (3.26)$$

where HK_{xx} , HK_{yy} and HK_{zz} [$L T^{-1}$] are the values of saturated hydraulic conductivity for the three axes x , y , and z , respectively. h is the potentiometric head (L), W represents sources and/or sinks of water as a volumetric flux [$L^3 T^{-1}$]; S_s

is the specific storage of the aquifer (T^{-1}), and t is time. All the simulations performed in this thesis implies unconfined aquifers, thus, for the remainder of this document, the S_s is substituted by the specific yield (S_y). Furthermore, the horizontal saturated hydraulic conductivity in the aquifer is considered homogeneous (i.e. $HK_{xx} = HK_{yy}$).

One of the characteristics of MODFLOW is its modularity, with each module grouping together all aspects related to a specific process. This approach allowed the UZM to be coupled to MODFLOW-2005 by replacing the ET package (EVT) with the output of the UZMs (UnSAT and SWAP), using the recharge (RCH) package to apply the calculated net-recharge to the cell-specific head.

The aquifer properties: saturated hydraulic conductivity (HK), specific yield (S_y), and model discretization are defined through FloPy (Bakker et al., 2016), a library that allows MODFLOW to be set up and run from a Python environment. The model runs at an 8-day time step, which is considered adequate for the groundwater dynamics. This choice was made to synchronize the models and assimilation time frequencies as the CMRSET data are available with a temporal resolution of eight days.

3.6 Model Coupling

A one-dimensional (1D) simplification of the unsaturated zone flow simulation is frequently accepted both at the field scale, where detailed simulation is needed for agriculture (van Dam et al., 2008) or solute transport (Daneshmand et al., 2019), and the regional scales (Zhu et al., 2011). Coupling a one-dimensional (1D) conceptual model for the unsaturated zone to a 3D, groundwater, physical model is a valuable solution for adequately modeling the two zones while maximizing the computational efficiency of the coupled model. This becomes a necessity when Monte Carlo like methods, such as the EnKF, are required. Coupling different models require a series of definitions and assumptions. The different time step definition for each model originated from the concept that the variability of the water content in the unsaturated zone is more pronounced than the WT dynamics (Xu et al., 2012). An appreciable variation of the regional WT often occurs over months or years. Therefore, a larger time step can be applied for the saturated model to reduce computational time (Facchi et al., 2004).

Alternatively, software like MIKE SHE (Diersch and Kolditz, 1998), Hydrogeosphere (Therrien et al., 2006) or MODHMS (HydroGeologic 2006) describe a fully coupled 3D unsaturated-saturated flow. These models inherently solve the issues related to the approximations and definitions associated with coupling distinct

models (i.e. different spatial and temporal scales, Barthel, 2006). However, these fully 3D models are not always computationally efficient for simulation at the regional scale. At the large scale, dimensional simplification to 1D unsaturated zone flow simulations has been shown to be sound. This is because the direction of the unsaturated zone flow is predominantly vertical (Zhu et al., 2011).

Other authors have dealt with the problem of mismatching time steps considering the vadose zone simply as a transition area between the surface and the water table, where the infiltration becomes potential recharge (Scanlon, Healy, and Cook, 2002). Other studies such as Batelaan and De Smedt (2007) used a definition of recharge as the results of a water balance over the unsaturated zone, accounting for ET losses. In these studies, the difference in time steps does not represent a problem either because the recharge is considered as an instantaneous input or because they are coupled to run at the same time step.

For the first configuration of the coupled model (Configuration-1), UnSAT was coupled to MODFLOW through the net-recharge flux, which acts as the MODFLOW upper boundary condition (Neumann conditions). MODFLOW passes back the new WT distribution on a raster basis to the UnSAT, which thus receives a lower Dirichlet boundary condition. This scheme, defined in Zeng et al., 2019 as the non-iterative feedback coupling model, is considered a trade-off between the computational cost of fully coupled or iterative schemes and the numerical accuracy. By specifically accounting for plant water extraction, through the calculation of fluxes due to transpiration from groundwater, the recharge to the WT takes the definition of net-recharge (Hopmans and Stricker, 1989; Doble and Crosbie, 2017).

Figure 3.8 on the left shows the coupling for two WT conditions and the flowchart of the coupling on the right hand. In the first case of the left hand side, the WT is within the root zone. Hence, the model simulates the root water uptake from all the layers. In the second case, the WT is below the root zone, the model is calculating the vegetation extraction from the layers forming part of the root zone but does not calculate extraction from the layers between the bottom of the root zone and the WT.

To optimize the computational requirements of running the coupled models, in Configuration-1 UnSAT runs at a short time step, either one hour or eight hours depending on the simulation, while MODFLOW runs with an 8-day simulation step that matches the CMRSET data frequency. A transformation function accounting for differences in the temporal resolutions is applied as part of the coupling (Besbes and De Marsily, 1984; O'Reilly, 2004). This accumulates the 8-days recharge from the UZMs and averages it to the time unit specified in the MODFLOW basic package (BAS), in this case a daily unit.

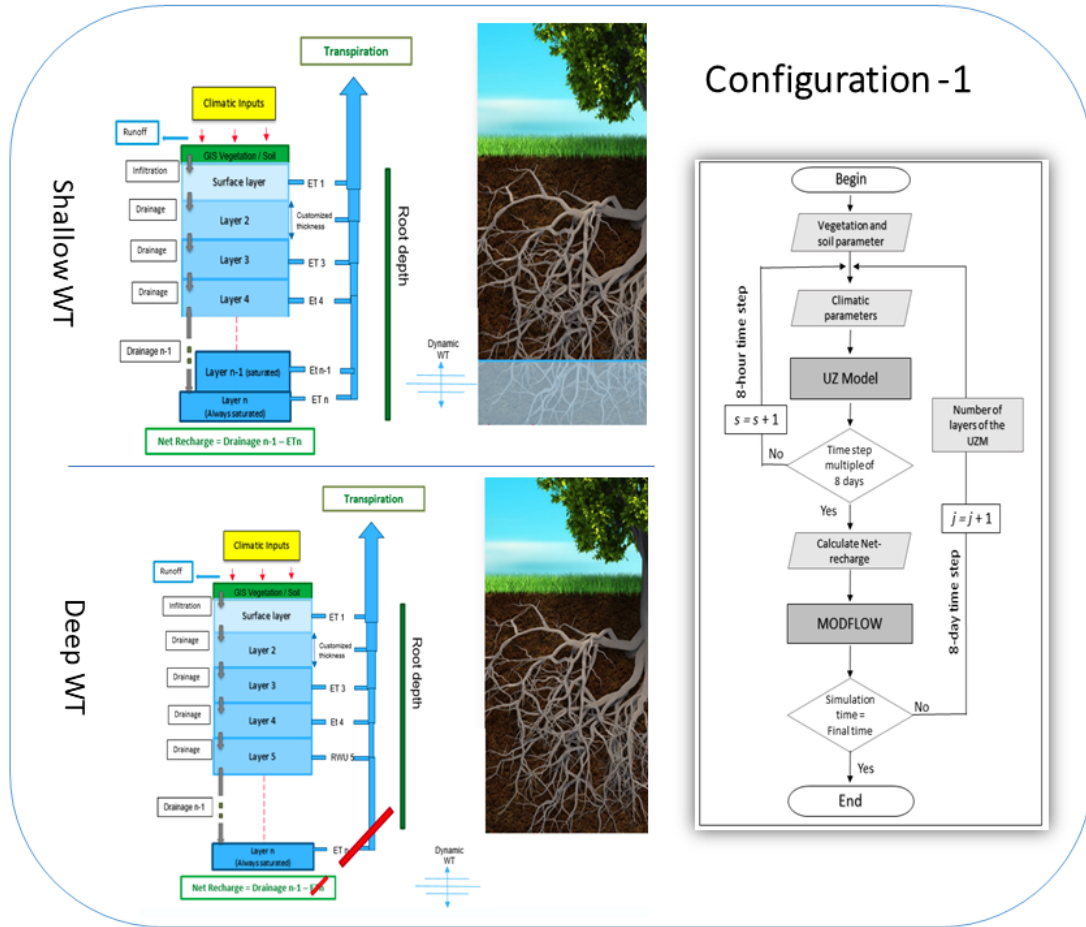


FIGURE 3.8: Configuration-1 coupling between UnSAT and MODFLOW. The two cases on the left represent different WT depths and corresponding number and saturation of modeled layers. On the right hand side, the coupling flowchart is represented. The UZM internal time step represented refers to the simulation of Chapter 4.

It reads

$$Cr = \frac{1}{8} \sum_{i=1}^N r(i), \quad (3.27)$$

where $Cr(t)$ is the recharge rate [L/T], $r(i)$ is the recharge as output of the UZM [L/T], and i goes from 1 to N . N is the number of UZM time steps contained in the simulation period, and eight is to obtain averaged daily recharge values. The simulation period for the coupled model is always eight days to match the MODIS frequency. In Chapter 4, the applied UZM time step is eight hours, while in Chapters 5 and 6 the UZM uses a hourly time step. Hence, the N number of UZM time step to cover the eight days is 24 and 192, respectively. Then, the MODFLOW RCH package internally multiplies the recharge value by the area of the cell.

$$QR_{i,j} = Cr_{i,j} DELR_j DELC_i, \quad (3.28)$$

where $QR_{i,j}$ [$L^3 T^{-1}$] is the recharge flow rate at the horizontal model cell location (i,j) , $Cr_{i,j}$ [$L T^{-1}$] is the cumulated net-recharge related to the area calculated as the product of the row dimension ($DEL R$) [L] multiplied by the column dimension ($DEL C$) [L]. In MODFLOW this value can be applied at a specified depth, according to the definition of recharge given above. We use the option that allows applying the $QR_{i,j}$ to the uppermost variable-head cell in the vertical column.

For the coupling of SWAP and MODFLOW-2005, identified as Configuration-2, the method reported in Xu et al. (2012) is applied. The models were coupled through the net-recharge similarly to Configuration-1. As the recharge rate is provided by SWAP as a daily value, in this case there is no need for a transfer function accounting for the time-step difference.

However, this way of coupling the models requires caution in the S_y parameter definition, which becomes part of the deterministic calibration and is further explained in chapter 5.

The two configurations (See figure 3.9) are fully implemented through Python scripts. However, Configuration-1 is entirely managed inside a Python console, while Configuration-2 needs to exchange the coupling variables by means of ASCII file output. Therefore, Configuration-2 requires a computationally intensive Inputs/Outputs procedure. As an example, SWAP is designed to use climatic forcing input divided into annual files, which increases the complexity when the model is applied to perform continuous simulations spanning over several years. Furthermore, when ensemble simulations are applied, the SWAP forcing input system needs to be carefully designed. For this reason, this study was performed using a script designed to generate, classify, store and recall the appropriate forcing input file.

However, the internal SWAP solver is optimized and efficient, resulting in solving time outperforming UnSAT in certain conditions. The performances of the latter are highly dependent on the root length extension and the depth to WT. In shallow WT (i.e. < 6 m) conditions, UnSAT is up to 40% faster than SWAP, whereas, for deeper WT, SWAP can be up to 25% faster. In summary, Configuration-II is not necessarily requiring greater computational resources, but it necessitates more inputs data preparation and is less flexible for applications to variable conditions. For example, the soil column vertical discretization has to be manually defined for Configuration-2, while is simply characterised by a single parameter in Configuration-1.

3.7 Data Assimilation

The EnKF was used as assimilation algorithm because of the reduced computational load, due to the propagation of a defined number of model application, and the ability with non-linear systems. The filter initially requires to establish a number of ensemble members, generated by perturbing the forcing inputs of precipitation and PET. The ensemble population size was set equal to 32 as in Mitchell, Houtekamer, and Pellerin (2002) and Pauwels et al. (2013).

In most data assimilation studies, the assimilated observations are states of the model. This thesis uses AET observations, which is a non-state variable of the coupled model. Thus, the required interaction between AET and the model states is performed in the UZM, of which AET is a product. AET data from the CMRSET dataset are assimilated into the coupled model.

The two configurations apply a similar scheme of the EnKF. The representation of the assimilation framework for Configuration-1 is shown in Figure 3.10. In the figure, the blue boxes are instances of MODFLOW, the bars are single instances of UnSAT (missing bars between boxes are for better visualization) and the green rectangles are the filter applications. The coupled configuration is represented in the blue shaded semi-ellipse, there are 32 coupled model instances for each assimilation time step. The green ellipse represents the data assimilation calculation. After the filter update, new initial conditions (SM and number of layers) are provided to the UZM. The difference between the two configurations lies in the composition of the state vectors, as the state variables of the UZMs are different. Specifically, for Configuration-1 the state vector for the single ensemble member ($i = 1, \dots, M$) is composed of the SM values from the UZM at time step k and reads

$$\mathbf{z}_{[1]k}^{i,f} = [\theta_1 \ \theta_2 \ \dots \ \theta_n] \quad (3.29)$$

where $\theta_1, \theta_2, \dots, \theta_n$ are the SM contents [$L^3 \cdot L^{-3}$] for each layer of the UZM, for the i -th ensemble member, and the superscript f means forecast.

For Configuration-2 the state vector is similarly composed, it reads

$$\mathbf{z}_{[2]k}^{i,f} = [p_1 \ p_2 \ \dots \ p_n] \quad (3.30)$$

where p_1, p_2, \dots, p_n are the pressure head values [mm] for each layer of the UZM, for the i -th ensemble member.

The aggregated state vector for the ensemble member i at the assimilation time step k is then composed in the same way for both configurations. Here, only the aggregated vector of configuration 1 is shown:

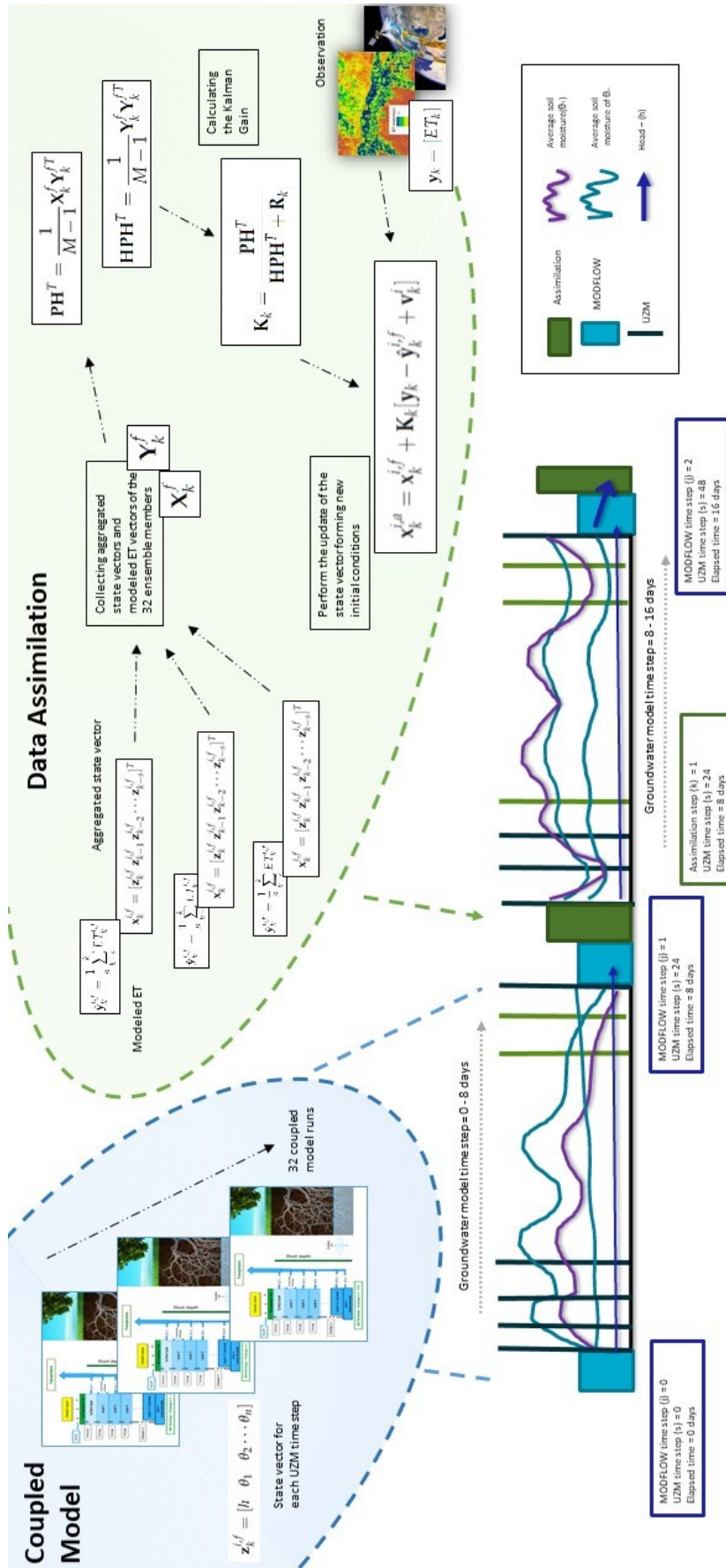


FIGURE 3.10: Schematic of the sequential data assimilation experiment for the first two assimilation time steps.

$$\mathbf{x}_{[1]_k}^{i,f} = [h^{i,f}, \mathbf{z}_{[1]_1}^{i,f}, \mathbf{z}_{[1]_2}^{i,f}, \dots, \mathbf{z}_{[1]_t}^{i,f}]^T, \quad (3.31)$$

where t is the number of times the UZM model is applied during the assimilation time-step and T indicates the transposed vector, and h is the WT level simulated by MODFLOW, which is a constant during the assimilation time step. The difference between the two configurations lies in the number (t) of the UZM time steps.

The average state vector is computed as:

$$\bar{\mathbf{x}}_k^f = \frac{1}{M} \sum_{i=1}^M \mathbf{x}_k^{i,f}. \quad (3.32)$$

The value of $\bar{\mathbf{x}}_k^f$ obtained is then subtracted from the state vector elements. This leads to the state deviation matrix, written as:

$$\mathbf{X}_k^f = [\mathbf{x}_k^{1,f} - \bar{\mathbf{x}}_k^f \quad \mathbf{x}_k^{2,f} - \bar{\mathbf{x}}_k^f \quad \mathbf{x}_k^{3,f} - \bar{\mathbf{x}}_k^f \cdots \mathbf{x}_k^{M,f} - \bar{\mathbf{x}}_k^f] \quad (3.33)$$

The CMRSET observation at time step k is the vector

$$\mathbf{y}_k = [AET_k]. \quad (3.34)$$

Because of the 8-days frequency of the observations, the average of AET over the eight days simulated by the model is

$$\hat{\mathbf{y}}_k^{i,f} = \frac{1}{8} \sum_{s=1}^t AET_s^{i,f}, \quad (3.35)$$

for the t UZM steps and its average over the size of the ensemble (M) is

$$\bar{\mathbf{y}}_k^f = \frac{1}{M} \sum_{i=1}^M \hat{\mathbf{y}}_k^{i,f}. \quad (3.36)$$

The observation-simulation deviation matrix reads

$$\mathbf{Y}_k^f = [\hat{\mathbf{y}}_k^{1,f} - \bar{\mathbf{y}}_k^f \quad \hat{\mathbf{y}}_k^{2,f} - \bar{\mathbf{y}}_k^f \quad \hat{\mathbf{y}}_k^{3,f} - \bar{\mathbf{y}}_k^f \cdots \hat{\mathbf{y}}_k^{M,f} - \bar{\mathbf{y}}_k^f]. \quad (3.37)$$

Then, the calculation of the state observation error covariance matrix, also called background state covariance matrix, is performed as

$$\mathbf{PH}^T = \frac{1}{M-1} \mathbf{X}_k^f \mathbf{Y}_k^{fT} \quad (3.38)$$

whete T indicates the tranposed matrix.

The observation-simulation error covariance matrix reads:

$$\mathbf{HPH}^T = \frac{1}{M-1} \mathbf{Y}_k^f \mathbf{Y}_k^{fT}. \quad (3.39)$$

The Kalman Gain (\mathbf{K}_k) is defined after the calculation of the deviation matrices as:

$$\mathbf{K}_k = \frac{\mathbf{PH}^T}{\mathbf{HPH}^T + \mathbf{R}_k} \quad (3.40)$$

where \mathbf{R}_k is the observation error covariance matrix.

Finally, with equation

$$\mathbf{x}_k^{i,a} = \mathbf{x}_k^{i,f} + \mathbf{K}_k [\mathbf{y}_k - \hat{\mathbf{y}}_k^{i,f} + \mathbf{v}_k^i], \quad (3.41)$$

the correlation between AET and the model states is reproduced through the Kalman gain. This maps the difference between observed and simulated AET to the model states. In equation 3.41, \mathbf{v}_k^i is a random number with mean 0 and standard deviation equal to the observation error.

3.8 Model Performances Evaluation

3.8.1 Assimilation Skills Verification

The evaluation of the assimilation results is performed through different metrics (Equations 3.42 to 3.45), which are the root mean square error (*RMSE*), the Pearson correlation coefficient (*r*), the mean bias (*b*) and the unbiased *RMSE* (*ubRMSE*) (Entekhabi et al., 2010) defined as

$$RMSE = \sqrt{\frac{1}{L} \sum_{k=1}^L (o_k - f_k)^2}, \quad (3.42)$$

$$r = \frac{\sum_{k=1}^L (o_k - \bar{o})(f_k - \bar{f})}{\sqrt{\sum_{k=1}^L (o_k - \bar{o})^2 \cdot \sum_{k=1}^L (f_k - \bar{f})^2}} \quad (3.43)$$

$$b = \left| \frac{1}{L} \sum_{k=1}^L (o_k) - \frac{1}{L} \sum_{k=1}^L (f_k) \right|, \quad (3.44)$$

$$ubRMSE = \sqrt{RMSE^2 - b^2}. \quad (3.45)$$

In Equations 3.42 - 3.45, o_k is observation and f_k is the modeled variable at time k and L is the size of the data set. For $RMSE$ and $ubRMSE$, the improvements were evaluated as a reduction of these errors compared to the respective open loop run.

This leads to the formulation of the $\Delta RMSE$ percentage increment used for the model performance evaluation in Chapter 4, which reads

$$\Delta RMSE = \frac{(RMSE_{OL} - RMSE_A)}{RMSE_{OL}} \cdot 100 \quad (3.46)$$

and similarly for the $ubRMSE$.

3.8.2 Additional Metric - CRPS

Squared error-based metrics (i.e. the $RMSE$) used to analyse model performance are sensitive to large errors that, in general, are relative rare, but can greatly influence the model skill evaluation (Schneider, Henriksen, and Stisen, 2020). The continuous ranked probability score (CRPS) (Hersbach, 2000) measures the difference between the predicted and occurred cumulative distributions, and was specifically designed to assess probabilistic simulations. The CRPS intrinsically weighs the errors by assigning a lower weight to the largest residuals (Schneider, Henriksen, and Stisen, 2020), which allows accounting for observations that in other cases are defined as outliers. For these reasons, the scientific community has recently adopted this metric alongside the more common evaluation criteria. In this thesis, the CRPS is used for the evaluation of the assimilation results in Chapter 6.

The CRPS for the $P(x)$ probability density function given by the ensemble simulation for the variable of interest x calculated at a specific time is

$$CRPS = \int_{-\infty}^{+\infty} (P(x) - P_o(x))^2 dx, \quad (3.47)$$

where P_o is the observation distribution at the same timestep. As the observation is usually a single value, P_o is given by the Heaviside function, which is equal to 0 for no observed value, and 1 when the observation is available.

According to this definition, the CRPS can be seen as the area between the cumulative probability function of the ensemble forecast and the observation function (which is linear in our case). According to Schneider, Henriksen, and Stisen (2020) the CRPS for a cumulative distribution can be defined as:

$$CRPS = \sum_{i=1}^M dx_i \cdot dP_i^2 \quad (3.48)$$

The expected value of zero is only possible in the case of a perfect deterministic forecast (Hersbach, 2000). An appealing characteristic of this metric is that it keeps the dimension of the parameter evaluated. Finally, the CRPS is usually calculated and averaged over a simulation period as follow:

$$\overline{CRPS} = \sum_{t=1}^T CRPS_t \quad (3.49)$$

where T is the number of observations. In this thesis, the \overline{CRPS} is calculated as in Eq. 3.49.

Chapter 4

Feasibility of improving groundwater modeling by assimilating evapotranspiration rates

This chapter is an extract of the article "**Feasibility of improving groundwater modeling by assimilating evapotranspiration rates**"¹ published in *Water Resources Research*.

4.1 Abstract

Water table dynamics are linked to the atmosphere through evapotranspiration and recharge. The assimilation of observed evapotranspiration values should thus improve groundwater model results. This chapter presents a method for assimilating evapotranspiration data into a coupled unsaturated zone and groundwater model using the Ensemble Kalman Filter. The method is tested for a synthetically generated losing stream system in climatic conditions common in South-Australia. The experiment focused on areas with a deep (recharge area) and a shallow (extraction area) water table, and an intermediate area showing seasonal variations between these two (transition area). The data assimilation algorithm consistently improved the model states in the three areas when the ensemble spread was adequate. Improvements were also obtained in the calculation of net-recharge and modeled actual evapotranspiration. The results indicate the potential to improve groundwater models using RS observations of actual evapotranspiration values.

4.2 Introduction

Recharge to the WT is one of the most important variables in groundwater management (Szilagyi et al., 2011), and it is driven by bio-physical processes, such as root water extraction, that take place in the unsaturated zone. By specifically

¹<https://doi.org/10.1029/2019WR025983>

accounting for plant water extraction, through the calculation of fluxes due to transpiration from groundwater, the recharge to WT takes the definition of net-recharge (Hopmans and Stricker, 1989; Doble et al., 2017). Representing fluxes associated with root water uptake correctly is important for the accurate calculation of net-recharge, particularly in environments characterized by shallow WT and groundwater dependent ecosystems (Orellana et al., 2012).

The aim of this chapter is to develop a method for the assimilation of AET data into a coupled unsaturated/groundwater model through the EnKF. In addition, we assessed the benefits of the data assimilation on the model state variables and how the updated states impact the calculation of AET and net-recharge fluxes. The assimilation sequence is devised to specifically account for the feedback between the assimilated non-state variable AET and the modeled SM and WT levels. This has been achieved by developing a simplified UZM, which links SM to AET, allowing for the assimilation of the latter. The UZM was then coupled to MODFLOW for the calculation of net-recharge, with a focus on shallow WT conditions. The coupled model was tested in a semi-synthetic study exploring the effects of the assimilation under different conditions of root-WT interaction and ensemble spreads.

4.3 Experiment Description

The experiment performed in this chapter uses the conceptual coupled model Configuration-1 (i.e. UnSAT + MODFLOW) introduced in Section 3.6. The EnKF was then used to perform the assimilation of synthetically generated AET into the model configuration. This section explains the EnKF requirements, the model domain, the data origin and the synthetic experiment set-up.

4.3.1 Data Assimilation

The EnKF as described in Section 3.7, requires to establish a number of ensemble members generated by perturbing the forcing inputs of precipitation and PET, which are discussed in the next section (4.3.3). The members of the ensemble population, set equal to 32 as in Mitchell, Houtekamer, and Pellerin (2002) and Pauwels et al. (2013), were generated maintaining statistical consistency. To verify the spread and accuracy of the ensemble, a number of statistical variables, originally developed for numerical weather forecast by Talagrand, Vautard, and Strauss (1997), are calculated on the ensemble population. In such a non-linear system, an ensemble that satisfies these statistics for AET may still introduce biases in other model products such as groundwater levels. This requires adequate evaluation metrics (i.e. ubRMSE) for the analysis of results.

To clarify the assimilation process, the sequence is presented here for a single ensemble member. As will be explained in Section 4.3.2, the WT levels provided by a MODFLOW steady state simulation is the initial condition of the coupled model, which is the same for all 32 members.

As each ensemble has different forcing inputs, the net-recharge values calculated by the UZM and passed to the groundwater model are different. Therefore, after the first groundwater model time step ($j = 1$), the new WT level head distributions are also different for each ensemble member. For this study, the assimilation time step (k), when the EnKF is applied, is equal to the groundwater model time step j (elapsed time = 8 days). The updated value of the WT levels and SM contents of the layers provide the new boundary condition for the UZM. At $j = 2$ (elapsed time = 16 days), a new groundwater model application is performed followed by another assimilation. This procedure is sequentially performed, every 8 days, for the simulation span of 8 years, resulting in 365 (L) applications of the EnKF.

To maintain a physical realistic system, which the EnKF does not necessarily represent, the updated state values may have to be constrained (Levy et al., 2010). For SM, this is automatically performed by the UZM which bounds the SM content between a residual value and complete saturation. The increase in the updated value is limited to $\pm 25\%$ for stability. This limitation avoids the SM content of the layers in proximity to the WT to be updated with high values that immediately becomes net-recharge at the first UZM time step after the assimilation. For the same stability reason, WT levels updates were also limited to within the thickness of 1 layer of the unsaturated zone (i.e. 200 mm). This prevents the updated WT levels to deviate significantly from the values being used to calculate recharge and the recharge delay associated with an increased thickness of the unsaturated zone. For these reasons, constraining the WT level updates to one layer preserves the physical meaning of the UZM net-recharge. These limitations are important mostly in the first time steps of the assimilation runs, because of the effect of the initial conditions of uniform SM profiles. After these initial time steps, the update limitations no longer needed to be applied.

4.3.2 Synthetic Experiment Domain

This study uses meteorological inputs of rainfall and PET obtained from the Coonawarra station located in the South-east of South Australia. The general description of the region and the location of the climatic station can be found in Sections 3.1 and 3.2. The forcing input provided cover the period between January the 1st 2000 and December the 31st 2007.

In semi-arid regions streams often lose water to the alluvial floodplain (local recharge) in addition to diffuse recharge across the catchment (Lamontagne and

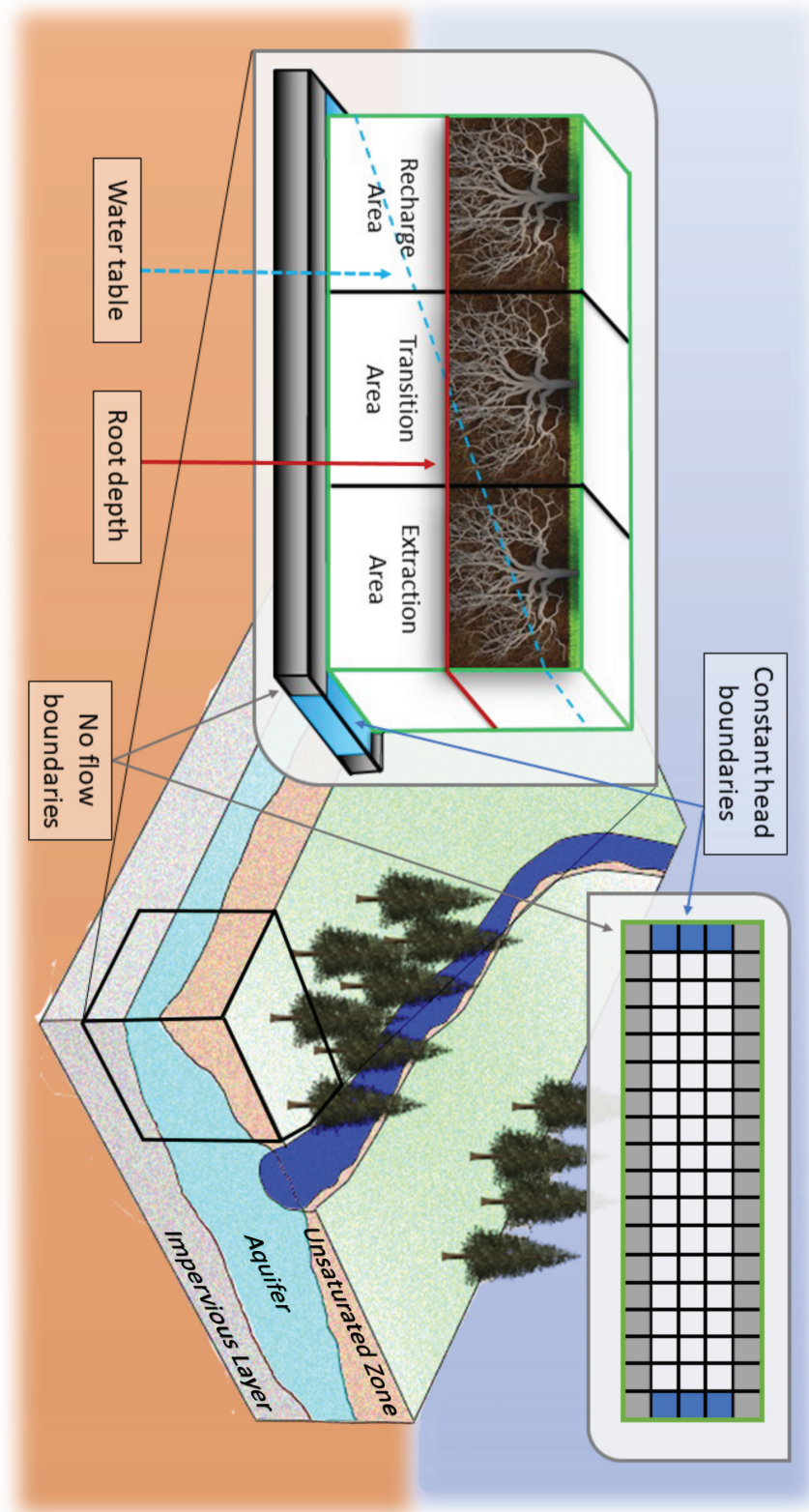


FIGURE 4.1: Representation of the losing stream-groundwater system interaction in a densely vegetated area. The unconfined aquifer overlies an impervious layer, the WT is declining moving away from the river interface. The model domain and boundary conditions are shown in the two insets. The right inset shows the top view of the domain formed by 18×5 cells. The blue cells indicate the constant head boundary, while grey cells indicate the no-flow boundary (inactive cell). In the left inset, the red line is the root depth, the light blue dotted-line is the initial water table distribution. These two lines divide the domain into three areas (Recharge, Transition and Extraction).

Herczeg, 2005). In these floodplains, pockets of dense forest vegetation can be planted and managed to take advantage of the shallow groundwater (Benyon, Theiveyanathan, and Doody, 2006). These conditions are ideal to explore the different interactions between vegetation and the water table. A simplified, synthetic model domain was developed (Figure 4.1) to incorporate a losing stream (right boundary condition) with a water table declining in depth away from the stream to the left of the figure.

The saturated groundwater model is comprised of 5 x 18 cells, each with a resolution of 1 km x 1 km (right inset of Figure 4.1). The top and bottom rows are no-flow boundary conditions (inactive cells) and the groundwater flow is perpendicular to the river, from right to left. The first and last columns are constant head boundary conditions, at a depth of 5 m (left) and 1 m (right) below the surface to represent the losing river system. The hydraulic conductivity is set to 1 m/d, and the specific yield is 0.4. The left inset of Figure 4.1 shows the domain set-up, in which the blue line represents the WT in steady state conditions. The red line marks the depth to which the vegetation root system is able to extract water. Three different areas are identified by the above configuration in steady state conditions. On the left side (Recharge Area), the WT is deeper than the root system, which is not able to extract water from groundwater. On the right side (Extraction Area), the WT is within the rooting zone, and plants extract groundwater. This area has the highest interaction between the vegetation and the WT. The central area is labelled as Transition Area. Here, the WT is frequently moving into and out of the root zone. The 1-D UZM is coupled to the groundwater domain independently for each cell. The model can process spatially distributed parameters of soil and vegetation parameters. Three cells in the central row are used as reference point for the analysis of the results of the effect of the assimilation, one for each of the three areas identified above.

4.3.3 Forcing Inputs Perturbation and Observations

Following Pauwels et al. (2013), an ensemble of 32 members was created by adding temporally varying, spatially homogeneous random numbers, sampled from a Gaussian distribution ($G_{(t,M)} \sim N(0, A \cdot SD)$), to the model forcing (rainfall and PET). A is a fraction, referred to as the input perturbation fraction for the remainder of the paper. SD is the standard deviation of the dataset, calculated throughout the entire simulation period, and M is the ensemble member. Only rainfall values greater than 0 are perturbed, negative perturbed values are set to 0. Similarly, PET inputs are generated using the same A values. For PET, all the dataset values are perturbed and, in case of negative values, these are replaced by their absolute value.

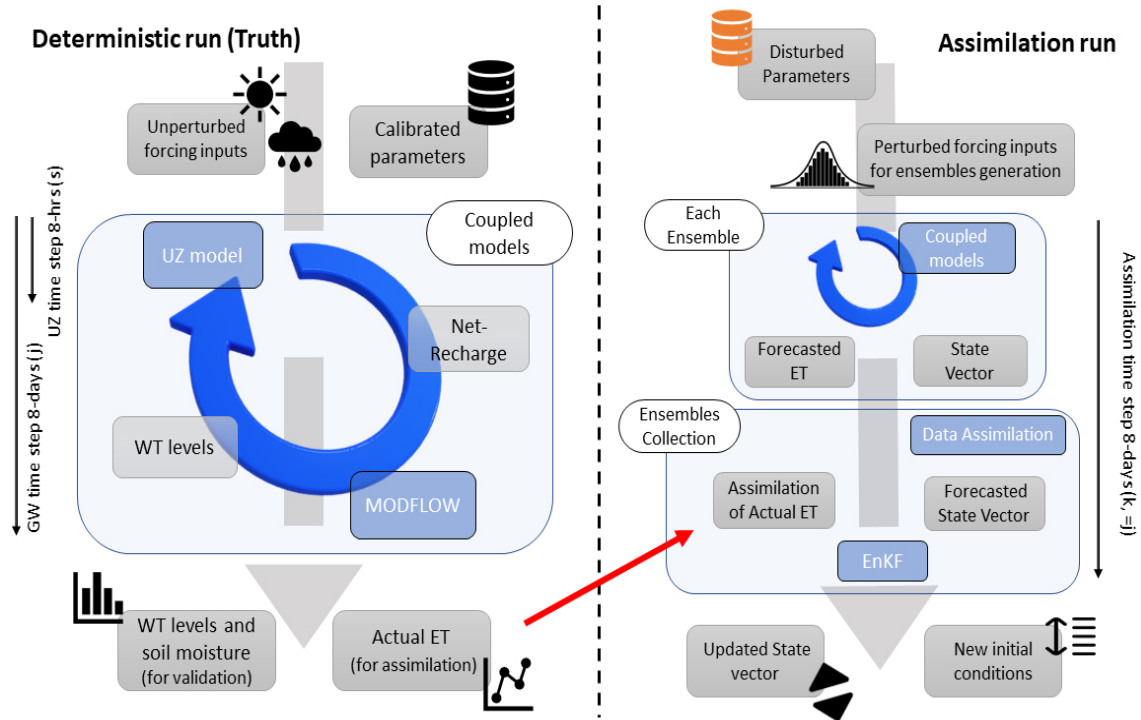


FIGURE 4.2: Schematic of the synthetic experiment set-up. The left panel illustrates the deterministic run of the coupled model. On the right, the flow path of a single ensemble member is represented. This run uses the synthetic actual ET from the deterministic run as observation to be assimilated.

The data assimilation works by updating the coupled unsaturated-groundwater model with AET observations. As the CMRSET observations are available at an 8-day interval, the synthetic AET data created for this experiment are provided as a daily value, which is the average for the modeled 8-day AET. These data are obtained from a deterministic run that is explained in section 4.3.4.

4.3.4 Experiment Description

A single deterministic simulation (Truth) was created using unperturbed forcing inputs of rainfall and PET and the parameter set listed in Table 4.1. The parameters of the deterministic run are saturated hydraulic conductivity (K_s), porosity, critical SM value for plant transpiration, SM residual value of the soil, root depth, root distribution, drainage empirical value, and parameter defining K_s decay with soil depth (Table 4.1). The experiment used modeled AET values from the deterministic run to generate observations for the assimilation procedure, and the SM content and WT levels for the validation of the assimilation results (Figure 4.2).

In particular, the AET values from three cells of the central row of the synthetic truth simulation were used to create the synthetic observations Rec-ET, Trans-ET, Ext-ET, referring to ET values for the Recharge, Transition, and Extraction areas,

TABLE 4.1: Parameters used for the simulations. Columns two to four report the parameters used for the Truth, the Disturbed Dataset 1 and the Disturbed Dataset 2

Model Parameter	Truth	Disturbed Dataset 1 (DD1)	Disturbed Dataset 2 (DD2)	Units
Hydraulic conductivity - K_s	4.3	4.9	4.75	$\text{mm} \cdot \text{hr}^{-1}$
Critical SM value for transp.	0.14	0.13	0.12	$\text{mm}^3 \cdot \text{mm}^{-3}$
Soil porosity	0.40	0.38	0.36	$\text{mm}^3 \cdot \text{mm}^{-3}$
Residual SM value for the soil	0.075	0.070	0.080	$\text{mm}^3 \cdot \text{mm}^{-3}$
Drainage empirical value	0.8	0.9	1.1	-
Root depth	2900	3200	2700	mm
Root distribution parameter	2.0	2.2	1.9	-

respectively. Because of the interaction between groundwater and vegetation, Ext-ET values are usually higher than Trans-ET, which are in turn higher than Rec-ET.

Accounting for parameter uncertainties, the set of calibrated parameters was disturbed twice by adding random numbers sampled from normal distributions with SD of 10% for each parameter, generating two slightly different disturbed datasets named DD1 and DD2, respectively (Table 4.1). The two ensembles of assimilation runs are both propagated with the perturbed forcing inputs and updated every time an observation is available. This permits the evaluation of the assimilation improvements independently from the parameters selected. The open-loop runs are generated by only propagating the ensembles from the initial states and are used as reference to measure the performance of the assimilation through the metrics reported in Section 3.8.1.

4.3.5 Ensemble Performance Verification

Following De Lannoy et al. (2006), the first and second moments of the probability distribution functions obtained by the ensemble run were calculated for the assimilated value of AET, these are the mean:

$$\bar{y}_k = \frac{1}{M} \sum_{i=1}^M (\hat{y}_k^i), \quad (4.1)$$

and the ensemble spread (*ensp*)

$$ensp_k = \frac{1}{M} \sum_{i=1}^M (\hat{y}_k^i - \bar{y}_k)^2. \quad (4.2)$$

M, i, k, y, \hat{y} are ensemble population size, ensemble member, assimilation time step, AET observation and AET modeled respectively. These equations can be used to verify the statistical accuracy of the generated ensembles (Talagrand, Vautard, and Strauss, 1997). More specifically, the average over the simulation period (indicated with $\langle \cdot \rangle$) of

$$\left\langle \frac{\overline{ensk}}{\overline{ensp}} \right\rangle \quad (4.3)$$

is an indicator of the ensemble spread, and should reach 1 to be considered adequate as shown in the study of De Lannoy et al. (2006). If this value is above one the ensemble spread is considered insufficient, while values below one indicate an excessive spread. In Equation 4.3 the ensemble skill (*ensk*) is defined as

$$ensk_k = (\bar{y}_k - y_k)^2. \quad (4.4)$$

For the truth to be statistically indistinguishable from a member of the ensemble (De Lannoy et al., 2006), the average of the ratio

$$\left\langle \frac{\sqrt{\overline{ensk}}}{\sqrt{\overline{mse}}} \right\rangle \quad (4.5)$$

should be equal to $\sqrt{(M+1)/2M}$, with mean squared error (*mse*) calculated as

$$mse_k = \frac{1}{M} \sum_{k=1}^M (\hat{y}_k^i - y_k)^2. \quad (4.6)$$

Thirty assimilation runs (15 for each dataset), formed as a combination between the input perturbation fractions *A* (0.05, 0.15, 0.25, 0.50, 1) and the observation errors *OE* (0.1, 0.2, 0.3 [mm/day]), were performed. These were grouped based on the cited ensemble verification methods and listed and discussed in section 4.4.

4.4 Results and Discussion

4.4.1 Ensembles Verification

Equations 4.3 and 4.5 were applied to verify the ensemble appropriateness; this classified the simulations in three groups named Adequate, Excessive and Insufficient (Pauwels and De Lannoy, 2009). For the analysis of results, one simulation per disturbed dataset of each group was chosen (2 × 3). These 6 simulations are listed in Table 4.2, which reports the forcing input perturbation fraction (*A*), the observation error (*OE*), the values of equations 4.3 and 4.5, and the appropriateness of the generated ensemble. Because observations are heterogeneous for the different areas of the domain, the ensemble skills are also slightly different. In Table 4.2, the values reported are averaged over the model domain. The results presented in the "State" and "Fluxes" parts of section 4.4.2 refer to the simulations classified as Adequate spread. These are DD1-I and DD2-I, which have the best ensemble performance skills (i.e. $\langle \overline{ensk}/\overline{ensp} \rangle$ about 1 and $\langle \sqrt{\overline{ensk}}/\sqrt{\overline{mse}} \rangle$ close to 0.71).

TABLE 4.2: Simulations classification and ensembles verification. The table is divided in two parts according to the parametric dataset used, reported in column 1. A is the input perturbation fraction which was used to generate the ensemble. OE is the observation error. Column 4 and 5 are the ensemble skills calculated on AET values averaged over the three areas, column 6 is the spread classification as described in Section 4.4.1.

Dataset	A	OE	$\frac{\langle \overline{ensk} \rangle}{\langle \overline{ensp} \rangle}$	$\frac{\langle \sqrt{\overline{ensk}} \rangle}{\langle \sqrt{\overline{mse}} \rangle}$	Appropriateness
DD1 - I	1	0.3	0.93	0.58	Adequate Spread
DD1 - II	0.15	0.3	0.50	0.30	Excessive Spread
DD1 - III	0.05	0.1	3.72	0.53	Insufficient Spread
DD2 - I	1	0.2	1.03	0.56	Adequate Spread
DD2 - II	0.50	0.2	0.70	0.43	Excessive Spread
DD2 - III	0.15	0.3	4.35	0.53	Insufficient Spread

4.4.2 Assimilation Performance

An example of the effects of the assimilation on SM content is presented in Figure 4.3, which shows rainfall, SM content of the shallow layers, and the simulated and assimilated values of AET for ensemble 21 in a simulation $A = 0.25$ and $OE = 0.1$ of dataset DD1. This simulation, which is not part of the 3 groups defined in section 4.4.1, serves as a representative example as these effects are seen for all the assimilation runs. When the observed AET is lower than the model results (i.e. box 1 in Figure 4.3), the data assimilation reduces the SM content of the layers. On the other hand, a higher observed AET (i.e. box 2 in Figure 4.3) produces an increment of SM in the most superficial layers. This increment is due to the filter update as no rainfall event occurs at this time. The data assimilation modifies the SM content of each layer independently allowing for depth specific updates. This is observable in box 3 of figure 4.3, where the SM content of all the layers is increased due to the higher value of the assimilated observation. However, layers 4 and 5 received the highest update and layer 7 and 1 were almost unchanged.

States

Table 4.3 presents an overview of the assimilation results on the state variables. It shows values for simulations with adequate spread divided into the three areas of the domain. An analysis of this table shows a similar improvement of assimilated WT levels $\Delta_{ub}RMSE$ (from +36% to +52%) for the two disturbed parameter datasets over the entire domain. The highest correlation and the lowest $ubRMSE$ value are seen in the Extraction area for both datasets, with DD1 showing the best values. The Recharge area has magnitudes of improvement similar to other part of the domain; however, it presents the highest $ubRMSE$ together with the lowest correlation. Hence, due to the greater interaction between roots and the WT, the assimilation shows the best result in the Extraction area. For SM values,

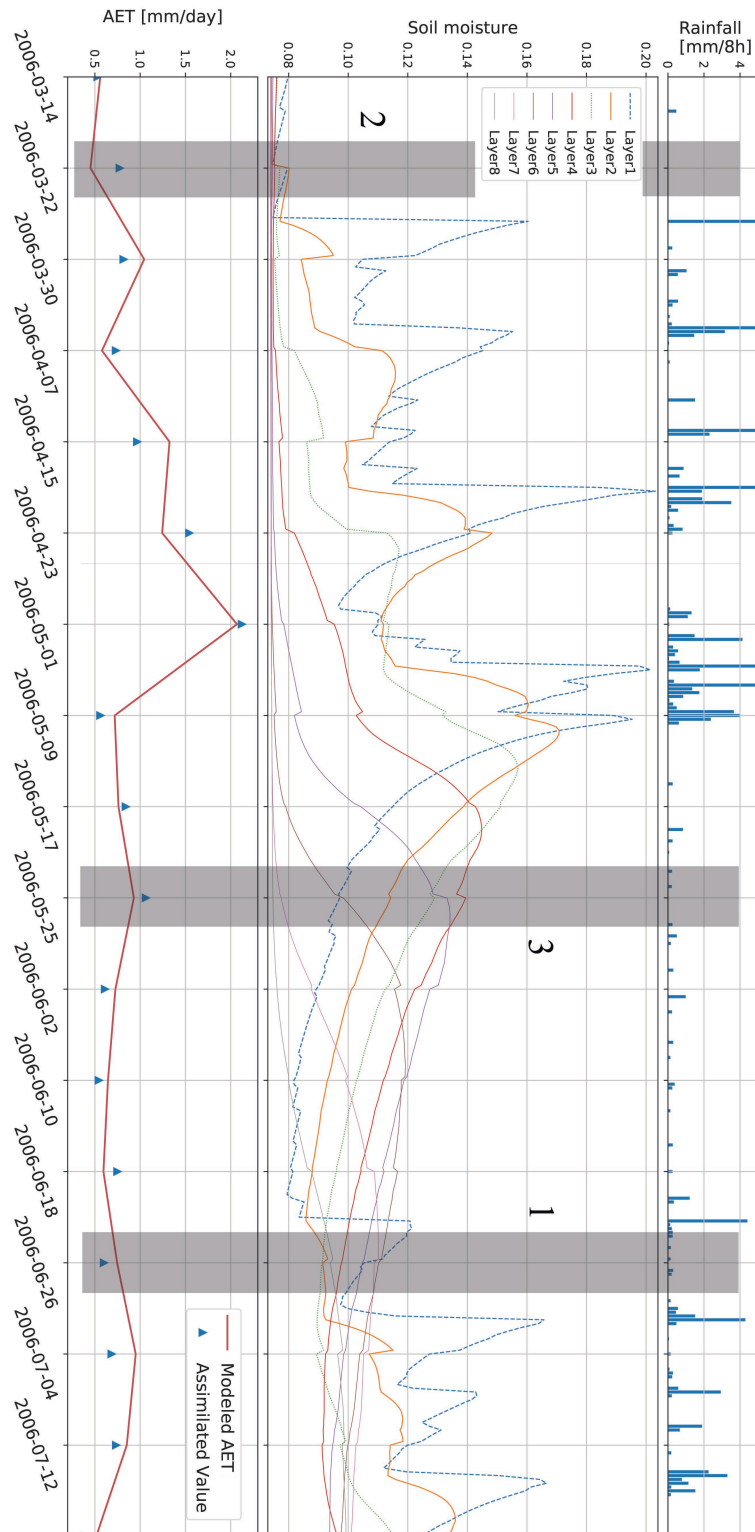


FIGURE 4.3: Results of simulation DD1 with $A = 0.25$ and $OE = 0.1$ for the extraction area. Top panel: rainfall input data. Middle panel: modeled SM values for ensemble member 21 (layer numbers increase with depth). Bottom panel: modeled AET and the assimilated observation for the same ensemble member. The grey boxes numbered 1, 2, and 3 are further explained in Section 4.4.2.

$\Delta ubRMSE$ improvements are again positive over the domain although the magnitude is diverse for the two datasets. DD1 has the highest improvements (+32%) for the Recharge area and the lowest (+8.2%) for the Extraction area, but $ubRMSE$ is the same for the three areas. DD2 gets the highest and lowest $ubRMSE$, respectively, in the Recharge area (0.033) and the Extraction Area (0.015). This behaviour may be related to the root depth and root distribution parameters. The shorter DD2 root depth (see Table 4.1) distributes the improvements of the AET assimilation differently between the two datasets. DD2 presents better improvements in the Extraction area compared to DD1. However, because of the smaller root depth, the assimilation has less impact on the Recharge area, which is deeper. The correlation coefficient sees improvements in every area, the best value being for DD1 in the Extraction area (0.95).

In Figures 4.4 and 4.5, the WT levels in the Extraction and Recharge areas are reported for the entire span of the simulation. For each figure, [a] and [b] show results for the datasets with adequate spread (DD1-I and DD2-I). Panel [c] shows results with insufficient spread, (DD2-II in Figure 4.4 and DD1-II in Figure 4.5). The effects of a different parameterization are clear for DD2 (Figure 4.4c and 4.5b). DD2 has a shorter root length that results in shallower WT levels when extraction from groundwater is dominant. This was expected for the Extraction and Transition area, where the groundwater-vegetation interaction is high. However, it was not expected for the Recharge area where, at least initially, the WT was below the root depth. This is because the perturbed forcing inputs changed this area from recharge to extraction/transition for part of the simulated period. The filter greatly limits this effect (Figure 4.5b) but is not able to correct the WT levels as seen in Figure 4.5a because the truth is not covered by the ensemble spread. This explains also the high $ubRMSE$ of Table 4.3.

The choice of parameters has an influence on the SM profiles. In Figure 4.6, the first two panels ([a], [b]) represent the SM of the sufficient ensemble spread for DD1-I and DD2-I, respectively. The main difference is the residual SM value (i.e. the lower boundary), which, in the case of [b], prevents the assimilation to provide results closer to the truth in dry periods. The third panel shows how an insufficient spread of the ensemble is not able to cover the truth for part of the simulation period [c]. In the case of SM, the effects of data assimilation are less area specific, resulting in a homogeneous behaviour over the entire domain.

Fluxes

Although the family of the Kalman filters is designed to update only modeled states without a specific effect on fluxes, the impact of the assimilation on the modeled AET and net-recharge is presented. In Table 4.4 the filter improved the $RMSE$

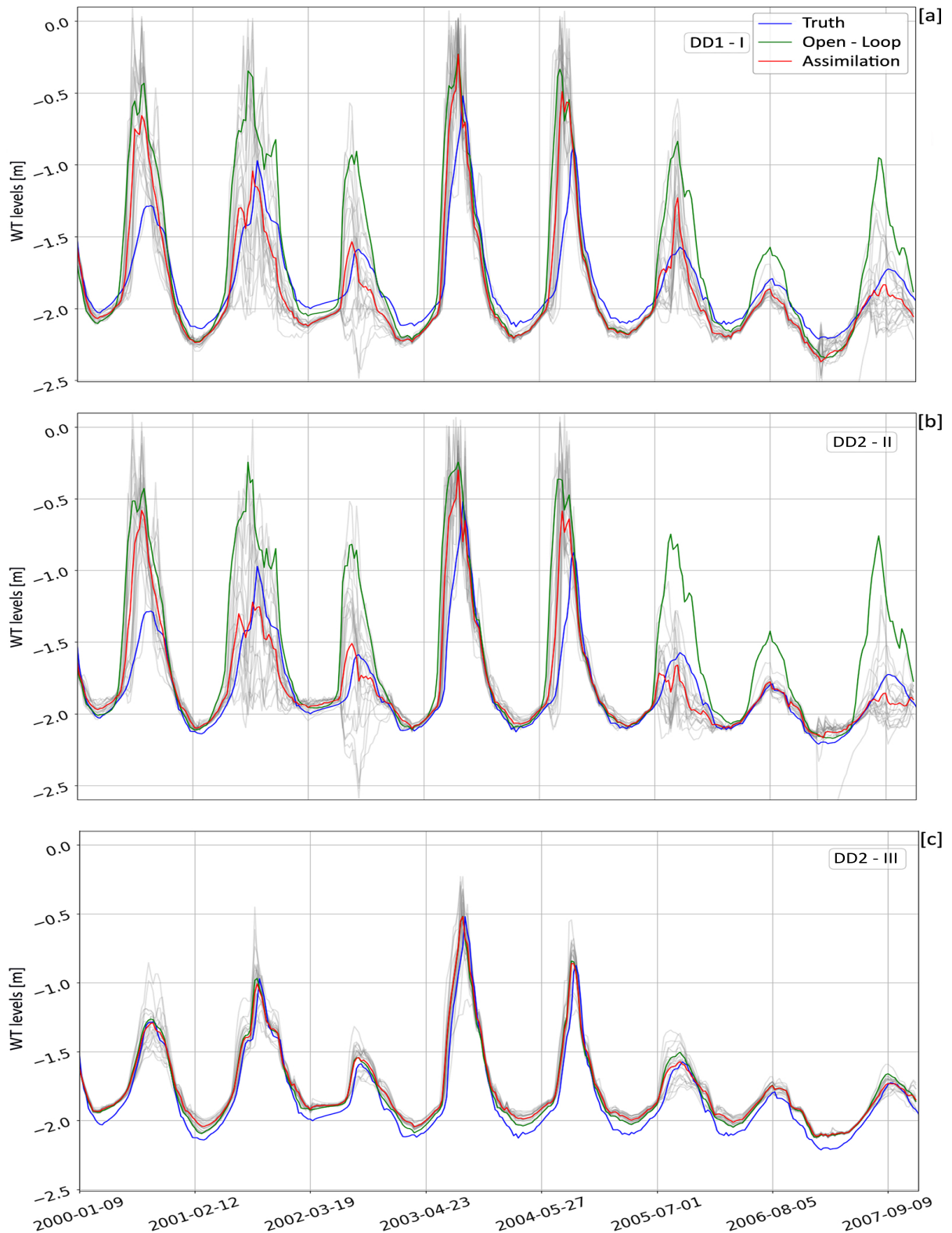


FIGURE 4.4: WT levels for the entire simulation period in the Extraction Area. The blue line is the deterministic truth, the green line is the Open-loop mean and the red is the mean of the assimilations runs. The individual ensemble runs are shown as gray lines. Panels [a] and [b] show results for the datasets with sufficient spread, i.e. DD1-I and DD2-I. Panel [c] shows results of DD2-III with insufficient spread.

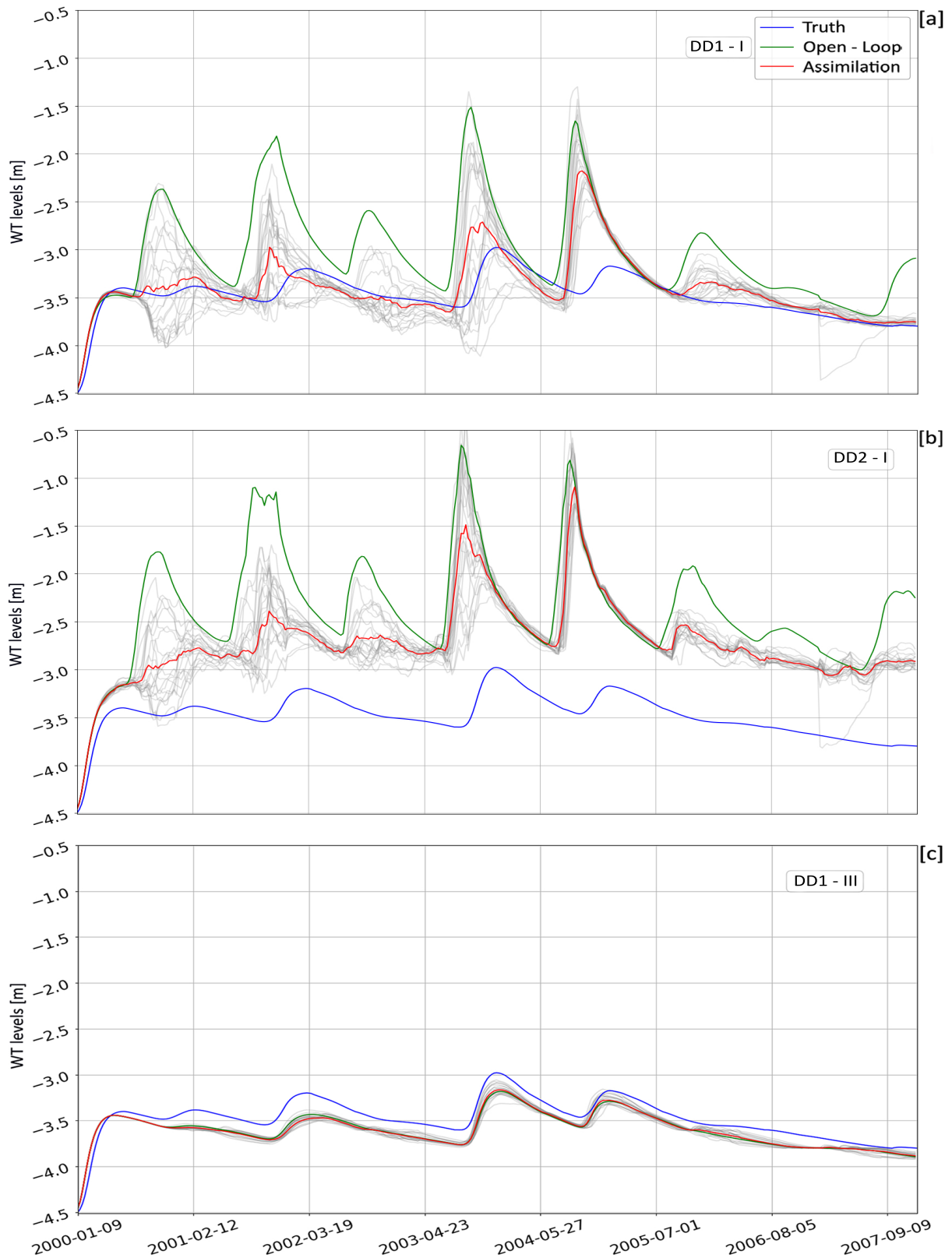


FIGURE 4.5: WT levels for the entire simulation period in the Recharge Area. Colors of lines as in figure 4.4. Panels [a] and [b] show results for the datasets with sufficient spread, i.e. DD1-I and DD2-I. Panel [c] shows results of DD1-III with insufficient spread.

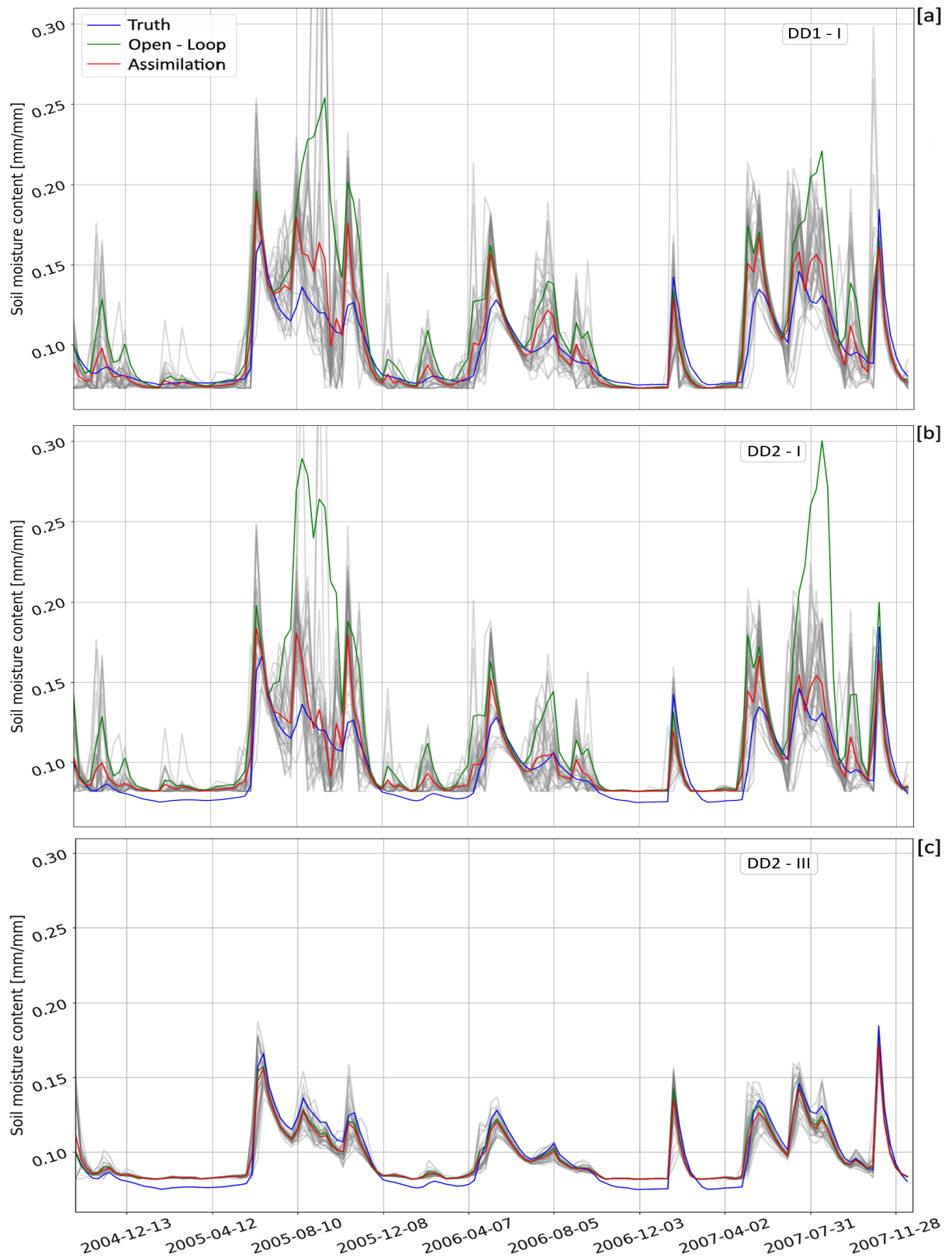


FIGURE 4.6: SM content at depth 900 [mm] for simulation period 2004-10-28 to 2007-12-11. Colors of lines as in figure 4.4. Panels [a] and [b] show results for the datasets with sufficient spread, i.e. DD1-I and DD2-I. Panel [c] shows SM profiles for the simulations of DD2-II with insufficient spread.

TABLE 4.3: State variables (i.e. WT levels and SM) results for the Adequate spread simulations (DD1-I and DD2-I). Column 1 and 2 report the area of the domain and the dataset considered. Columns 3 through 5 report the $ubRMSE$ and r of the WT levels between the assimilation run and the deterministic truth. The $\Delta ubRMSE$ % is the percentage of improvements (if positive) or worsening (if negative) of the $ubRMSE$ of assimilation and OL. R is the correlation, the sign in parenthesis is positive in case of the assimilation improving the correlation, negative otherwise. Columns 6 to 8 refer to SM.

Area	Dataset	WT levels			Soil Moisture		
		$ubRMSE$ [m]	$\Delta ubRMSE$ %	r	$ubRMSE$ [$\frac{mm}{mm}$]	$\Delta ubRMSE$ %	r
Recharge	DD1	0.228	+49.0%	0.70 (+)	0.021	+32.0%	0.80 (+)
	DD2	0.340	+36.0%	0.60 (+)	0.033	+16.0%	0.74 (+)
Transition	DD1	0.210	+45.8%	0.83 (+)	0.021	+16.0%	0.91 (+)
	DD2	0.207	+52.0%	0.80 (+)	0.021	+27.0%	0.90 (+)
Extraction	DD1	0.171	+43.0%	0.93 (+)	0.021	+8.2 %	0.95 (+)
	DD2	0.156	+49.0%	0.91 (+)	0.015	+25.0%	0.93 (+)

TABLE 4.4: Fluxes results for the Adequate spread simulations (DD1-I and DD2-I). Column 1 and 2 report the area of the domain and the dataset considered. Columns 3 through 5 report RMSE and r of the AET between the assimilation run and the deterministic truth. The $\Delta RMSE$ % is the percentage of improvements (if positive) or worsening (if negative) of the RMSE of assimilation and OL. R is the correlation, the sign in parenthesis is positive in case of the assimilation improving the correlation, negative otherwise. Columns 6 to 8 refer to net-recharge.

Area	Dataset	AET			Net-Recharge		
		$RMSE$ [$\frac{mm}{day}$]	$\Delta RMSE$ %	r	$RMSE$ [$\frac{mm}{day}$]	$\Delta RMSE$ %	r
Recharge	DD1	0.43	+42.1%	0.978 (+)	0.247	+46.0%	0.280 (+)
	DD2	0.44	+35.0%	0.956 (+)	0.370	+39.0%	0.050 (+)
Transition	DD1	0.41	+44.0%	0.977 (+)	0.365	+35.0%	0.590 (+)
	DD2	0.42	+36.0%	0.955 (+)	0.386	+40.0%	0.455 (+)
Extraction	DD1	0.40	+41.0%	0.977 (+)	0.398	+32.0%	0.678 (+)
	DD2	0.38	+36.0%	0.955 (+)	0.395	+32.0%	0.620 (+)

of the fluxes to magnitude similar to the states. This is one of the key findings of the study.

ET fluxes had high percentages of $\Delta RMSE$ improvement and good correlation values for both datasets over the entire domain. This is consistent with the nature of the assimilated observed quantity. The $RMSE$ is around a value of 0.4 [mm/day], which is the same order of magnitude of the error perturbing the observations.

The magnitude of net-recharge improvements is similar to AET (i.e. +30% - +45%), with the greatest improvements experienced in the Recharge area. This can be explained by the combination of WT levels and SM improvements for this area. The enhancement of net-recharge is consistent with a number of studies (Doble et al., 2017; Crosbie et al., 2015) that have shown how net-recharge is dependent

on the groundwater level; therefore, improving the WT levels could produce an indirect improvement of the net-recharge flux. The correlation coefficient of net-recharge is improved for all the simulations, but presents low values particularly for the Recharge area. This is an effect of the continuous filter updating of both SM and WT levels. By updating the latter in particular, the net-recharge flux at the WT interface is delayed or anticipated in time, resulting in poor correlation with the deterministic truth.

Group Comparison

Figures 4.7 and 4.8 show a comparison for the Extraction area of the WT levels and SM *ubRMSE*, respectively. The simulations are grouped according to the ensemble performance of Table 4.2. The simulations with Adequate spread are consistently showing improvements for both WT levels and SM across the 2 datasets.

For WT levels (Figure 4.7), the OL *ubRMSE* of the Adequate group is up to one order of magnitude higher than the other two groups. This is a combined effect on WT levels of the parametrisation and forcing inputs perturbation fraction A . The model response to large A (i.e 1 of SD) produced a rise in WT levels due to an increase in high rainfall events that can supply water to the system until it is completely saturated. This is not counterbalanced by high PET because the water extraction is limited by both the maximum root depth and the availability of water in the system at that particular time. In this situation, the high *ubRMSE* of the OL is improved by the filter, but it is not the optimal value found across all the simulation groups. These results indicate that WT levels generated by applying the adequate-spread ensemble are not necessarily the optimal choice. It might be necessary to apply different ensemble verification statistics particularly if the focus of the modeler is on WT levels. However, this would only be possible if WT observations were available.

For SM (Figure 4.8), the OL *ubRMSE* is similar for all the three groups and the assimilation *ubRMSE* presents the largest improvements for the Adequate spread group. This indicates that the assimilation improvements are less dependent on the ensemble perturbation fraction, and the adequately generated ensemble performs well.

4.5 Conclusion

A simplified UZM was coupled to MODFLOW-2005 to investigate the potential to improve the groundwater model results through the assimilation of AET values. The framework that was implemented explicitly models the feedback between AET

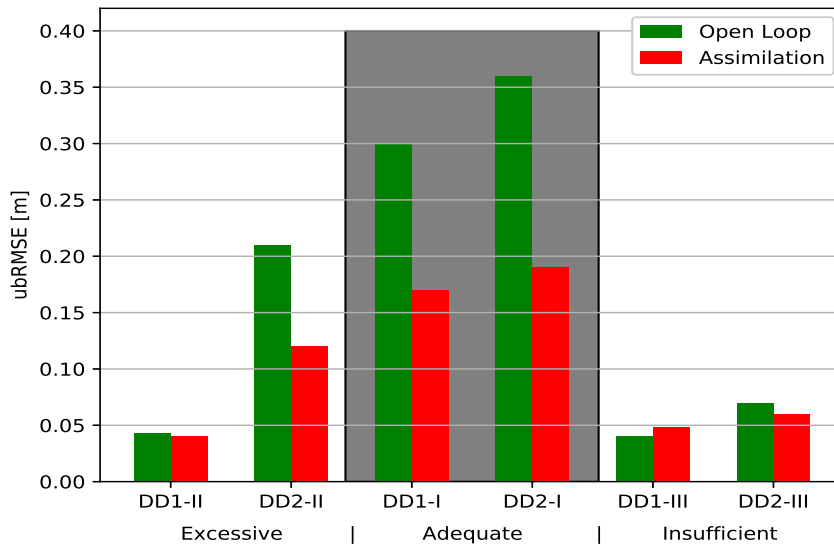


FIGURE 4.7: Comparison of the WT levels ubRMSE for the Extraction area across all the simulation groups. The red bar is the assimilation ubRMSE and the green bar is the associated open loop ubRMSE. The colored area highlights the adequately generated ensemble.

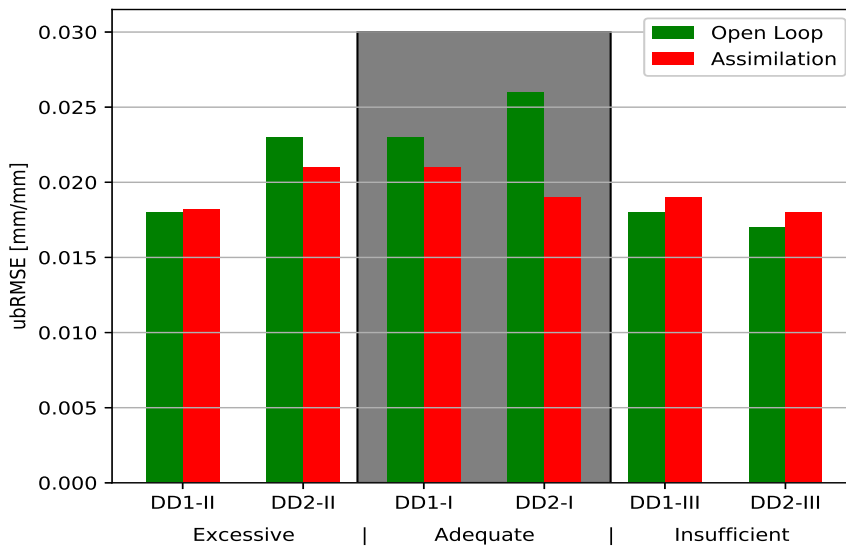


FIGURE 4.8: Comparison of the SM ubRMSE for the Extraction area across all the simulation groups. The red bar is the assimilation ubRMSE and the green bar is the associated open loop ubRMSE. The colored area highlights the adequately generated ensemble.

and both state variables (i.e. SM and WT levels).

The assimilation of a synthetically generated AET dataset into the coupled unsaturated-groundwater model was presented and tested on a scenario representing a losing river in the South-East of South Australia. A domain with 5 x 18 cells was generated, with gradually deepening WT levels from one boundary to the other. Three cells were used for the evaluation, representing a recharge area (with a consistently deep WT), an extraction area (with a consistently shallow WT), and a transition area (with seasonally varying WT).

In all areas the assimilation consistently improved the modeled WT levels and SM when the ensemble was adequately generated according to the ensemble verification metrics calculated over AET. Reduced errors were also seen in the case of fluxes regardless of the groundwater level. Specifically, AET fluxes were improved for all the datasets over the entire simulation domain because of the nature of the observation assimilated (i.e. AET estimates). Net-recharge fluxes have seen an improvement both in RMSE and correlation. However, the correlation value in the recharge area remained low due to the filter continuously updating SM and WT levels, thus anticipating or delaying the time when net-recharge was delivered to (or extracted from) groundwater.

These results are consistent with the EnKF objective of improving the modeled state variables without directly affecting the fluxes. By means of the feedback between AET and SM, and the relationship between net-recharge and the state variables, fluxes are indirectly improved.

In the case of WT levels, the assimilation run *ubRMSEs* for the appropriately generated group were higher than the correspondent values seen in other groups. This was primarily due to the high magnitude of the perturbation used to create the forcing inputs. A highly perturbed rainfall dataset, homogeneous over the relatively small domain, produced an increment in positive net-recharge that was not counterbalanced by high PET values because of the limits imposed by parameters (i.e. root depth) and water availability at the time (i.e. a deep WT with high PET). Therefore, the ensemble verification metric calculated on AET resulted to be adequate in the case of SM. However, it led to an excessively perturbed ensemble in the case of WT levels. This might indicate that a different ensemble verification metric has to be applied if the objective of the modeller is mainly focused on WT levels.

By assimilating AET fluxes, synthetically generated from a deterministic run of the coupled model, the study did not thoroughly explore the biases likely to be seen in a real case scenario. This was partially accounted for by the two disturbed

model parameter datasets, but cannot account for other sources of bias (e.g. WT level and SM observation error or forcing input bias). A real-world case study would require a careful calibration of the model on AET and WT in order to reproduce the link that in this study was inherently embedded in the synthetically generated observations.

Nevertheless, the findings of this study indicate that groundwater models can be improved by the assimilation of remotely sensed AET values, and the use of a relatively simple UZM could be sufficient for this purpose. Future testing of this framework on a more complex UZM will help define the level of details required for assimilating remotely sensed AET.

Chapter 5

Unsaturated zone models complexity for the assimilation of evapotranspiration rates in groundwater modeling

This chapter is extracted from the article "**Unsaturated zone model complexity for the assimilation of evapotranspiration rates in groundwater modeling**"¹ preprint *Hydrology and Earth System Sciences* .

5.1 Abstract

The bio-physical processes occurring in the unsaturated zone have a direct impact on the water table dynamics. Conceptual models, with a simplified representation of the unsaturated zone dynamics, are often selected for coupling to groundwater models, while physically-based models are widely used, particularly at the field scale, for an accurate representation of the water and solute transport. The recharge rates estimated by these UZMs can then be used as input for groundwater models. Because recharge estimates are always affected by uncertainty, model-data fusion methods, such as data assimilation, can be used to reduce the uncertainty in the model results. In this study, the required complexity (i.e. conceptual versus physically-based) of the unsaturated zone model to update groundwater models through the assimilation of ET rates is assessed for a water-limited site in South Australia. ET rates are assimilated because they have been shown to be related to the groundwater table dynamics, and thus form the link between RS data and the deeper parts of the soil profile. It has been found that, under the test site conditions, a conceptual UZM can be used to improve groundwater model results through the assimilation of ET rates.

¹<https://doi.org/10.5194/hess-2020-252>

5.2 Introduction

ET and recharge to the WT are two major components of the water cycle. Because ET is a function of the soil water content within the root zone, as the root water uptake is distributed along the entire root system (Grinevskii, 2011; Neumann and Cardon, 2012), improving ET estimates, by means of a detailed modeling of the soil water transport, can lead to better simulation of recharge and WT dynamics. This is particularly important when the WT is within the reach of the roots, as it is common in Australian semi-arid catchments (Banks, Brunner, and Simmons, 2011), where the direct transpiration from the WT is a major contribution to the total ET (Mensforth et al., 1994; Orellana et al., 2012).

This chapter aims to perform a validation of the ET assimilation framework proposed synthetically in Chapter 4 (also Gelsinari et al. (2020)) and to assesses the UZM complexity required for the assimilation to positively update groundwater models. A conceptual and a physically-based UZM are coupled to MODFLOW, and applied to a water-limited study site in the South-East of South Australia. Remotely sensed ET observations are assimilated into both these coupled models, and an assessment of the improvements in the model results is made. Based on this assessment, a number of recommendations regarding the required UZM complexity to obtain a positive impact on the modeled WT dynamics are made.

5.3 Experiment Set-up

The study site is a *Pinus Radiata* plantation next to the Mount Gambier airport (Figure 5.1[b]). The area was originally planted in July 1996 with a density of 1225 trees/ha, there was no thinning of the plantation during the observations. The survey performed by Benyon, Theiveyanathan, and Doody (2006), classified the soil as duplex. This type of soil presents a contrast between the upper part, which features sandy-loam characteristics with high hydraulic conductivity, and the lower part, classified as clay, with a finer texture and lower hydraulic conductivity. The average WT depth, from the observations at one bore, is reported at approximately 6 m below the surface. SM observations were taken at an interval of 30 cm up to 3 m with a neutron probe. The campaign was conducted from August 2000 to January 2005 with an average measurement frequency of 4 weeks. Because in the area more than 90% of the available groundwater is in shallow aquifers, these plantations have been shown to have direct access to groundwater (Benyon and Doody, 2004)

Remotely sensed data of AET from the CMRSET algorithm (Guerschman et al., 2009) were used. These values are obtained by rescaling the PET rates calculated with the Penman-Monteith algorithm using the Enhanced Vegetation Index and

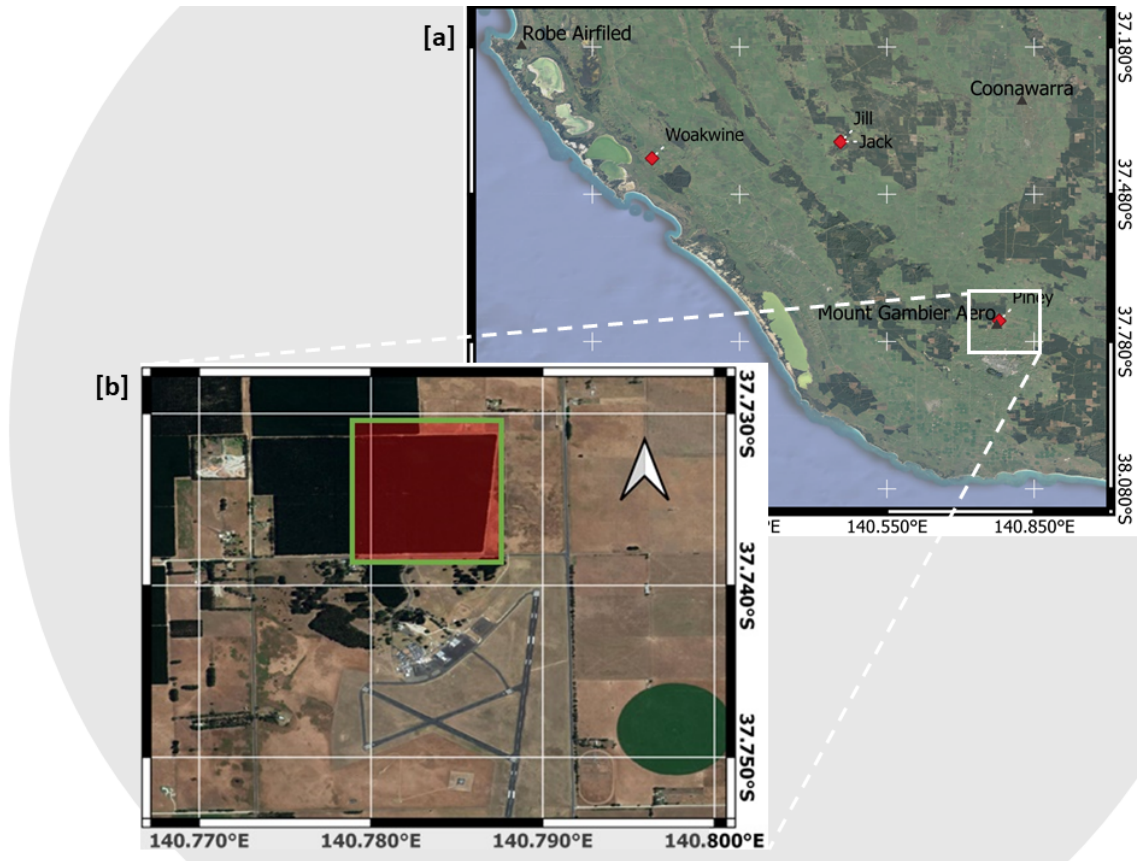


FIGURE 5.1: Localization of the study area within the South East of South Australia [a] and detail of the forest plantation [b]. The red square indicates the CMRSET tile.

Global Vegetation Moisture Index obtained from the MODIS spectroradiometer (Swaffer et al., 2020). The observations are available every 8 days with a finest spatial resolution of 250 by 250 m.

5.3.1 Model Description

Two different configurations of coupled groundwater-unsaturated zone models were tested. The UZMs conceptualization and the coupling to the groundwater model are described Section 3.6 and depicted in Figure 3.9. This section presents the model domain and introduces the multi-objective calibration function.

5.3.2 Model Domain and Calibration

The coupled model configurations were applied to a domain of 1×5 cells of 1 km^2 each, and a single vertical unconfined layer (Figure 5.2). The boundary cells were set to a constant head obtained via calibration (See Section 5.4.1). UnSAT can account for the decrease of K_s along the soil column, whereas SWAP is capable of explicitly accounting for the heterogeneity of the soil column, as described in Section 5.3. Thus, For Configuration-1, the decay of K_s is a result of the calibration,

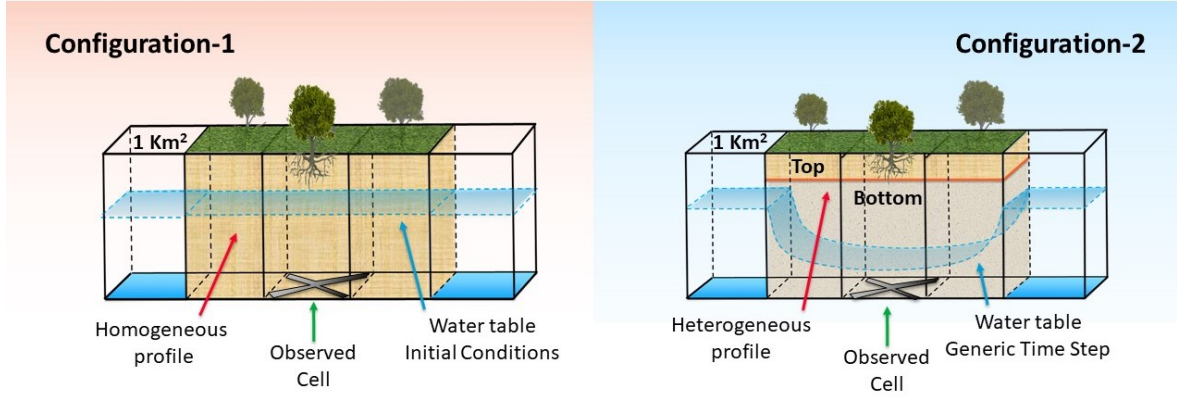


FIGURE 5.2: Schematic of the simulation domain. Configuration-1 models the unsaturated zone as a homogeneous profile with UnSAT. Configuration-2 models the soil heterogeneity by accounting for the change in soil properties with SWAP. The WT is represented at initial conditions on the left-hand side, and at a generic simulation time, showing the depression caused by the root water extraction, on the right-hand side.

while other soil parameters are homogeneous along the soil column length (i.e. 10 m). In Configuration-2, the first (Upper) 1.5 meters of soil is classified as "Sandy-Loam" soil and the second (Lower) is a "Loam-Clay" soil spanning the rest of the simulated soil column (i.e. 8.5 m).

Preliminary analyses of this study (not shown) indicated that, in order to get significant improvements in the model outputs, the link between WT depth and ET had to be accurately reproduced. For both configurations, attempting to assimilate ET fluxes, without reproducing the interdependence between WT and actual ET, yielded poor filter performances. To account for this interdependence, and reduce the order of freedom of the ill-posed problem of calibration, a multi-objective function (MOF) which combines WT depths and actual ET values was introduced. Then, SM observations were used for refinement and to set boundaries to the soil parameters. The algorithm Particle Swarm Optimization (PSO) (Kennedy and Eberhart, 1995; Shi and Eberhart, 1998) was used for calibration minimizing the specifically defined MOF:

$$\text{MOF} = \frac{\text{RMSE}(WT)}{\sigma(WT)} + \frac{\text{RMSE}(ET)}{\sigma(ET)}, \quad (5.1)$$

where RMSE is the Root Mean Square Error, and σ is standard deviation. PSO searches the n-dimensional solution space, where n is the number of parameters given, in order to minimize equation 5.1. The calibrated parameters are listed in Table 5.1. The drainage empirical value and root distribution parameter apply only to Configuration-1. The oxygen stress values, one of which indicates the upper pressure head limit for no extraction and the other the start of the plant transpiration

reduction, apply to Configuration-2. The other values are for both configurations.

For each configuration, the observation data set was divided into two periods used for calibration and validation. For calibration, 46 8-day time steps covering roughly the year 2001 were used, while the rest of the data set (4.5 years in total) was used for validation.

Ensemble Generation

The generation of a statistically meaningful ensemble, which preserves the relationship between ET and WT levels obtained during the calibration, is crucial for the application of the EnKF (Gelsinari et al., 2020). A number of ensemble generation techniques were applied to the two configurations, and a consistent approach for both configurations was adopted. First, a simple perturbation of forcing inputs, by adding a random number sampled from Gaussian distributions with different standard deviations, as performed in Chapter 4, was tested. Then, a mixed method involving the perturbation of both inputs and the parameters, with the latter perturbed by adding a random number proportionally to the calibrated value, was applied. For the UZMs, the parameters selected for the perturbation were K_s and root depth, and for MODFLOW the saturated K_h and S_y . Initial conditions of WT levels were also perturbed to induce a good spread in the ensemble from the early stages of the simulation. This ensemble of simulations is defined as the open loop, which represents the "prior" distribution. After applying the filter, the resulting distribution is called the assimilation run and represents the "posterior".

In such a non-linear configuration, it is a challenge to generate ensembles that maintain the statistical accuracy, and simultaneously preserve the ET - WT relationship. The most adequate ensembles for the two configurations, obtained by calculating the ensemble validation skills on the modeled ET based on the method explained in Talagrand, Vautard, and Strauss (1997), were retained (De Lannoy et al., 2006; Pauwels and De Lannoy, 2009). Results are shown in Section 5.4.2.

5.4 Results and Discussion

5.4.1 Deterministic Runs

During the calibration with the PSO, the dynamics of the parameter optimization algorithm was monitored, showing that the MODFLOW saturated hydraulic conductivity (K_h) had a consistent tendency towards high values (100 m d⁻¹ or higher) in order to minimize Equation 5.1. This was interpreted as an effect of the ET component on the objective function, which was inducing the UZMs to transpire water directly from the WT to compensate for the low ET values. The boundary conditions for the groundwater model were thus modified by imposing a constant head

TABLE 5.1 : Calibrated parameter values used for the simulations and their perturbation fraction.

Model Parameter	Configuration 1	Configuration 2		Perturbation Fraction
	UnSAT + MODFLOW Homogeneous	SWAP + MODFLOW Top Bottom	SWAP + MODFLOW Top Bottom	
Hydraulic conductivity - K_s	25 [mm · hr ⁻¹]	24 41 [mm · hr ⁻¹]	30%	
Drought Stress (Reduction)	-	-3000 [mm]	-	
Drought Stress (No extraction)	-	-30000 [mm]	-	
Oxygen Stress (Reduction)	-	-100 mm	-	
Oxygen Stress (No extraction)	-	+ 5 mm	-	
Soil porosity	0.35 [mm ³ · mm ⁻³]	0.36 0.36 [mm ³ · mm ⁻³]	-	
Critical SM for transpiration	0.12 [mm ³ · mm ⁻³]	-	-	
Residual SM (θ_r)	0.03 [mm ³ · mm ⁻³]	0.01 0.02 [mm ³ · mm ⁻³]	-	
Drainage empirical value	2.50	-	-	
Root depth	8000 [mm]	2900 [mm]	10%	
Root distribution parameter (Vr)	0.5	-	-	
MODFLOW K_h	10.0 [m · d ⁻¹]	8.0 [m · d ⁻¹]	10%	
MODFLOW S_y	0.12	0.11	10%	

boundary with shallower WT depth, which maintained K_h at a plausible order of magnitude. Conceptually, these boundary conditions represent the water supplied from the regional aquifer to the plantation, and induce the WT depression shown on the right hand side of Figure 5.2.

With the calibration technique proposed in Section 5.3.2 the coupled models were able to simultaneously reproduce the dynamics of both the WT and ET for the two configurations. (See Figure 5.3). Configuration-1 performs better overall in the representation of the WT dynamics with a RMSE of 0.23 [m], while the RMSE of Configuration-2 is slightly larger (i.e. 0.36 [m]). Configuration-1 also shows a higher correlation coefficient (0.790 vs 0.400) for the WT. Configuration-1 shows a lower temporal variability than Configuration-2, but the latter better matches the temporal evolution of the WT. There is a time lag between groundwater observations and model WT fluctuation for Configuration-2, which also explains the higher RMSE and lower correlation. This lag may be induced by preferential flow that the Richards equation does not account for, or to a slower response of the WT to the meteorological input that is discussed later in this section.

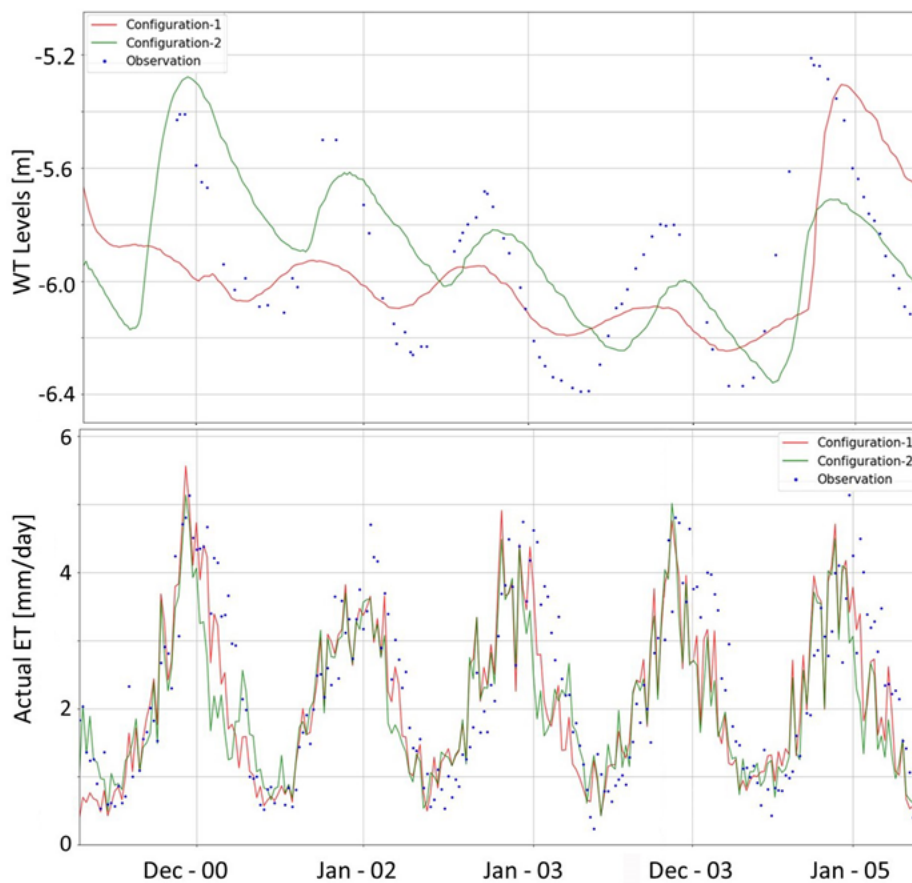


FIGURE 5.3: Combined WT fluctuations [a] and AET [b] for both configurations.

TABLE 5.2: Results for the calibrated runs.

Variable	Configuration	RMSE	r
WT	1	0.230 [m]	0.790
Levels	2	0.360 [m]	0.400
SM	1	0.049 [mm ³ mm ⁻³]	0.410
Upper	2	0.045 [mm ³ mm ⁻³]	0.610
SM	1	0.085 [mm ³ mm ⁻³]	0.592
Lower	2	0.018 [mm ³ mm ⁻³]	0.850
ET	1	0.791 [mm day ⁻¹]	0.811
	2	0.870 [mm day ⁻¹]	0.788

The capillary fringe and soil heterogeneity are represented differently by the two configurations. For physically-based Configuration-2, the detail of the capillary fringe is represented in Figure 5.4 [d] by the blurred area above the saturated zone (i.e. dark blue). Configuration-2 is also able to represent the heterogeneity of the soil column, as shown in Figure 5.4 [d] where a sharp variation of the SM content at 1.5 m depth is caused by the different soil parameters. Configuration-1 has no ability to represent the capillary fringe effect, and it does not explicitly account for duplex soil. However, it can account for a decay of the hydraulic conductivity along the soil column. Because of these reasons, the modeled SM from Configuration-2 shows a good agreement with the observations, especially in the lower soil (Figure 5.4 [f]). Configuration-1 has a low SM RMSE (0.049 [mm³ mm⁻³]) and a reasonable agreement in terms of the Pearson correlation coefficient r (0.410) for the upper soil [b], but the resulting SM is consistently below the observed values in the bottom soil (panel [c]), with an RMSE of 0.137 [mm³ mm⁻³]. Both configurations report a higher correlation for the lower soil.

For ET, Configuration-1 yields good results with a lower RMSE and similar correlation when compared to Configuration-2. In particular, the physically-based Configuration-2, underestimates the simulated ET for the Southern hemisphere late summer/early autumn as shown in Figure 5.3 [b]. In this period, the soil water content is low, as shown in Figure 5.4 [d], and the system is actively transpiring from the groundwater. This can be interpreted as an effect of the coupling to the groundwater model. The conceptually based Configuration-1, with a rooting depth of 8.0 m, is able to extract water directly from the water table and immediately transforms it into ET. Configuration-2, with a rooting depth of 2.9 m, achieves this by reducing the pressure head along the soil column. Thus water has to flow across a part of unsaturated zone before becoming available for direct plant transpiration, reducing the rapid response of the model to the forcing inputs. This also explains the lag in the WT dynamics described precedently. Another possible reason for the underestimation of ET are the two oxygen stress parameters that reduce transpiration in conditions close to saturation (Table 5.1). These parameters are calibrated and kept constant during the simulation period. Configuration-2

has shown to be highly sensitive to these parameters, while Configuration-1 does not include this process.

5.4.2 Ensemble Simulations

The generation of the ensemble is also found to be a key step of the method. The simple perturbation of forcing inputs was not able to generate a sufficiently broad ensemble spread, particularly for Configuration-2. For both configurations, the combined perturbation of parameters and forcing inputs was found to produce adequate ensembles. This is obtained by applying the ensemble validation, as discussed in Section 5.3.2, to the first year of the data set, excluding the first 10 time steps to avoid the influence of the initial conditions (i.e. from the 10 to the 45th time step). For the meteorological data, the best candidates are obtained by perturbing the input with a random number sampled from a Gaussian distribution having a standard deviation proportional to the value of the forcing inputs (i.e. 50% for Configuration-1 and 10% for Configuration-2). The difference in the percentage is motivated by the different time frequency of the models' forcing inputs (i.e. hourly vs daily). For the parameters, the last column of Table 5.1 lists the perturbation fractions. Additionally, for Configuration-2, S_y has a lower limit of 0.1 to preserve numerical stability of the coupled models.

In the case of the conceptual Configuration-1, the WT level spread of the open loop ensemble is consistently covering the observations (Figure 5.5[a]). The mean of the ensemble is close to the observations, but does not follow the seasonal variability appropriately. The associated spread of the actual ET for Configuration-1 is wider than that of Configuration-2. More specifically, the latter is narrow during wet periods (i.e. April to November) and becomes wider for the dry period (Figures 5.5[c] and 5.5[d]). A similar effect, with a larger magnitude, was reported during the ensemble generation phase and led to the double perturbation of the meteorological inputs and the parameters as explained in Section 5.3.2. The spread of the WT levels for Configuration-2 (see panel [b]) covers the WT observations for most of the simulations and is wider than for Configuration-1. The mean represents the amplitude of the seasonal fluctuations better as compared to Configuration-1, but leads to a shallower WT as a result of the perturbation of the forcing inputs.

Table 5.3 summarizes and compares the results between the open loop and the assimilation for actual ET, WT levels, and SM contents of the upper and lower soil layers. For both configurations, the ET assimilation slightly decreases the RMSE and improves the correlations. In particular, the RMSE of ET for Configuration-1 reduces from 0.76 [mm day⁻¹] for the open loop to 0.73 [mm day⁻¹]. The RMSE for the ET for Configuration-2 reduces from 0.83 [mm day⁻¹] for the open loop to 0.81 [mm day⁻¹].

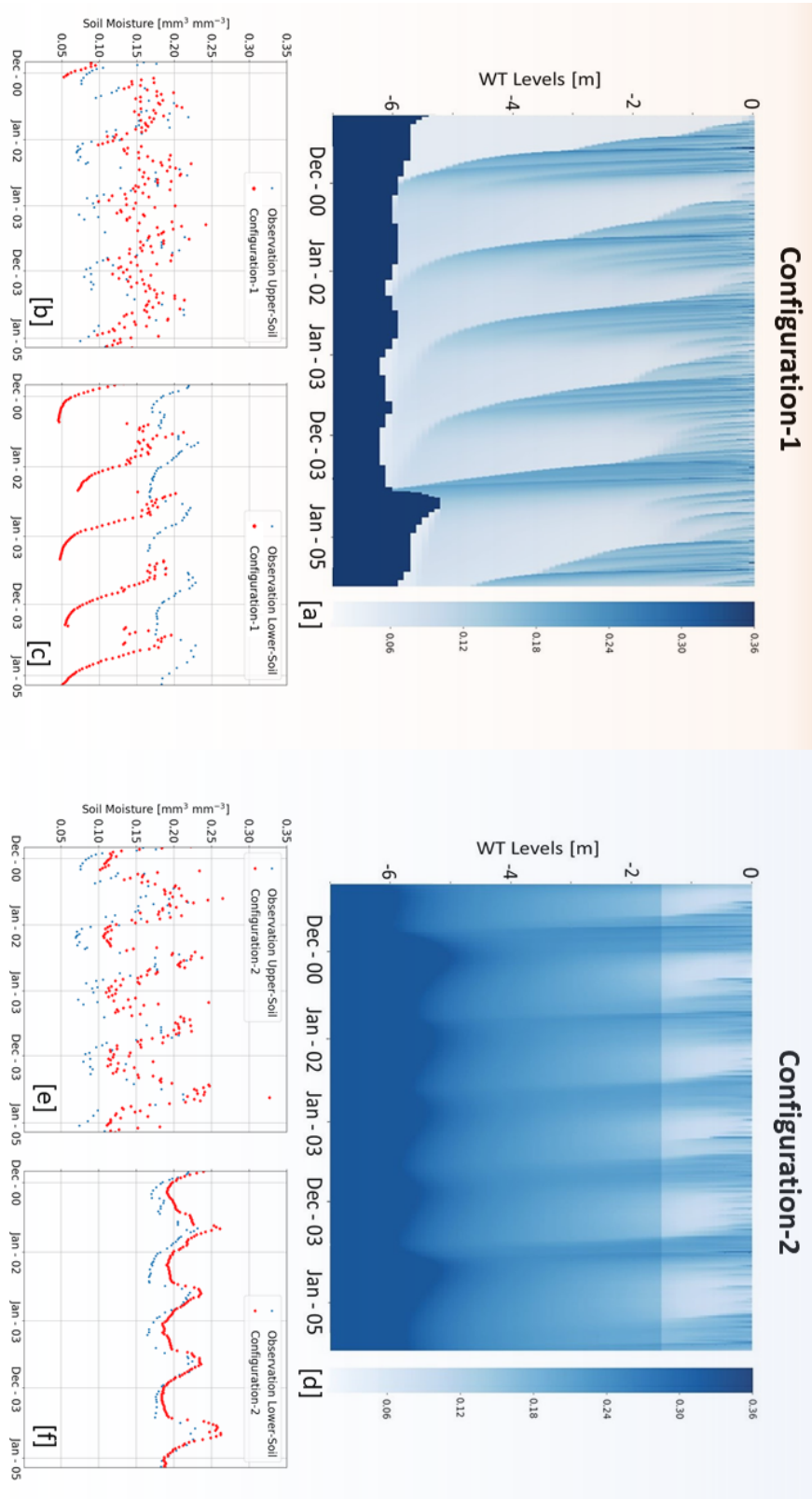


FIGURE 5.4: Temporal evolution of the soil moisture contents. Panels [a] and [d] show the entire modeled column, including the fluctuation of the WT (i.e. the dark blue area). Panel [b] and [e] represent the modeled and observed water content for the upper soil (averaged over 0-300 mm depth). Panel [c] and [f] show these results for the lower soil (averaged of the interval 1500-1800 mm depth).

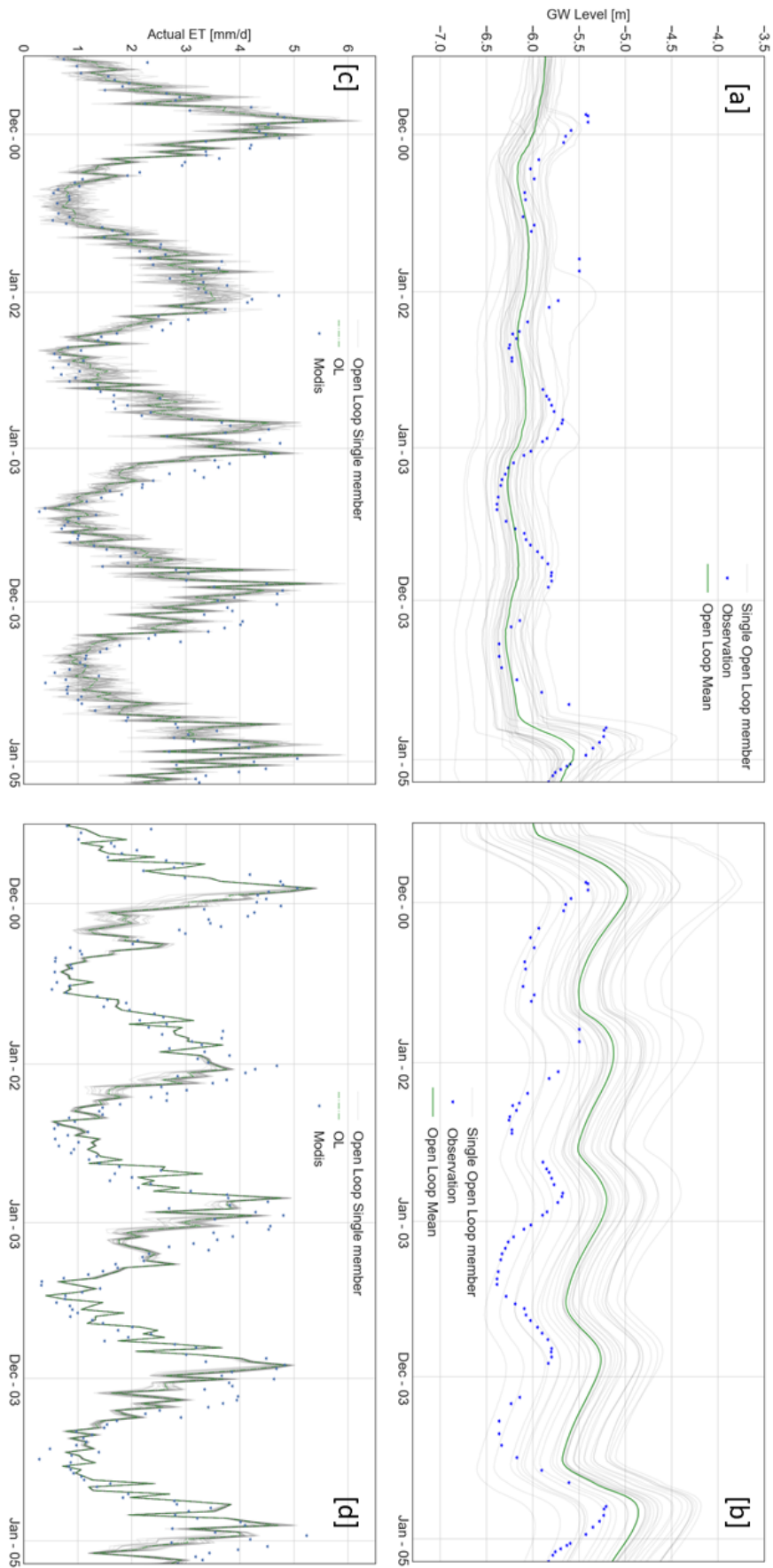


FIGURE 5.5: WT levels and AET and spread of the Open Loop ensembles for Configuration-1 [a,c] and Configuration-2[b,d]

TABLE 5.3: RMSE and correlation for three variables between the open loop and the assimilation.

Config	Type	Actual ET		WT Levels		SM Upper Soil		SM Lower Soil	
		RMSE	r	RMSE	r	RMSE	r	RMSE	r
1	Open loop	0.760	0.820	0.280	0.730	0.045	0.497	0.102	0.468
	Assimilation	0.730	0.830	0.236	0.734	0.044	0.498	0.098	0.428
2	Open loop	0.830	0.810	0.626	0.880	0.041	0.888	0.019	0.940
	Assimilation	0.810	0.820	0.307	0.675	0.042	0.864	0.017	0.900

The correlation also improves marginally for both configurations (i.e. + 0.01). However, these are non-trivial results as the data assimilation, through the EnKF, is designed to improve the model states. Therefore, the reduction of the ET errors suggests that the improved state variables are contributing to a better modeling of other hydrological quantities.

In Configuration-2, the assimilation is not able to improve ET in the Summer of 2000/2001 and 2002/2003. This results in poorer WT simulations during these periods (Figure 5.6[b]). Here, the filter is trying to increase the amount of water in the system to match the higher assimilated observation, which is a correct application of the methodology. Thus, the WT is made shallower by the filter but this does not reflect in a higher modeled ET. The reason for this is the behaviour of the SWAP vegetation parameter oxygen stress. The filter is increasing the pressure head of the system, in an attempt to provide more water to transpire, but the actual transpiration from the plant is hindered by SWAP, which recognizes the soil to be too saturated for the plant to transpire. The EnKF then causes the WT to rise, and increases the amount of recharge entering the groundwater. When the observed ET is lower than the simulations, the filter reduces the pressure head and the model allows the plant to transpire. Therefore, in the two time steps after this effect, the modeled ET is higher than the observation, after which this phenomenon disappears. This artefact is not seen in Configuration-1 as the oxygen stress is not accounted for.

Figures 5.7 and 5.8 show the observations, the mean of the open loop (blue dash-dotted line) and the mean of the assimilation runs (red dot line), for Configuration-1 and Configuration-2, respectively. For both configurations, the assimilation improves the RMSE when compared to the open loop runs. The best results are obtained for Configuration-1, showing an RMSE of 0.236 [m] with a 15 % error reduction compared to the open loop. Configuration-2 resulted in a substantial error reduction of 38.9 % as compared to the open loop. However, the overall RMSE value (0.307 [m]) is still higher than Configuration-1.

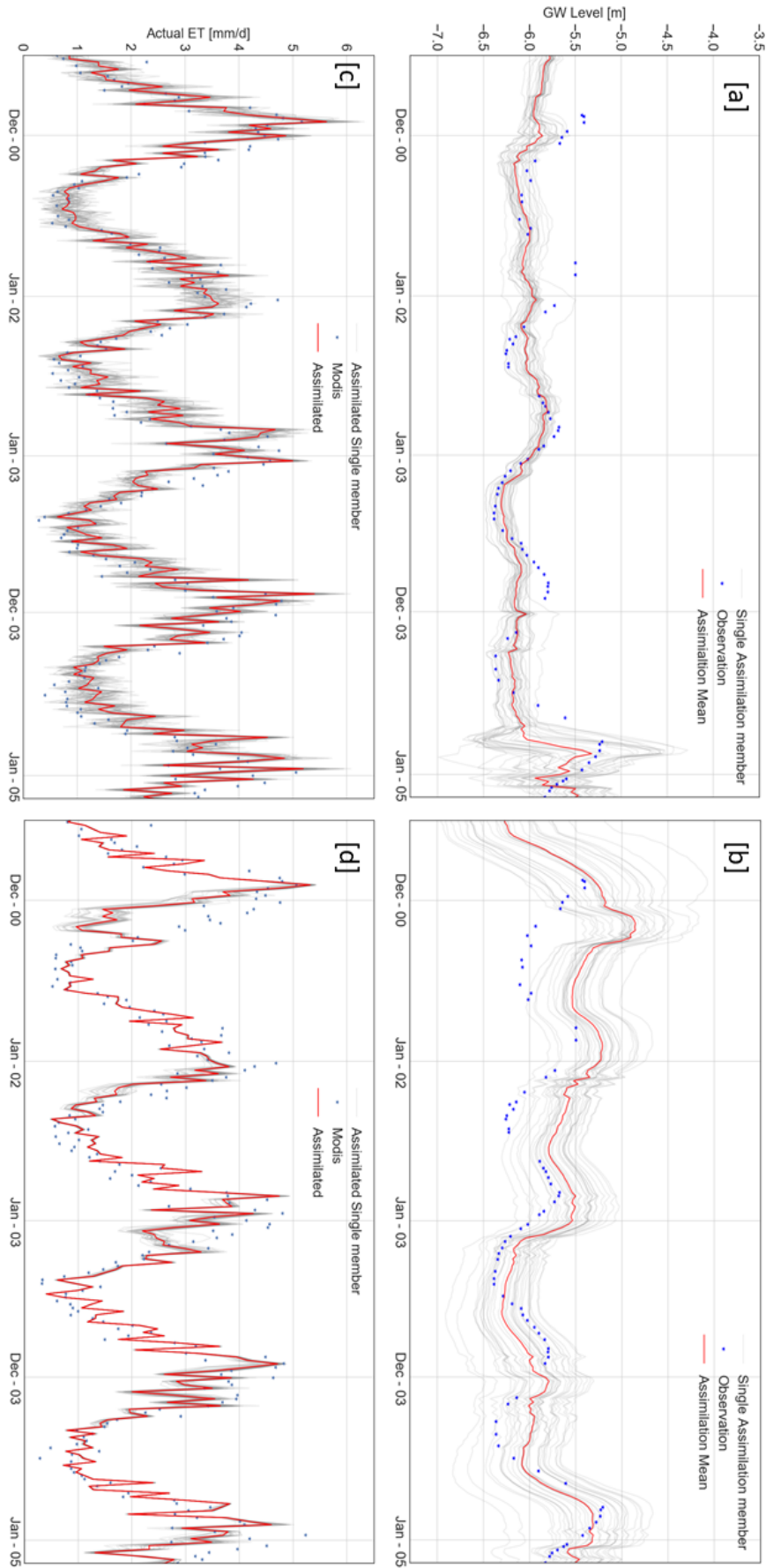


FIGURE 5.6: WT levels and AET and spread of the assimilation run for Configuration-1 [a,c] and Configuration-2[b,d]

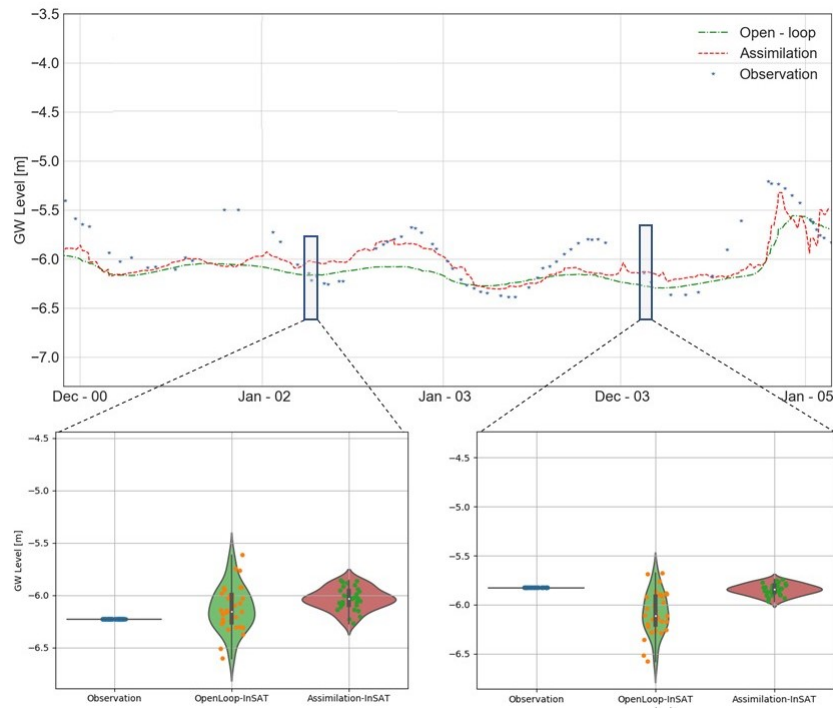


FIGURE 5.7: Observations, open loop and assimilation means for Configuration-1. In the insets, green and red surfaces represent the violin plots of the open loop (Prior) and the assimilation runs (Posterior) distributions, for two dates indicated by the boxes.

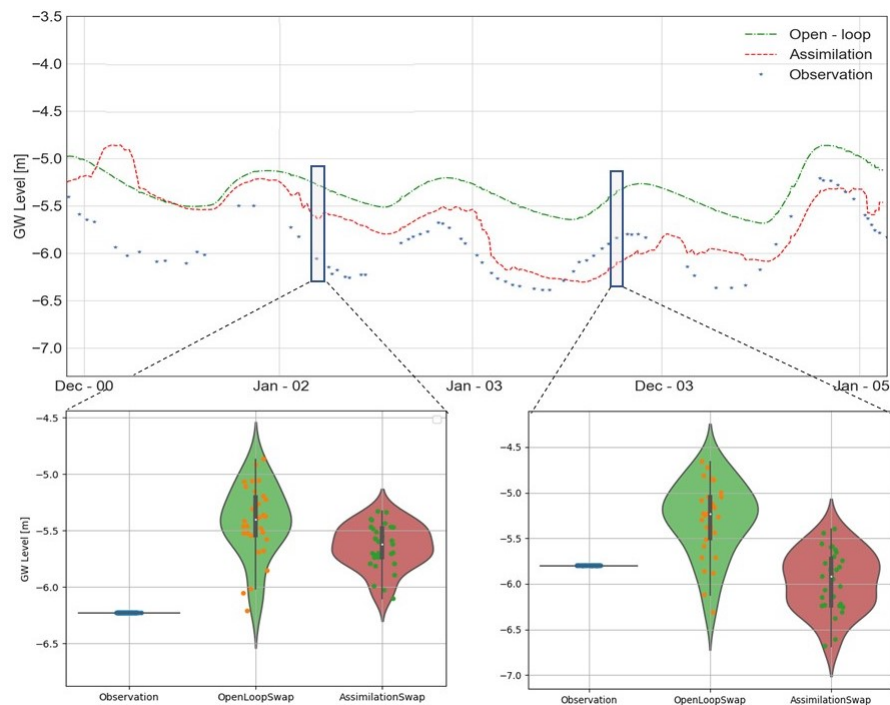


FIGURE 5.8: Observations, open loop and assimilation means for Configuration-2. In the insets, green and red surfaces represent the violin plots of the open loop (Prior) and the assimilation runs (Posterior) distributions, for two dates indicated by the boxes.

Apart from the oxygen stress artefacts explained above, the assimilation run of Configuration-2 is consistently better than the open loop. This is not always the case for Configuration-1, where the open loop was already performing well. The correlation remains largely unchanged for Configuration-1, and reduces for Configuration-2 mainly due to the updates during the summers of 2000/2001 and 2002/2003.

The two violin plots shown in the insets to Figure 5.7 and 5.8 provide a visual representation of the magnitude of uncertainty before (prior) and after (posterior) the assimilation. In general, the spread of the WT levels for Configuration-1 is narrower than the equivalent for Configuration-2. Even when the mean of the open loop is closer to the observation, as in the first violin plot of figure 5.7, the assimilation helps in reducing the uncertainty around the WT levels. The second violin plot shows an ideal situation, where the assimilation mean is very close to the observed value and the uncertainty interval is narrow. This combination was not obtained for Configuration-2. As shown in the violin plots of figure 5.8, the posterior covariances (i.e. the red violin plot) are still large after the assimilation. This means a lower uncertainty reduction compared to Configuration-1.

Figure 5.9 presents the scatter plots of the SM in the top (at a depth of 300 mm) and bottom (1800 mm) parts of the soil for each configuration. The open loop of Configuration-1 has an RMSE of 0.045 [$\text{mm}^3 \text{mm}^{-3}$] for the upper soil and 0.102 [$\text{mm}^3 \text{mm}^{-3}$] for the lower soil. In the latter, the simulated water contents are consistently lower than the observations. This is mainly due to the model's inability to represent capillary rise. The assimilation only marginally improved the SM content, with slightly better results for the bottom part of the soil, where the RMSE was reduced to 0.098 [$\text{mm}^3 \text{mm}^{-3}$]. The open loop of Configuration-2 has a lower RMSE, 0.041 and 0.017 [$\text{mm}^3 / \text{mm}^{-3}$] for the top and bottom part of the soil, respectively. However, it is slightly overestimating the SM content for the entire column. This is consistent with the shallower WT (i.e. more water in the system) observed for the WT levels in the open loop (Figure 5.5[d]).

The assimilation did not improve the top layer SM content, with an RMSE of 0.042 [$\text{mm}^3 \text{mm}^{-3}$]. However, the assimilation improved the SM content of the bottom part (Figures 5.9[g] and [h]), for which the best results are obtained (i.e. 0.015). The updating of the entire soil column is a positive result of the assimilation of ET rates, as opposed to the assimilation of remotely sensed SM values. The latter usually results in stronger updates in the upper parts of the soil, because of the reduced correlation between the SM contents in the upper and deeper parts of the soil column.

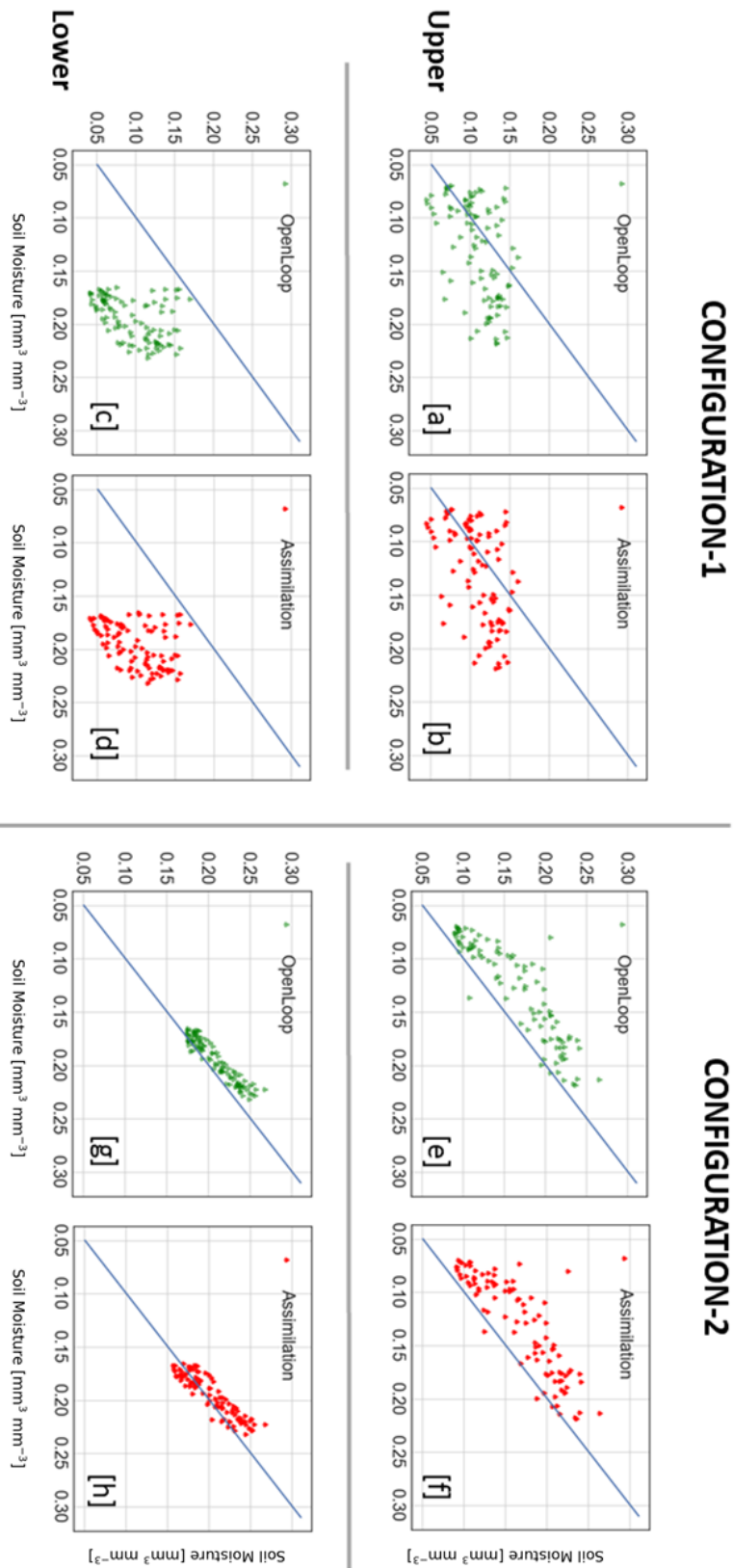


FIGURE 5.9: Scatter plots of the upper [a,b,e,f] and lower [c,d,g,h] soil water content. Configuration 1 Open-Loop [a,c], Assimilation [b,d]. Configuration 2 Open-Loop [e,g], Assimilation [f,h]. N.B. Observations are reported on the x axes.

Generally, these results consolidate the synthetic approach in Gelsinari et al. (2020), and further confirm that the assimilation framework is not only able to update and improve the WT level, which is a prognostic variable of the coupled model, but also the modeled ET, and consequently the recharge to the WT. In addition, albeit marginally, the filter improves the unsaturated zone state variables regardless of the manner in which the SM content is calculated (volumetric SM or pressure head).

5.5 Conclusions

This study validates the assimilation of the satellite-based evapotranspiration (ET) data set (CMRSET) into two coupled unsaturated zone-groundwater configurations. Specifically, these configurations are composed by a conceptual water balance model (UnSAT) and a physically-based agro-hydrological model (SWAP), respectively, coupled to MODFLOW and applied to a semi-arid, pine plantation in the south-east of South Australia.

The most important findings can be summarized as:

Calibration. This study shows the need to calibrate the model using a multi-objective function, with normalised components of water table (WT) and actual ET. In this way, both configurations are representing the WT-ET relationship in an appropriate manner and benefit from the assimilation of ET observations.

Configuration-1. The assimilation of ET values through the Ensemble Kalman Filter (EnKF) using a conceptual unsaturated zone model, produced the best results for the prognostic variable WT levels and the diagnostic fluxes of actual ET. SM values were also slightly improved in both the upper and lower parts of the soil column. However, because of the model conceptualization the mismatch in the lower part of the soil is considerably larger than for Configuration-2. The reduced number of parameters of this configuration allows for a simpler calibration, which is able to represent the WT dynamics. Similarly, the generation of an appropriate ensemble is more straightforward mostly due to the model conceptualization, which allows the WT to respond quickly to direct root water extraction by transpiration.

Configuration-2. The ET assimilation into a physically-based unsaturated zone model, based on the Richards equation, produced the largest improvements to the WT levels with a larger uncertainty reduction and an adequate representation of the capillary fringe. Improvements to actual ET fluxes were similar to Configuration-1. For SM, generally the impact of the assimilation algorithm was small, with a positive update for the lower soil layers, and a

negative update for the upper layers. Here, the calibration involved a larger number of parameters and produced a good representation of the SM dynamics. However, due to the non-linearity introduced with the coupling (e.g. capillary fringe), errors in the WT levels and ET fluxes are higher. In addition, the ensemble generation is constrained by the high model parameterization, making it more difficult to produce an appropriate ensemble that preserves the ET-WT relationship.

ET information. The updating of the entire soil column is an advantage of the assimilation of remotely sensed ET over satellite SM retrievals. ET rates express the moisture status of the entire root zone. Thus, assimilating ET overcomes the SM assimilation tendency to produce stronger updates in the most superficial part of the soil because of the reduced correlation between the upper and lower SM contents.

In conclusion, it is possible to use either a conceptual or a physically-based unsaturated zone model in the assimilation of satellite-based ET estimates to inform hydrogeological models. Both model coupling configurations reduce the uncertainty related to state variables (such as WT and SM) and fluxes of actual ET. The findings indicate that a simple conceptual model may be sufficient for this purpose, thus using one configuration over the other should be only motivated by the specific purpose of the simulation and the information available. This study represents a step towards the use of satellite-based ET retrievals for water resources management. For future applications at larger scales, more research is to be conducted in areas with different groundwater, vegetation and soil conditions, with the intent of prioritizing regions where the ET assimilation is more effective.

Chapter 6

Prioritizing regions for the assimilation of evapotranspiration rates into hydrogeological models

This chapter is based on the article "Prioritizing regions for the assimilation of evapotranspiration rates into hydrogeological models" In preparation for *Journal of Hydrology*.

Abstract

This chapter describes the ET data assimilation performed at four silvicultural sites within the study area presented in Chapter 3. These plantation sites differ in their soil profile, average depth to WT and vegetation type. This variation of conditions allows for an analysis of their effects on the assimilation of ET. The conceptual Configuration-1 is applied and calibrated to reproduce the WT-ET dynamics. Satellite remotely sensed ET rates from CMRSET are assimilated through the Ensemble Kalman Filter. The results are investigated through two commonly recognised metrics (i.e. root mean square error and correlation) and the continuous ranked probability score, which is specifically designed for ensemble predictions. Results show that the most influential condition is the depth to WT, with positive impacts of the ET assimilation recorded up to a depth of 6.5 m. Whereas no clearly defined impact of the vegetation type and soil profile characterizations results from the analysis.

6.1 Introduction

A general decline of groundwater levels in arid and semi-arid regions throughout most of the globe has been observed due to climate change (Taylor et al., 2013). Some predictions indicate that this trend will further increase due to reduced or irregular rainfall events (Leblanc et al., 2012) combined with high PET and low soil moisture (Swaffer et al., 2020). The AET component plays a fundamental role in the hydrological cycle, especially in water-limited regions, because it influences the recharge to the WT. AET also provides a link between the bio-physical and

hydrological processes. For example, some vegetation types, like forestry plantations, use more water than crop field and other natives species because they have higher rainfall interception and generally deeper root systems (van Der Salm et al., 2006; Benyon, Theiveyanathan, and Doody, 2006). Recognising the impact of forest plantation on the water balance, countries like Australia and South Africa have put in place water policies that require forest managers to comply with regulations and sometimes water licensing (Dye and Versfeld, 2007; GSA, 2009). Thus, the assimilation of satellite-based ET retrievals can provide information to constrain the uncertainty related to the water cycle components under these plantations, and potentially become a tool to assist regulators issuing water licences.

This chapter aims at identifying the conditions for which the ET data assimilation reports the improvements in prediction of hydrological quantities. The plantations selected for this study present a mix of characteristics, but they have been shown to directly access the groundwater (Benyon and Doody, 2004). Hence, updating the model with readily available satellite-based ET data, and improving the estimates of water balance components by accounting for the vegetation water extraction, is a potential benefit for water resource managers.

6.2 Experiment Description

This section introduces the locations and the simulation set-ups used to test the ET assimilation under different soil, vegetation and depth to WT conditions. The conceptually based, coupled, Configuration-1 (see Section 3.6), was selected for this task based on the findings of Section 5.5, which indicated a good versatility and a reduced computational burden for this coupling configuration.

6.2.1 Site Description

Four silviculture sites, located within the study site described in Section 3.1, were selected from field studies conducted in the area. These studies have produced datasets which include a number of observations (e.g. SM, WT levels) and land classifications (Benyon and Doody, 2004; Benyon, Theiveyanathan, and Doody, 2006; Benyon et al., 2008). In particular, these four locations cover different combinations of soil, vegetation, and depth to WT conditions and represent a good sampling of the diversified settings found in the area. These conditions and the coordinates of the four sites are reported in Table 6.1 with the names (i.e. *Jack*, *Jill*, *Woakwine* and *Piney*) attributed following the nomenclature used by previous studies. For each location, the vegetation type (i.e. Tasmanian blue-gum (EG - *Eucalyptus globulus Labill.*) or Pinus (PR - *Pinus radiata*)), soil characterization, depth to the WT observations, rainfall & net irrigation, PET and AET are available.

TABLE 6.1: Name, coordinates and characteristics of the silviculture sites

Name	Latitude	Longitude	Soil Profile	Average WT	Vegetation
Jack	-37.4361	140.5810	Heterog.	Shallow (3 m)	EG
Jill	-37.4361	140.5630	Homog.	Deep (10 m)	EG
Woakwine	-37.4067	140.0716	Homog.	Shallow (2.5 m)	EG
Piney	-37.7377	140.7790	Heterog.	Deep (6 m)	PR

The remotely sensed ET rates retrieved from the CMRSET and the applied assimilation algorithm (i.e. EnKF) were introduced in Sections 3.2 and 3.7 respectively. Similarly to the simulations described in Chapters 4 and 5, the CMRSET values are rescaled to the model grid size (1 Km²) as a result of averaging the sixteen 250 x 250 m tiles. Figure 6.1 shows the individual CMRSET tiles, in transparency, while the lined squares represent the model cell and the CMRSET averaging area.

To further evaluate the results from the tests performed in this chapter, a number of extra simulations were performed. Two of these simulations were based on extended WT observations at Jack and Piney, while a third one assimilated the bias-corrected CMRSET at Jack. The details of these are explained below.

For the extended simulations, the WT observations of two locations with deep and shallow WT conditions (Jack and Piney) were extended with additional monitoring bores obtained from the South Australian government webpage (www.waterconnect.sa.gov.au). This enabled longer simulations that covered exceptional dry conditions associated with the "Milleinum Drought" (van Dijk et al., 2013), and prominent groundwater depletion, observed at both sites. Results of these two sites are reported separately for the period referring to the dataset collected in Benyon and Doody (2004) and the extended period. The deep WT levels with *Pinus Radiata* (Piney) site was the test case for the simulations covered in the previous chapter.

In addition to the data extension, the *Eucaliptus globulus* plantation (Jack) was also selected to perform a bias correction of the CMRSET dataset using field ET data recorded during the Benyon and Doody (2004) study. The motivation for the bias correction lies in investigating, by comparing to the standard CMRSET retrievals, the possible improvements obtained by correcting the CMRSET to the specific location. The first step of the bias correction process consisted in the temporal rescaling of the averaged 8-day CMRSET values to the variable intervals of the field data collections. Then, a regression analysis between these data sets was performed, identifying the linear regression equation shown in Figure 6.2[a]. Figure 6.2[b] shows the original CMRSET in blue, the field data in red and the CMRSET bias-corrected in black. The CMRSET tends to underestimate the ET in the cool period and slightly overestimates it in summer. Generally, the bias-corrected ET



FIGURE 6.1: Satellite images of the 4 locations. Piney [a], Woakwine [b], Jack and Jill [c]. Note: [c] refers to a time beyond the simulation period, taken after the harvesting of the plantation.

reduces the underestimation in winter and corrects the overestimation in summer.

6.2.2 Site Location and Model Conceptualization

The model conceptualizations of the four sites are shown in Figure 6.3, all of which are modelled individually. The figure shows the average WT level, constant head boundaries, vegetation and the soil characteristics for each location. Similarly to the experiment in Chapter 5, the domains consist of 5×1 cells, where the first and the last are constant head boundaries, and one convertible vertical layer for the saturated zone simulating the unconfined aquifer. The magnitude of the cone of depression induced by the plant transpiration is also represented in these conceptualizations. This is more pronounced for Jack, Piney and Woakwine and just

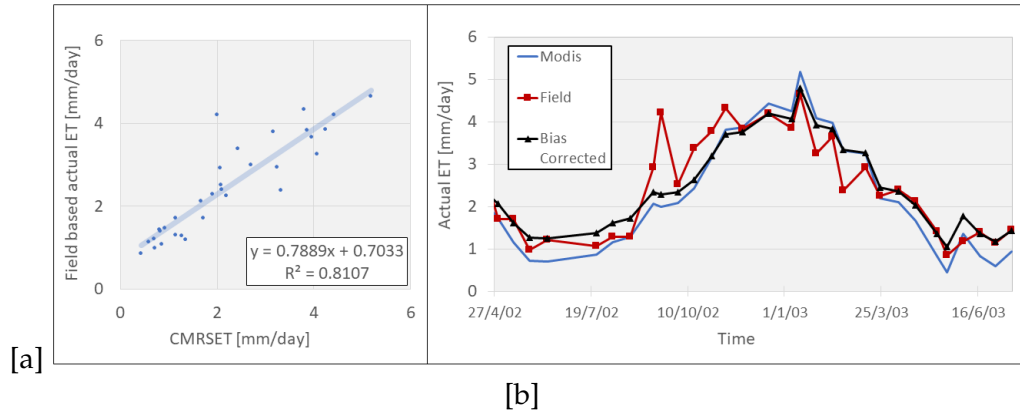


FIGURE 6.2: Bias correction of ET. [a] Regression analysis. [b] Comparison of the three AET as per legend.

TABLE 6.2: Parameters, perturbation fractions, and forcing input generation fractions used for the simulations.

Model Parameter	Jack	Jill	Piney	Woakwine	Param. pert. fraction (%)
Hydraulic conduct. K_s [mm/h]	32	50	25	22	30
Soil porosity [mm^3/mm^3]	0.29	0.29	0.35	0.32	-
Critical SM [mm^3/mm^3]	0.14	0.14	0.12	0.10	-
Residual SM [mm^3/mm^3]	0.046	0.046	0.03	0.06	-
Drainage empirical value	1.9	0.5	2.50	2.0	-
Root depth [mm]	7200	26000	8000	5000	10
Root distribution parameter	0.14	0.01	0.5	0.10	-
MODFLOW K_h [m/d]	43	10	10.0	80	10
MODFLOW S_y	0.113	0.35	0.12	0.11	10

noticeable in the case of Jill due to the deep WT.

The two sites Jack and Jill are located 110 meters apart within the same *Eucalyptus Globulus* plantation which has an average age of 5.5 years and a stock density of 0.1175 (trees m^{-1}). The two locations present a prominent difference in the depth to WT conditions due to local surface undulations (See Figure 6.4, left). Jack is located at the level of the surrounding plain, with an average depth to WT of four m on a duplex soil (sand - clay). Jill is at the top of a local dune, a condition that increases the depth to WT to around 10 m, and the soil texture is mostly sandy. The field-based annual water balance reports an average rainfall of 669 mm/year for Jack and 701 mm/year for Jill, with a PET for both sites of 980 mm/year, resulting in the lowest amongst the considered sites. The observed AET for Jack is 904 mm/year and for Jill is 713 mm/year for Jill. There is, therefore, a deficit of approximately 235 mm/year between rainfall and ET for Jack, while Jill shows a net water balance close to zero (Rainfall - PET). The forcing input PET dataset at Jack has a long gap between April and September 2002. The gap was filled with a simple interpolation between the observations, which have been shown to affect some

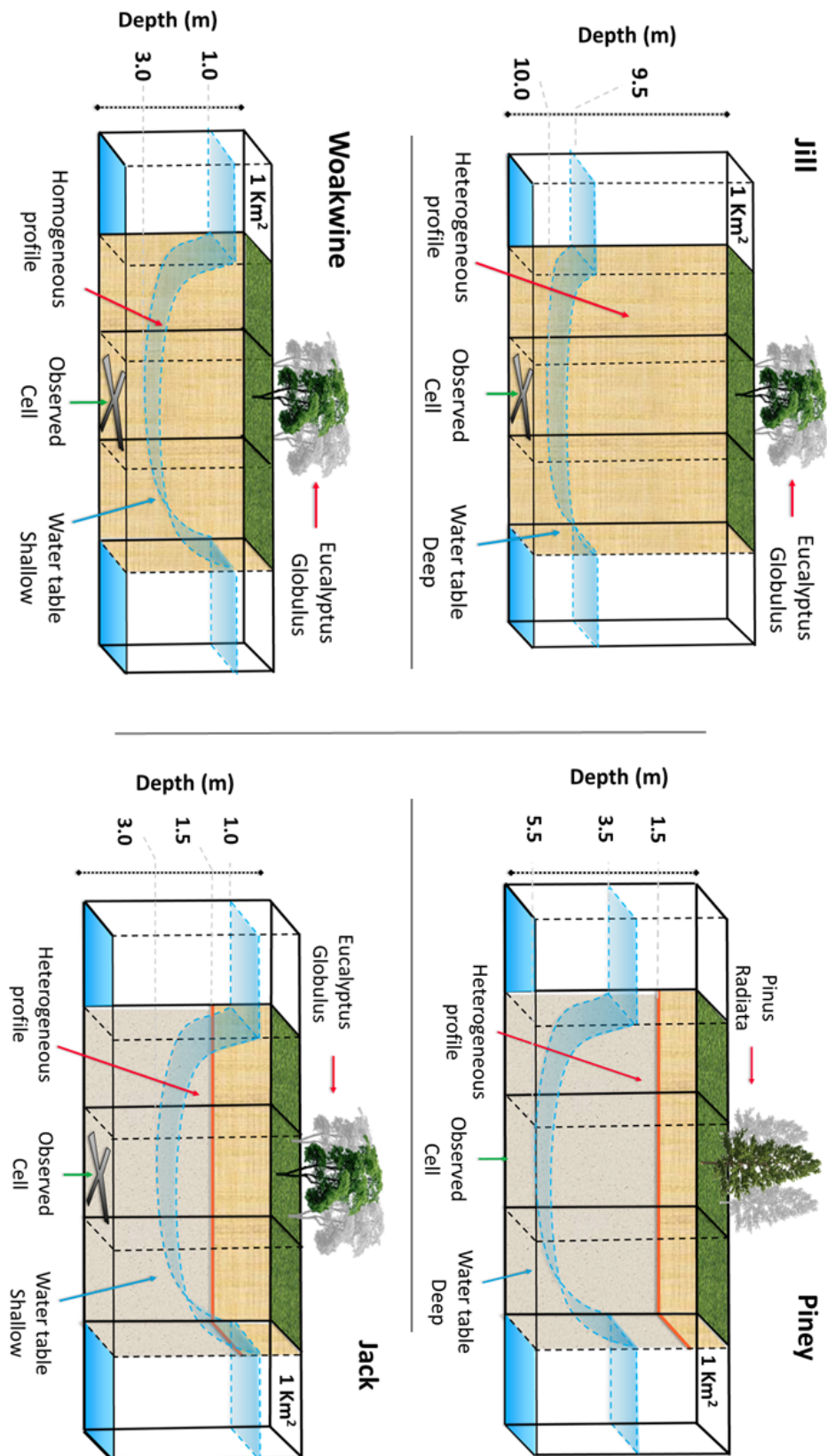


FIGURE 6.3: Conceptual representation of the four locations.

of the assimilation results. For this reason, this period is omitted in the calculation of the model evaluation. The right panel of Figure 6.4 shows the field measured ET at Jack and Jill and the 1-Km averaged ET value from CMRSET used for the assimilation. The higher ET rates at Jack in summer (i.e. up to ≥ 1 mm/day higher) are due to the direct transpiration from the groundwater when the WT levels are shallow. This is not possible for Jill due to the rooting depth. The higher AET rates of Jack from May to August are due to a slightly larger amount of rainfall recorded at Jill (i.e.+5%). This further confirms that, for the conditions of the study area, trees have the capacity to extract water from groundwater when the WT is up to about 6 m deep (Benyon and Doody, 2004). The assimilation run performed at Jill provides a valuable source of information not only to assess the soil and depth to WT conditions, comparing it to Jack, but also on the effect of the CMRSET tile resolution.

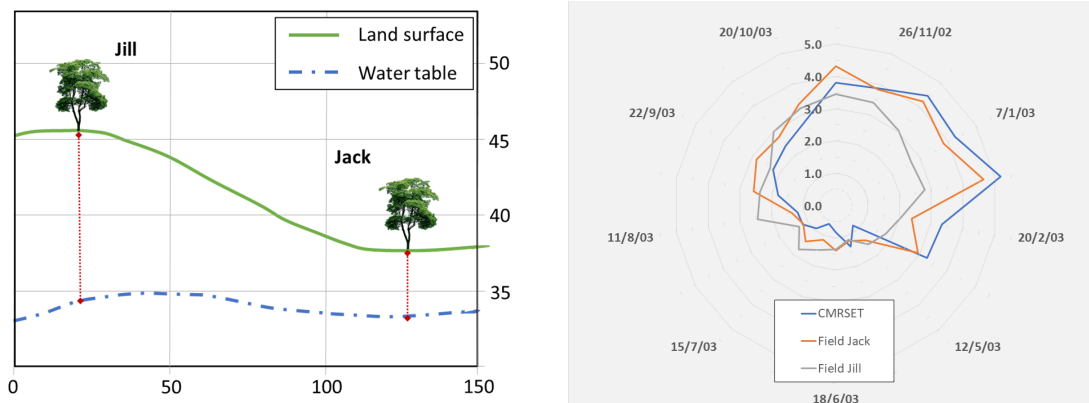


FIGURE 6.4: Conceptual representation of the local depth to WT. AET from the CMRSET averaged over 1 km² and field data of Jack and Jill].

The Woakwine site is located within an *Eucalyptus Globulus* plantation which has an average age of 7.5 years and a tree density of 0.0818 (trees m⁻¹). This location has a shallow WT (3 m) with a homogeneous sandy soil profile. The annual water balance reports the lowest rainfall 545 [mm/year], together with a high PET 1180 [mm/year] and an AET of 1193 [mm/year]. This combination produces the highest deficit of 636 mm/year.

Piney is located within a *Radiata Pine* plantation that is, on average, 7 years old and has a tree density of 0.120 (trees m⁻¹). The plantation is located on a duplex sandy-clay soil profile, in the proximity of a meteorological station used to provide the forcing inputs. Rainfall, PET and AET are all the highest of the four sites (i.e. 747, 1230, 1343 mm/year, respectively), resulting in a deficit of 561 mm/year. The WT depth is around 6 m, which is considered to be the threshold depth for the direct transpiration from the groundwater. Thus, at least in part, the WT characteristics of this location are classified as deep.

Extensions of the depth to WT observation datasets were performed at Piney and Jack. At Piney, the readings used for the extended simulation are from the bore identified with the number 7022-9409, which is part of the same plantation (as shown in Figure 6.1[a]). After a correction using an overlap period of 1.5 years, the depth to WT dataset is extended from the 15/01/2005 to the 23/05/2007, as shown in Figure 6.5. A similar method is used to extend the depth to WT dataset at Jack. In this case, the bore is located in a similar plantation 8 km away (Bore 7023-2123), and the dataset is extended until the end of February 2008.

The motivation for including the soil profile characteristics in this experiment arose from the results of Chapter 5. The conceptual UZM was able to sufficiently reproduce the WT level dynamic and the AET pattern, but the SM content was poorly represented for the deeper part of a duplex soil, due to the model simplifications. Notwithstanding this, the ET assimilation improved both the state variables (i.e. SM and WT levels) and the ET rates. In this chapter, the focus is the assimilation performance in relation to either homogeneous or heterogeneous soil profiles and by specifically assessing WT levels and AET. The specific SM assessment, which was conducted in Chapter 5, is left for more specific agro-hydrological applications.

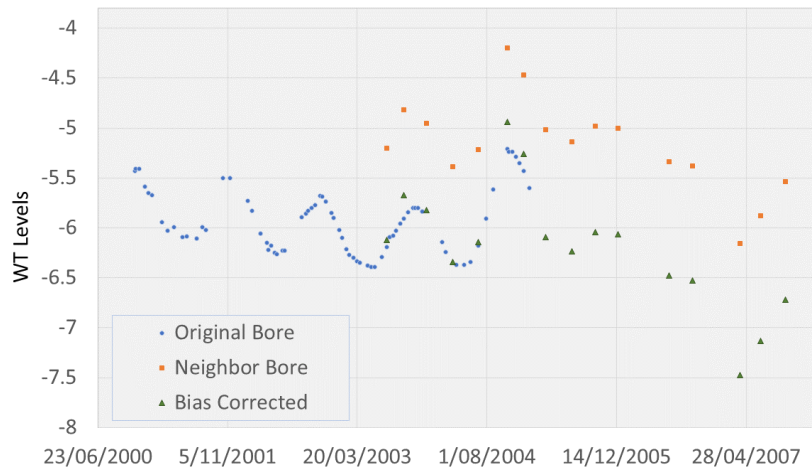


FIGURE 6.5: Bore observations at Piney, at the neighbour bore, for the extended corrected dataset.

6.2.3 Model Calibration

The model was calibrated for the four sites using the MOF based on WT levels and AET in order to reproduce the behaviour which has been shown to be a requisite for the ET assimilation. This method is explained in section 5.3.2. For all locations, the WT observation datasets were split and used for a calibration/validation approach, with the calibration period consisting of 50 8-day intervals.

6.3 Results and Discussion

6.3.1 WT Levels

The simulation performances based on the evaluation of model skill presented in Chapter 3 are summarized in Table 6.3 for the WT levels. Jack and Piney were tested for an extended simulation, which uses independent WT level observations from an additional monitoring well. Results are presented independently for the simulation calibrated and validated with the field data and for the simulation using the extended dataset.

TABLE 6.3: Results for the WT dynamics. In green the values where the assimilation is improving the WT levels compared to the open loop. In red the cases when the open loop performs better than the assimilation.

Location	Simulation	RMSE	CRPS	Correlation (r)
Jack	Assimilation	0.338	0.202	0.76
	Open Loop	0.348	0.205	0.85
	Bias Corrected as.	0.534	0.185	0.80
Extended	Assimilation Ext.	0.652	0.405	0.67
	Open Loop Ext.	0.761	0.454	0.58
	Bias Corrected as. EXT	0.870	0.404	0.58
Jill	Assimilation	0.291	0.165	0.89
	Open Loop	0.290	0.160	0.89
Woakwine	Assimilation	0.285	0.200	0.64
	Open Loop	0.300	0.200	0.63
Piney	Assimilation	0.240	0.151	0.73
	Open Loop	0.280	0.144	0.73
Extended	Assimilation Ext.	0.305	0.179	0.67
	Open Loop Ext.	0.312	0.171	0.68

At Jack, improvements in the RMSE and CRPS are seen for the field-based assimilation run compared with the open loop. However, the r in this simulation is reduced by the ET assimilation, which can be explained by the continuous WT level updating by the filter. Overall, the filter updating results in a better RMSE value, but produces a jagged WT level dynamic, clearly visible for the second part of 2003 (See the first panel of Figure 6.6), which reduces the r . The abrupt change of September 2002 is likely due to the interpolated PET values used to fill the data gap. A similar trend is observed for the open loop run as well, indicating that the effect is not due to the filter updating. Because of this, the period from 2002/04/01 to 2002/10/31 was removed from the calculation of the metric. The extended simulation, indicated by the purple stars in the first panel of Figure 6.6, shows a higher RMSE, CRPS and lower r than the shorter simulation. This is a consequence of

the groundwater storage depletion induced by the "Millennium Drought" period that triggered a general decrease of WT levels. Under these new conditions, the model is not able to properly capture the WT fluctuation because the calibration was based on different conditions. However, the ET assimilation improves the model prediction of the WT levels, especially for the summer periods.

The reduction of the RMSE and CRPS values seen here represents the potential of the filter to improve models results in challenging, variable conditions, such as situations of climate change.

The bias-corrected assimilation run (yellow line with markers in Figure 6.6 at Jack), was performed to investigate the possible improvements given by the local calibration of the CMRSET. For the short simulation, the bias-corrected run reduces the CRPS to the lowest value among all simulations. Besides, it increases the r compared to the standard assimilation run, but it also further increases the RMSE. This is possibly due to the temporal window for which the linear regression was performed, which results in good coverage of the period 2001/11/01 - 2003/03/08 (RMSE 0.1 lower than the standard assimilation run) but does not continue with a similar performances afterwards. This is confirmed by the higher RMSE for the extended simulation when the bias-corrected ET run tends to underestimate the depth to WT (i.e. shallower WT level). These dissimilar results are not sufficient to affirm that the ET bias correction is to be discarded. A regression analysis with a longer simulation period could potentially lead to improved bias-corrected values, which in turn are likely to perform similarly to the 2001/11/01 - 2003/03/08 period described above. However, long, field-based, ET observations are expensive and would then provide the best ET dataset candidate to be used for the assimilation, reducing the benefits of using RS observations.

Figure 6.7 shows the values of the CRPS for the assimilation, open loop and bias-corrected runs at Jack. Each bar is a time when a WT level observation is available, which produces an unequally distributed X-axis. The larger values from October 2010 to April 2008 compared to the rest of the datasets are due to the decreased WT levels already discussed above.

The CRPS values represent the WT level distribution of the ensemble around the observation, with a low value indicating a good agreement and thus reduced uncertainty. The assimilation CRPS values (dark blue bars) are lower than the corresponding open loop values (i.e. light blue bars) for large parts of the datasets. The magnitude of the improvements is remarkable for the periods June-October 2003, and June-November of the years 2004 and 2005. These periods cover the rising limb and the peak of the WT level and include some days of high PET.

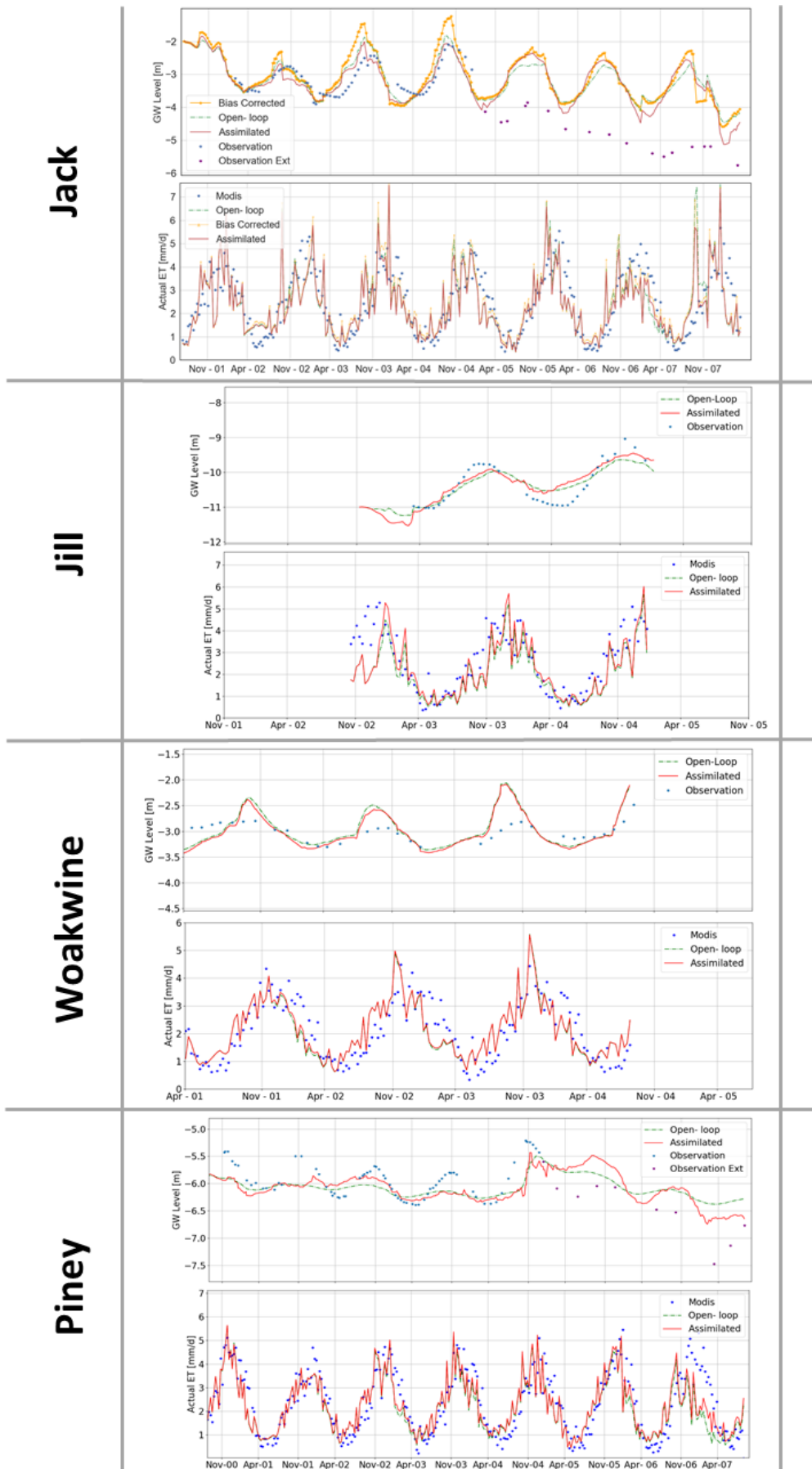


FIGURE 6.6: Depth to WT and AET at Jack, Jill, Woakwine and Piney.

This combination can present strong groundwater-vegetation interaction, where the ET assimilation has shown to perform well. The improvements in the last part of the observation dataset further confirm the ability of the ET assimilation to improve model results when altered conditions occur. The large CRPS values for the second part of 2002 are again affected by the interpolated ET forcing inputs. These are shown in the figure but, similarly to RMSE and r , they do not contribute to the values reported in the tables.

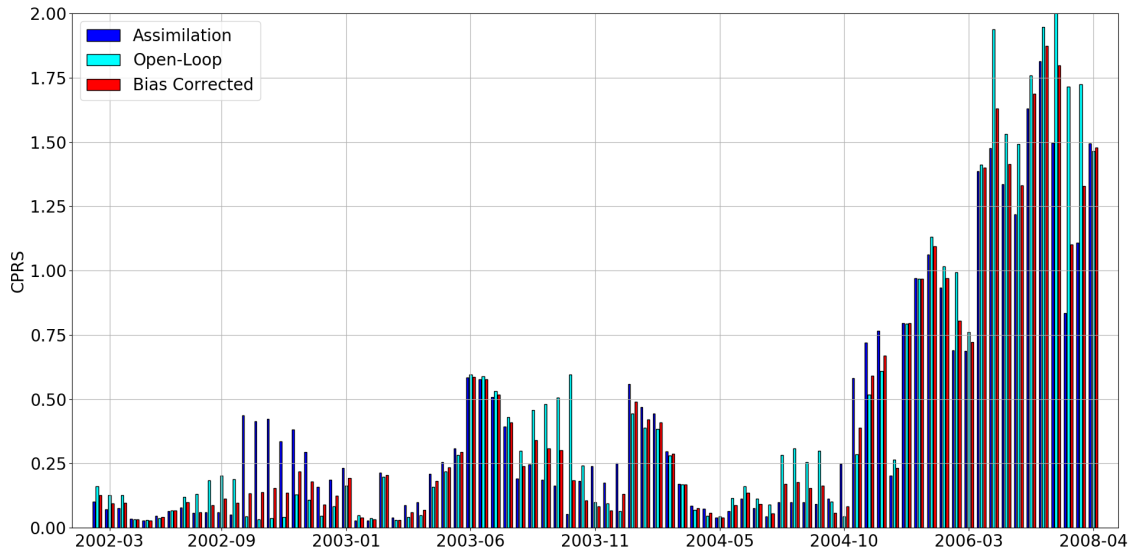


FIGURE 6.7: CRPS values are computed for the assimilation, open-loop and bias corrected runs each time an observation is available.

The second location, Jill, is located into the same, averaged 1 Km² CMRSET tile, as Jack. However, it has a deeper WT level condition which results in overall lower transpiration rates compared with Jack (Figure 6.4), particularly in summer. Due to the field observations available, this simulation is the shortest of the four, covering the period 28th October 2002 - 8th January 2005. Both the RMSE and CRPS see a slight increment when compared to the respective open loop values, while r does show noticeable changes. Overall, the three metrics indicate that the open loop simulation already performed well with low residuals related to the average depth to WT (10 m). The filter has an attenuated effect for this deep WT condition, with an overall tendency to produce a shallower WT. This agrees with the assimilated averaged CMRSET value, which was higher than the field-based ET. Generally, the damped effect of the ET assimilation on the dynamics of deep WT is consistent with the lack of direct correlation between AET and WT when the latter is deeper than 6 m.

The ET assimilation for the Woakwine plantation improved the model's ability to simulate the WT dynamics as indicated by all metrics. This location presents the shallowest averaged depth to WT and the highest negative water balance thus it is

the site that has the strongest groundwater-vegetation interaction. The calibration of this location was particularly challenging, as the observed magnitude of the WT fluctuation is only about 0.5 m while the ET fluctuation is comparable to other locations. Thus, the calibration with the MOF led to high values of K_h , which tended to overestimate the peaks of recharge, resulting in a shallower WT.

The Piney simulation shows similar improvements to the RMSE and r compared to the simulation performed in Chapter 5, where the small differences are related to the aleatory of the observation error in the formulation of the EnKF. Despite the CRPS value being the lowest of all the simulations, according to this metric, the open loop performs better (0.144 vs. 0.151). Similarly to the results of the previous chapter, the r value is not improved. When analyzing the extended simulation, the RMSE and CRPS values are in general higher. As for the case of Jack, this is due to the calibration. At this location, the root depth parameter is set to 8000 mm from the calibration, limiting the model in reproducing deeper WT levels. The assimilation partially corrects this effect and maintains a better seasonality of the WT levels as shown in the last panel of Figure 6.6 and by the improvements in the RMSE values. This is not reflected by a reduction of uncertainty as expected in the CRPS.

6.3.2 Evapotranspiration

For the AET, the simulation performances are summarized in Table 6.4. Consistently with the results of Chapters 4 and 5, the ET assimilation improves the RMSE and the r in all cases apart from the deep WT location of Jill. Overall, the best results for RMSE and r are obtained at Piney. Similarly to the WT levels, the largest improvements are for both the extended simulations. High RMSE reductions are recorded at the shallow WT level location (Woakwine), for which the reason is twofold. Firstly, this location shows strong groundwater-vegetation interaction, and that is a condition where the ET assimilation has been shown to perform better. The second reason can be related to the calibration of this location which overestimates modeled AET in the winter periods, leaving more room for improvement. At one deep WT location (Jill), the results show little improvement for the RMSE, combined with a slightly lower r and a higher CRPS. This indicates that the averaged 1 km² CMRSET tile, which is the same for Jack and Jill, was not a completely adequate representation of the AET rates for this location. This study also shows that there are no clear differences in the assimilation of AET between plantation of *Eucalyptus Globulus* and *Pinus Radiata* under similar climatic and depth to WT conditions. These results are consistent with the findings of Benyon and Doody (2015) based on field observations.

TABLE 6.4: Results for the AET. In green the values where the assimilation is improving the AET compared to the open loop. In red the cases when the open loop performs better than the assimilation.

Location	Simulation	RMSE	CRPS	Correlation (r)
Jack	Assimilation	1.025	0.804	0.69
	Open Loop	1.035	0.807	0.67
	Bias Corrected As.	1.100	0.903	0.67
	Assimilation Long	1.025	0.790	0.69
	Open Loop Long	1.100	0.826	0.67
	Bias Corrected As. Long	1.106	0.898	0.67
Jill	Assimilation	1.150	0.883	0.67
	Open Loop	1.154	0.872	0.70
Woakwine	Assimilation	0.832	0.605	0.74
	Open Loop	0.857	0.621	0.72
Piney	Assimilation	0.797	0.645	0.81
	Open Loop	0.810	0.656	0.80
	Assimilation Long	0.839	0.703	0.79
	Open Loop Long	0.892	0.728	0.77

It is worth to note that, because of the high non-linearity between the ET and WT levels of the ensemble, and because ET is the quantity being assimilated, ensemble distributions that are improved by the assimilation are more frequent for ET than for WT levels. This is also shown by generally reduced CRPS values, meaning a more defined uncertainty characterization, calculated on the AET.

This consideration suggests a use of the ET assimilation focused on the quantitative aspect of ET, and as a possible relevant tool for water resources managers. The AET ratios for the four locations, which are volumes divided by the cell area [mm/Km^2], are calculated by integrating the averaged daily ET value over the respective 8-day windows. Table 6.5 summarizes the RMSE of the assimilated and open loop ratio calculated with respect to the CMRSET, and Figure 6.8 shows the 6-month aggregated values for the assimilation and open loop runs. In the figure, values above zero show an overestimation of modeled ET compared to the remotely sensed observations, whereas values below zero are underestimations. Better estimates of AET, as per all the locations in the table, can lead to improved quantitative management of the groundwater resources. This concept becomes more important when the volumes of water transpired by the plantations are underestimated, as in the case of the values below zero in Figure 6.8, because of the possible risk of depleting groundwater resources. In the case of underestimation, the ET assimilation shows the ability to reduce the errors at all locations for the entire simulation length. An exception is the case of the second semester of 2002 at

TABLE 6.5: RMSE values calculated for the integral of the ET ratios.

Location	Simulation	RMSE [mm / Km ²]
Jack	Assimilation	53
	Open Loop	72
	Bias Corrected Ass.	62
Jill	Assimilation	63
	Open Loop	81
Woakwine	Assimilation	71
	Open Loop	76
Piney	Assimilation	69
	Open Loop	82

Jack (first panel), which has been shown to be affected by an approximate interpolation of the PET forcing input. On the other hand, the assimilation clearly reduces the overestimation at Jack, but it does not improve the over-estimations at Piney, and only marginally at Woakwine. This shows that the filter is able to correct for residuals of both signs.

Finally, the results of this analysis do not show a clear role of the soil profile for the assimilation performances on WT levels and AET. The objective of this chapter is to identify if specific conditions or parameterizations encourage (or prevent) the improvements provided by the assimilation of remotely sensed ET rates. The modeled SM contents would likely be differently distributed because of the homogeneity or heterogeneity of the soils. Thus, it is acknowledged that a specific assessment of the SM content at all the locations could provide more insights to help better define the impact of the ET assimilation. However, this methodology implies the use of ET fluxes that are a proxy for the water content of the entire soil column. Thus, for the application of the ET assimilation to the strategic management of groundwater resources, a detailed SM content analysis is assumed to be unnecessary.

6.4 Conclusions

This chapter focused on the satellite-based ET dataset (CMRSET) assimilation into a coupled unsaturated zone-groundwater model (Configuration-1). The assimilation was applied to four plantations of the water-limited, south-east of South Australia. The combination of WT depth, soil profiles and vegetation type for each of the locations, is representative of the numerous other plantations in the area. Thus, they provide insights into the ET assimilation improvements on hydrogeological quantities for the area.

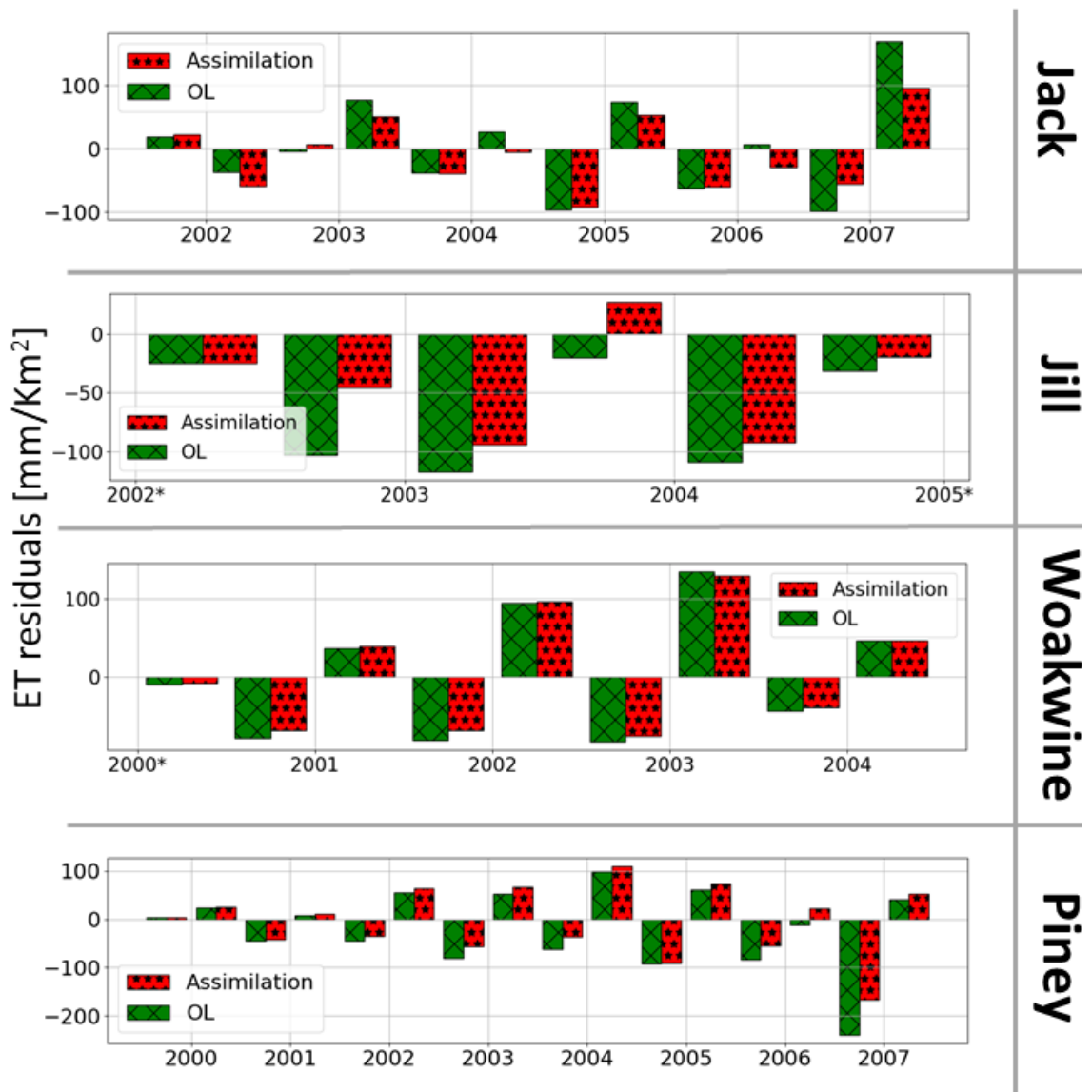


FIGURE 6.8: Residuals of the AET volumes calculated over 6 months. NB. the mark indicates a partial year.

Overall, the findings of this chapter show that the impact of the ET assimilation is mostly affected by the depth to WT. Vegetation with direct access to groundwater presents a higher transpiration component, which is a condition where groundwater models become highly non-linear with complex feedbacks. Thus applying the ET assimilation to these locations reduces the WT levels errors and also marginally improve the ensemble distribution as indicated by the CRPS values. The extended simulations, performed at a shallow and a deep WT location, included a sharp WT level reduction triggered by a major drought. For these changed conditions, the errors were larger as the model was not parameterized for this case, however, the assimilation was able to reduce the RMSE at both locations and improve the CRPS and the correlation (r) at the location with higher ET WT interaction (Jack). On the other hand, the location with deep WT (Jill) had a reduced filter effect, which is in

agreement with the lack of direct correlation between AET and WT when the latter is deeper than 6 m.

At the *Eucalyptus globulus* location with a deep WT (Jack), the assimilation of a bias-corrected CMRSET scored the overall best CRPS value but did not show direct benefit in the RMSE or r . This is mostly due to the length of the dataset used for the bias correction, which should be extended for a better regression. However, the findings of this experiment are not sufficient to show the benefit of using a locally bias-corrected CMRSET and may not be sufficient to justify the investment of long field data collection campaigns.

For AET, the RMSE, CRPS and r values were improved for all the locations, with the exception of the CRPS and r in the case of deep WT levels (Jill). These good performances for ET are consistent with the findings expressed in Chapters 4 and 5, and have to do with the nature of the assimilated observations. The degraded results at Jill are related to overestimated CMRSET observations, which are averaged over an area dominated by trees able to access groundwater while Jill was not showing this ability.

These findings underpin the use of the ET assimilation as a valuable tool for the quantitative management of groundwater resources in silvicultural areas. It has been shown that there is a substantial reduction of the residuals for the AET volumes, which are more evident in the cases of changing conditions (i.e. simulations including a major drought event). This can help in better assessing the actual water consumption of forest plantations accessing groundwater in semi-arid environments.

Chapter 7

Overall Discussion and Conclusions

7.1 Overview

The literature review in Chapter 2 highlights the scientific knowledge gaps in the field of the data assimilation into hydrogeological models. These gaps were identified in the representation of the intricate unsaturated-groundwater system through models of different complexity and in the novelty of using the EnKF to assimilate ET fluxes into such a system to constrain coupled saturated-unsaturated models. The research performed as part of this thesis contributed to assessing the potential of the ET assimilation in reducing the uncertainties linked to the groundwater model products and to increase the understanding of the soil water-groundwater-vegetation system.

Initially, the coupling of UZMs of different complexity to a commonly used groundwater model was explored. The EnKF was used to assimilate satellite-based ET fluxes to constrain estimates of WT and AET. Finally, the conditions associated with vegetation, soils, and depth to WT that provided the greatest improvements were identified. The findings of this thesis contribute to knowledge required for an increased use of satellite-based hydrological quantities to promote a better characterization of hydrogeological model's uncertainty.

In the next sections, the contributions of the thesis are summarized based on the three main research questions expressed in Section 2.4.

7.2 Summary of the Finding

7.2.1 Feasibility Study

This section lists the contributions of Chapter 4, which were triggered by the first research question:

Is it possible to assimilate remotely sensed ET to improve UZM-groundwater model outputs?

The fulcrum of this question was the interaction between ET and WT levels. A key aspect was to analyze if the updated state variables (i.e. WT levels and SM) were, in turn, improving the values of modeled ET and net-recharge.

In this phase, a conceptually-based model for the water flow in the unsaturated zone (UnSAT) was developed with the specific intent to account for the dynamics of ET. UnSAT was coupled to MODFLOW through a net-recharge flux, with a non-iterative feedback scheme which was a considered trade-off between numerical accuracy and the computational cost of fully coupled or iterative schemes. By specifically accounting for plant water extraction due to transpiration from groundwater, these coupled models (Configuration-1) explicitly modeled the feedback between AET and the state variables.

Configuration-1 was used to investigate the potential for improving hydrogeological model results through the assimilation of a synthetically generated AET dataset. The method was tested on a scenario representing a losing river in the South-East of South Australia. A domain with gradually deepening WT levels from one boundary to the other was generated. The evaluation was conducted on three different parts of the domain, representing a recharge, an extraction, and a transition area, respectively.

In all areas, the data assimilation consistently improved the modeled WT levels and SM values if the ensembles were adequately generated according to the verification metrics calculated for ET. Reduced errors were also seen in the fluxes, regardless of the WT levels. AET fluxes were improved for all the datasets over the entire simulation domain because the observation assimilated was an ET flux. Net-recharge fluxes have seen improvements both in RMSE and correlation. However, the correlation value in the recharge area remained low due to the filter continuously updating SM and WT levels, thus anticipating or delaying the time when net-recharge was delivered to (or extracted from) the groundwater.

These results were consistent with the EnKF objective of improving the modeled state variables without directly affecting the fluxes. But, by means of the feedback between AET and SM, and the relationship between net-recharge and the state variables, fluxes were also indirectly improved.

In the case of WT levels, the errors of the group considered appropriate were higher than the corresponding values seen in other groups. This was primarily due to the high magnitude of the perturbation used to create the forcing inputs. A

highly perturbed rainfall dataset, homogeneous over the relatively small domain, produced an increment in positive net-recharge that was not counterbalanced by high PET values because of the limits imposed by parameters (i.e. root depth) and water availability at the time (i.e. a deep WT with high PET). The ensemble verification metric calculated on the AET resulted to be adequate in the case of SM but led to excessively perturbed WT level ensembles. This suggested that a different ensemble generation method and verification metric have to be applied if the objective of the modeller is mainly focused on WT levels.

By assimilating AET fluxes, synthetically generated from a deterministic run of the coupled model, this part of the thesis did not thoroughly explore the biases likely to be seen in a real case scenario. This was partially accounted for by the two disturbed model parameter sets but cannot account for other sources of bias (e.g. WT level and SM observation error, forcing input bias, or AET observation error). It was acknowledged that a real-world case study would require careful calibration of the model on AET and WT to reproduce the link that in this study was inherently embedded in the synthetically generated observations. Nevertheless, the findings of this study were sufficient to indicate that groundwater models can be improved by the assimilation of remotely sensed AET values. They motivated the next stage of testing the synthetic approach by applying it to a real-case.

7.2.2 Model Complexity Assessment

This section summarizes the contributions of Chapter 5 that arose from the second research question:

What level of complexity of the unsaturated zone model is needed for the assimilation of ET into groundwater models?

The study explored the trade-off between model complexity and accuracy of the outputs. A simplified conceptual UZM and a detailed physically-based UZM were coupled to MODFLOW and calibrated to represent the link between WT levels and AET. This link was found to be a key aspect for the ET assimilation.

In this phase, a validation of the assimilation of satellite-based ET data (CMRSET) into the two coupled unsaturated zone-groundwater configurations was performed by applying the models to a water-limited pine plantation in the south-east of South Australia.

The key findings related to three main points were: the calibration on WT-ET, the effects of the assimilation on the configurations, and the information held by the ET. For the calibration, the study required to simultaneously calibrate the model on WT and AET. In this way, the groundwater-vegetation relationship is

represented and the assimilation of ET observations can positively inform the models.

The ET assimilation into the conceptual UZM produced the best results for the prognostic variables (WT, SM) and the diagnostic fluxes (AET, net-recharge). SM values were also slightly improved in both the upper and lower parts of the soil column. The reduced number of parameters of this configuration allowed for a simpler calibration, which was able to represent the WT dynamics. Similarly, the generation of an appropriate ensemble was more straightforward, mostly due to the model conceptualization, which permitted the WT to respond quickly to direct root water extraction by transpiration.

The ET assimilation into a physically-based UZM produced the largest improvements to the WT levels with a larger uncertainty reduction. This configuration was also capable of an adequate representation of the capillary fringe. The impact of the assimilation algorithm on SM was generally small, with a positive update for the lower soil layers, and a negative update for the upper layers. Calibrating this configuration involved a larger number of parameters and produced a good representation of the SM dynamics. However, due to the non-linearity introduced with the coupling, errors in the WT levels and ET fluxes were higher. The ensemble generation was constrained by the high model parameterization, making it more difficult to produce an appropriate ensemble that could preserve the ET-WT relationship.

Updating the entire soil column is an advantage of the assimilation of remotely sensed ET over satellite SM retrievals. ET rates are based on the influence of the moisture status of the entire root zone. Thus, assimilating ET overcomes the SM assimilation tendency to only produce stronger updates in the most superficial part of the soil because of the reduced correlation between the upper and lower SM contents.

This part of the thesis showed that the use of either a conceptual or a physically-based UZM for the assimilation of satellite-based ET estimates to inform hydrogeological models is possible. This was validated by the experiment conducted using real field and satellite data. The findings indicated that a simple conceptual model is sufficient for this purpose, thus using one configuration over the other should only be motivated by the specific purpose of the simulation and the information available.

This study represented a step towards the use of satellite-based ET retrievals for water resources management. With this in mind, and to prioritize areas for the effective use of the ET assimilation, the need for conducting more investigation in

areas with different groundwater, vegetation and soil conditions was made clear.

7.2.3 Area Prioritization

This section extends the work of Chapter 6, which was motivated by the final remarks of the previous section and the third research question:

Under which soil, vegetation, and depth to WT condition does the assimilation improve model performance?

At the origin of this question is the hypothesis of a greater impact of ET assimilation for shallow WT conditions with more prominent interaction with vegetated areas. Thus, the object of the investigation was primarily the effect of the depth to WT. Other parameters were the soil column characterization, the vegetation type, and bias correction of the assimilated values.

The last phase of the project focused on the assimilation of the CMRSET into the conceptual UZM configuration, which was shown to be adequate for this region and purpose by the findings of the previous research question. Configuration -1 was applied to four plantations selected because they showed a combination of WT depth, soil profiles and vegetation characteristics, representative of other plantations in the area.

The findings of this chapter indicated that the depth to WT had the greatest impact in affecting the ET assimilation outputs. As hypothesized, the ET assimilation resulted in reduced WT level errors, and improved ensemble distributions, for the cases where the vegetation had a direct access to groundwater, and thus a higher transpiration component. This experiment also included simulations with major drought events. For these cases, despite larger errors due to the model having been calibrated to different climate conditions, the assimilation was able to improve the model performance. On the contrary, at the location with deep WT the filter had a reduced effect, which was expected given the lack of direct correlation between AET and WT when the latter is deeper than 6 m.

The assimilation of AET that had been bias-corrected to enhance the localization of the CMRSET was also performed. This experiment rescaled and then assimilated the CMRSET observations to adjust the RS values closer to the field-based ET. It was concluded that the experiment was not sufficient to show the benefits of assimilating a locally bias-corrected CMRSET.

Errors in the AET fluxes were improved by the ET assimilation at all of the four locations except for the deep WT condition. These good performances for ET were consistent with the findings expressed in Chapters 4 and 5, and had to do with the

nature of the observations assimilated (i.e. AET fluxes). The degraded results at Jill are related to overestimated CMRSET observations, which are averaged over an area dominated by trees able to access groundwater while Jill was not showing this ability.

7.3 Contribution

This thesis explored the use of remotely sensed ET data for constraining unobservable estimates (i.e. net recharge) calculated by hydrogeological models. As a result of the filter update, improving the AET fluxes led to better net-recharge estimates. Thus, as net-recharge is the quantity that drives the WT dynamics, the modelled link between AET and WT is strengthened, especially when the water table levels are within about 6 m from the soil surface.

As hypothesized in Chapter 2, the locations with high interaction between WT and vegetation (i.e. root water extraction from WT) showed the highest data assimilation improvements for WT levels, SM, and AET estimate. The maximum depth to which there is a benefit in assimilating AET estimates is not clearly defined. However, it was seen that a positive filter update was occurring for WT levels up to -6 m.

The findings suggested that the use of ET assimilation in groundwater models is also a valuable tool for the quantitative management of groundwater resources in silvicultural areas. In Chapter 6, the ET assimilation provided a substantial reduction of the residuals seen for the AET fluxes throughout all the experiments. The error reduction, in turn, led to improved AET volumes, particularly in changing climatic conditions. Thus, it was recognized to be a useful tool for the assessment of the water consumption of plantations accessing groundwater.

However, the anticipated advantage of updating the entire soil column by assimilating ET, based on ET being influenced by the moisture status of the entire root zone, could not be entirely demonstrated. It was shown that assimilating ET overcomes the SM assimilation artifact of mostly updating the upper soil fringe, but the updates of the deep SM content were marginal and cannot be considered conclusive.

7.4 Limitations & Future Developments

The purpose of this thesis is to pave the way for the ET data assimilation into hydrogeological models at an operational level. In order to foster the use of this methodology, it is important to illustrate the limitations encountered in the development of this technique and identify possible developments.

The experiments described in Chapters 4, 5 and 6 use climatic inputs from an area characterized by semi-arid, vegetated conditions. Further testing is required for other climatic types, such as energy limited areas, or different vegetation types, such as grasses or sparse vegetation.

A further note involves the generation of the ensembles. A large effort was made in generating correct AET ensembles which maintained the ET-WT level relationship. It can be summarized as an evolution from the simple forcing inputs perturbation, applied for Chapter 4, to a more advanced ensemble generation in Chapter 5 and 6, combining parameters and forcing inputs. However, as required from the Kalman Filters, the added perturbation was sampled from normal distributions, which meant that some datasets had to be limited to preserve physical meaning (e.g. no negative rainfall). This part of the method would be interesting to improve and further investigate. At the same time, the use of other assimilation techniques, such as variational algorithms (Reichle, McLaughlin, and Entekhabi, 2002) or particle filters (Nejadi, Trivedi, and Leung, 2012), which have been proven to perform well in non-linear/non-Gaussian distributions, could improve or overcome the problems with the ensemble generations.

The literature review identified a number of algorithms based on satellite RS data which were capable of providing ET estimates at a continental scale (AWRA, CMRSET, ET-Look, NDTI) (King et al., 2011). Although CMRSET is one of the most accurate products for Australian conditions at a continental scale, the assimilation of other algorithms may perform better. This can be the case with ET datasets calibrated on a smaller scale and for specific conditions.

The natural development for the methodology described in this thesis is the application to larger regions. The challenges of this upscaling are not merely related to the computational burden required by running ensemble simulations for large scale, coupled saturated/unsaturated models. For instance, issues may arise from the spatial covariance of forcing inputs. In the experiments described in this thesis, not all locations had the same forcing input perturbation fraction, but this did not create a problem for the simulations as they were individually performed. At a large scale, either applying a constant perturbation fraction on interpolated climatic inputs or introducing spatially variable perturbation fractions, could lead to

instabilities and inconsistencies that have not yet been explored. In a similar way, the spatial covariance of the assimilated ET values can lead to skewed updates of neighbour cells, potentially generating numerical instability for the groundwater model. Although the model framework introduced in this thesis is ready to be used at larger scales, these last aspects were not explored as we focused on point scale simulations.

The value of remotely sensed ET data has been shown to be high for constraining hydrogeological models. The assimilation of RS AET in combination with field-based groundwater levels may significantly improve the characterization of the entire soil column. The use of techniques based on Bayesian inference for the quantification of model's uncertainty (e.g. conceptual) is an active research field. Information, obtained from the updates performed with data assimilation, may be used to improve the understanding of processes taking place in the soil column. Hence, data assimilation can contribute to the goal of improving the structure and conceptualization of hydrogeological models.

Appendix A

UnSAT - Sensitivity Analysis

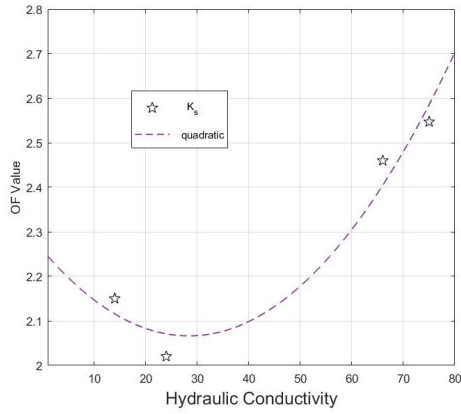
The sensitivity analysis of the model can be seen as a One-At-a-Time methodology. In this kind of tests only one parameter per time is changed and the values of an objective function (OF) compared. The OF is defined as a normalized RMSE following De Lathauwer et al. (2011):

$$RMSE = \frac{RMSE_{\theta_1}}{\sigma_{\theta_1}} + \frac{RMSE_{\theta_2}}{\sigma_{\theta_2}} + \dots + \frac{RMSE_{\theta_n}}{\sigma_{\theta_n}}, \quad (\text{A.1})$$

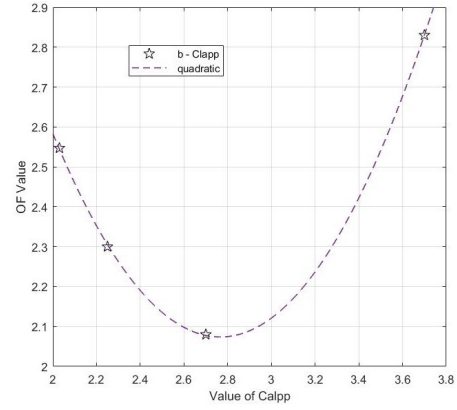
where the $RMSE_{\theta_n}$ and σ_n are the RMSE between model simulation and observation from the dataset for the $n - th$ bucket. Dividing the $RMSE_n$ by the standard deviation of the associated variable, the weight of each component is normalized.

This analysis provided information about the relative effect of parameters on the model results. Results of the sensitivity analysis were used to reduce the range values of the parameters for the PSO calibration.

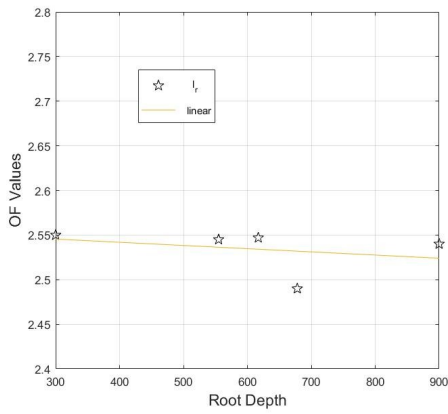
The model sensitivity is almost equal for the hydraulic conductivity K_s (Figure A.1 (A)), the value of p_z (Figure A.1 (D)), and the decay of hydraulic conductivity through the Wang parameter (Figure A.1(E)). UnSAT shows a greater sensitivity to the Clapp value for the drainage (Figure A.1 (B)), and appears to be less influenced by the variation of the root depth (Figure A.1 (C)). However, the latter consideration is not valid for the coupled configuration, where the root depth becomes an important parameter of the model.



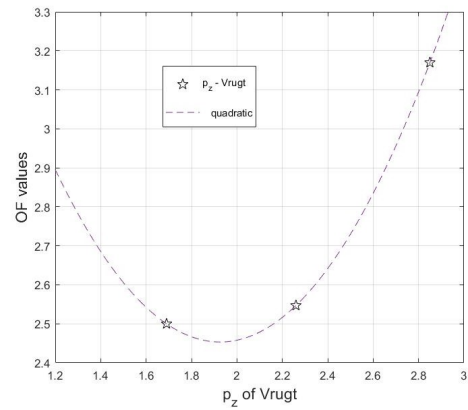
(A) Sensitivity to K_s



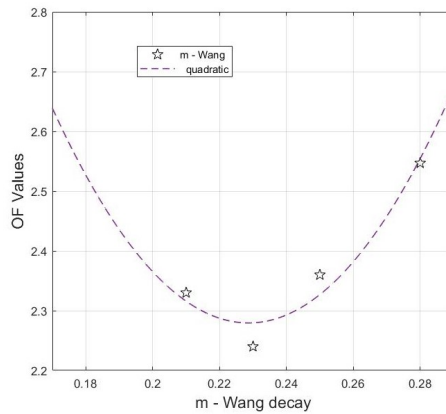
(B) Sensitivity to the drainage value



(C) Sensitivity to the root depth



(D) Sensitivity to p_z



(E) Sensitivity to Wang decay

FIGURE A.1: Results of the sensitivity analysis.

Appendix B

UnSAT - Calibration

B.1 Inputs and Calibration

UnSAT was firstly calibrated against the AgriSAR data set. This was a campaign run during the 2006 crop growing season in the North-east of Germany. The data set provided climatic input at the hourly frequency. The PET values are calculated by applying the surface energy balance to the values obtained from Bowen Ratio Energy Balance (BREB) station. The latent heat of vaporization, λ [J kg^{-1}], is a function of air temperature ($Temp$) and was calculated as in Shuttleworth (1992):

$$\lambda = 2.5 \cdot 10^6 - 2361 \cdot Temp. \quad (\text{B.1})$$

Values of PET [mm h^{-1}] were obtained from the latent heat flux LE [W m^{-2}] through

$$PET = \frac{LE \cdot 3.6 \cdot 10^6}{\lambda \cdot 1000}. \quad (\text{B.2})$$

The BREB dataset is composed of 1287 observations, with a total AET of 128.92 [mm]. These are spread over three periods roughly identified as April, May and June, and defined the calibration period.

B.1.1 Calibration Algorithm

The PSO used for the calibration is explained in Kennedy and Eberhart (1995) where an inertia weight factor ω is added to the original algorithm. For the purposes of this document only a reduced explication of the PSO is provided, the detailed solution can be seen in Shi and Eberhart (1998).

According to Scheerlinck et al. (2009) the iterative process updates position x_i and velocity v_i of each particle from the step k to $k + 1$ as

$$\begin{cases} v_i(k+1) = \omega \cdot v_i(k) + c_1 \cdot r_1(k) \cdot [\mathbf{p}_i(k) - \mathbf{x}_i(k)] + c_2 \cdot r_2(k) \cdot [\mathbf{p}_g(k) - \mathbf{x}_i(k)] \\ x_i(k+1) = x_i(k) + v_i(k) \end{cases} \quad (\text{B.3})$$

where c_1, c_2 are constant and referred to as cognitive and social parameters respectively. Here, $r_1(k)$ and $r_2(k)$ randomly vary between 0 and 1.

The PSO aims to search the best position of each particle that is placed in the space of the solution, thus find the optimal solution. Functions of OF as defined in equation B.5 are the initial positions $x_i(k)$ of the particles. Velocities $v_i(k+1)$ are then transmitted to these particles in order to find new positions $x_i(k+1)$ that are evaluated and stored if considered better than the previous. After a specified number of iterations (36 for our purposes) and considering the interaction with a population of other 30 particles that share information about the best position to find the optimal solution, the PSO stops (Kennedy and Eberhart, 1995). Results of this process are described in the section below.

B.1.2 Calibration

The AgriSAR campaign also measured hourly values of soil moisture at five depths, 50, 90, 150, 290, and 470 mm respectively. The calibration of the model is performed by minimizing the objective function (De Lathauwer et al., 2006):

$$RMSE = \frac{RMSE_{\theta_1}}{\sigma_{\theta_1}} + \frac{RMSE_{\theta_2}}{\sigma_{\theta_2}} + \dots + \frac{RMSE_{\theta_n}}{\sigma_{\theta_n}}, \quad (B.4)$$

where the $RMSE_{\theta_n}$ is the RMSE between the simulated soil moisture and the observations for the n -th bucket, and σ_n is the standard deviation of the soil moisture. Dividing the $RMSE_n$ by the σ_n normalized the weight of each component.

To maintain consistency between the depth of the observations and the discretization of the simulated soil column, layer one, two and five and observation at 50, 150 and 470 mm were considered. Thus, Eq. B.4 becomes

$$RMSE = \frac{RMSE_{\theta_1}}{\sigma_{\theta_1}} + \frac{RMSE_{\theta_2}}{\sigma_{\theta_2}} + \frac{RMSE_{\theta_5}}{\sigma_{\theta_5}}. \quad (B.5)$$

Six parameters were selected for the calibration through the PSO, each of them having an associated range in the algorithm. For the hydraulic conductivity (K_s) a range 1 – 200 mm/h was selected. The critical SM value (θ_*) has to be constrained between the wilting point and the saturation; in the literature this is usually found closer to the first rather than the latter (Laio et al., 2001). Therefore, the associated selected range was 0.1 – 0.3 mm³/mm³. The empirical factor p_z of Eq. 3.16 was tested between zero and four, as represented in figure B.1. Other values are the parameter b , in Eq. 3.3.1. The drainage between the layers and deep drainage from the lowest layer are sensitive to this parameter. The m value of the parabolic

TABLE B.1: Parameter, range, calibrated values and RMSE

Parameter	Range	Calibrated Value	Units
K_s	1-200	15	mm/h
θ_*	0.1-0.3	0.14	mm^3/mm^3
b	1 - 3.5	2.294	-
Z_m	100-2000	1290	mm
p_z	0.1-4	1.65	-
Overall RMSE	-	2.62	-

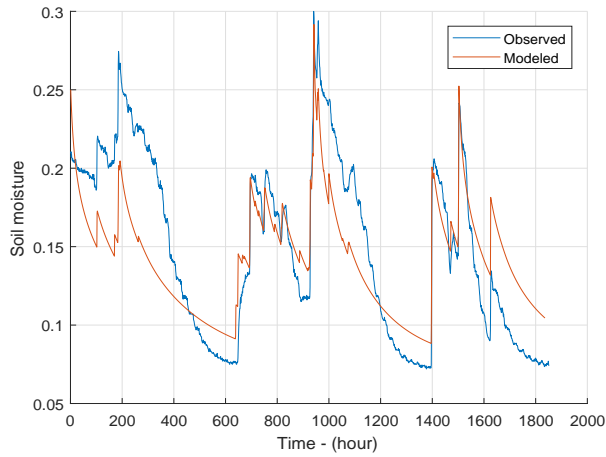


FIGURE B.1: Results of calibrated soil moisture values for the 50 mm depth observation and first model layer.

decay 3.25 is also part of the calibration; however, for the experiments presented in this thesis the exponential decay was used, thus this parameter is reported only for completeness. Another important parameter is the maximum root depth Z_m ; the results of the coupled models are sensitive to this value because it defines the maximum depth the root system is able to extract water from the soil.

Table B.1 shows the parameters that were calibrated, their range, and the results proposed by the PSO. Results of the soil moisture calibration with the parameters listed in the table are shown in figures B.1 to B.4, for depth 50, 150, 290 and 470 mm, respectively.

Hydraulic Conductivity Decay

Two possible hydraulic conductivity decay functions are implemented in the model as explained in section 3.3.4. The empirical parameter m was the object of the calibration for the parabolic decay, while for the exponential decay the parameter Z is a function of the maximum modelled depth and was not part of this calibration. Results of the simulations are shown in Table B.2, which reports the root mean square error (RMSE) between modeled and observed soil moisture, divided by the

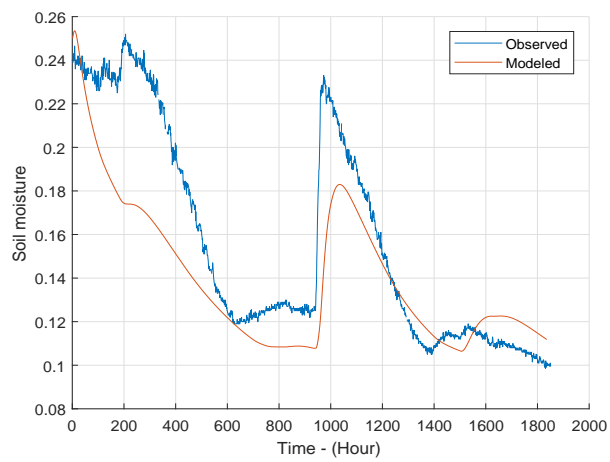


FIGURE B.2: Results of calibrated soil moisture values for the 150 mm depth observation and the second model layer.

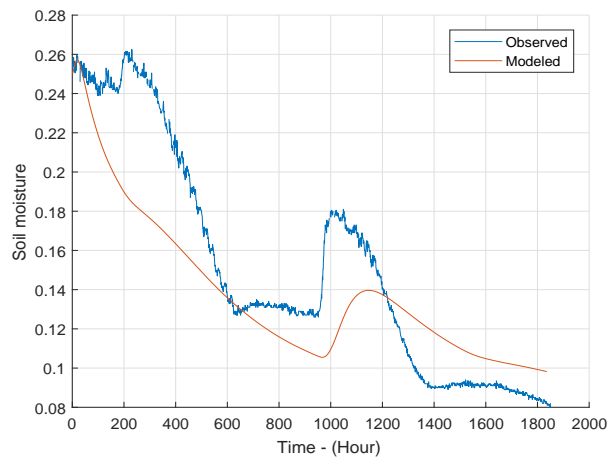


FIGURE B.3: Results of calibrated soil moisture values for the 290 mm depth observation and the third model layer.

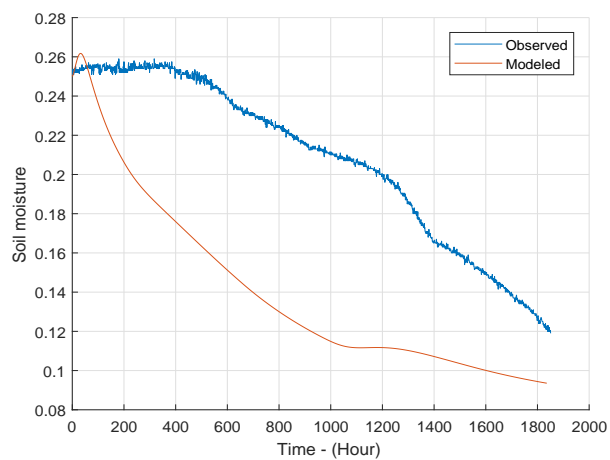


FIGURE B.4: Results of calibrated soil moisture values for the 470 mm depth observation and the fifth model layer.

standard deviation (σ). This is further described in section B.1.2. The best performance was obtained when the parabolic decay function was used; however, as the exponential decay is a function of the maximum root depth, it avoids to introduce another parameter in the calibration. For this reason, when detailed data are available for calibration, the m parameter can be an useful tool to tune the model. In less constrained situations the use of the $B = f(MD_{max})$ simplifies the calibration.

TABLE B.2: Parameters and normalized error for the different decay profiles.

Decay Type	Parameter	RMSE/SD
Linear	$m = 0.233$	3.06
Parabolic	$m = 0.260$	2.62
Exponential	$B = 1/1290$	2.80

Appendix C

Domain Sensitivity Analysis

This appendix presents the result of the sensitivity analysis of the model domain. The choice of the simple model domain is a result of numerical experiments which have shown us how it is possible to obtain similar water table dynamics with both a fine (20 cells in the x-axis) and coarse (5 cells in the x-axis) model domain. Figure C.1 shows the water table fluctuation, calculated with Configuration-1, in the central cell of the two domains simulating a similar location in the same study area. It is worth to say that the run-time for the fine set-up is roughly 5 times larger than for the coarse set-up.

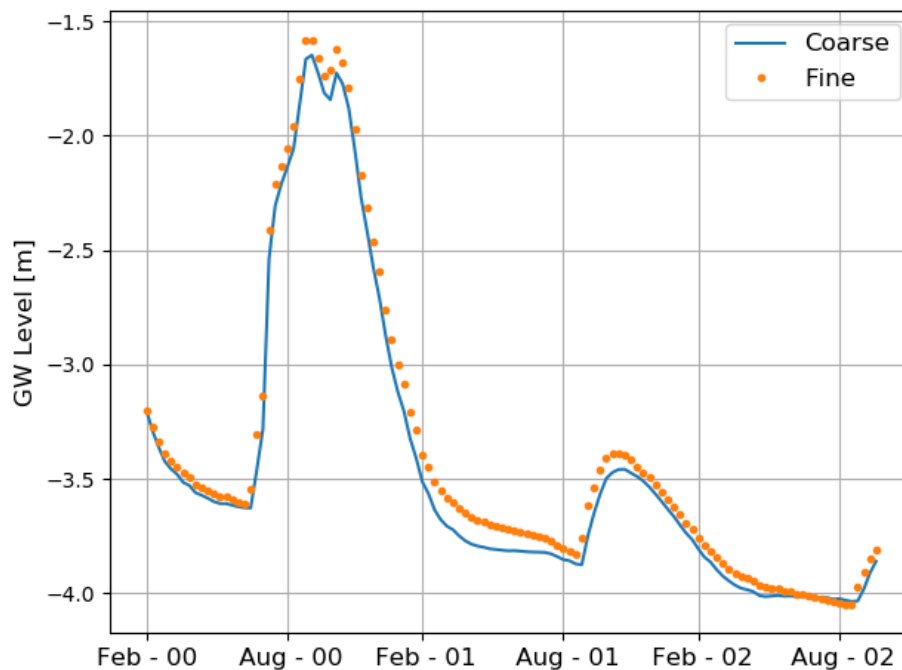


FIGURE C.1: Water table fluctuation at the cell in the centre of the domain for Configuration-1 after calibration. The simulation is based on real forcing inputs. The “Coarse” resolution is a 5 X 1 cell domain, the same as the one used for the experiment in this paper. The “Fine” resolution is a 20 X 1 cell domain.

Bibliography

- Abbaszadeh, P., H. Moradkhani, and D. N. Daescu (2019). "The Quest for Model Uncertainty Quantification: A Hybrid Ensemble and Variational Data Assimilation Framework". In: *Water Resour. Res.* 55.3, pp. 2407–2431. ISSN: 19447973. DOI: [10.1029/2018WR023629](https://doi.org/10.1029/2018WR023629).
- Allen, R. G., M. Tasumi, and R. Trezza (2007). "Satellite-Based Energy Balance for Mapping Evapotranspiration with Internalized Calibration (METRIC)—Model". In: *J. Irrig. Drain. Eng.* 133.4, pp. 380–394. ISSN: 0733-9437. DOI: [10.1061/\(ASCE\)0733-9437\(2007\)133:4\(380\)](https://doi.org/10.1061/(ASCE)0733-9437(2007)133:4(380)).
- Bakker, M. et al. (2016). "Scripting MODFLOW Model Development Using Python and FloPy". In: *Groundwater* 54.5, pp. 733–739. ISSN: 17456584. DOI: [10.1111/gwat.12413](https://doi.org/10.1111/gwat.12413).
- Banks, E. W., P. Brunner, and C. T. Simmons (2011). "Vegetation controls on variably saturated processes between surface water and groundwater and their impact on the state of connection". In: *Water Resour. Res.* 47.11, pp. 1–14. ISSN: 00431397. DOI: [10.1029/2011WR010544](https://doi.org/10.1029/2011WR010544).
- Barnes, W.L., T.S. Pagano, and V.V. Salomonson (1998). "Prelaunch characteristics of the Moderate Resolution Imaging Spectroradiometer (MODIS) on EOS-AM1". In: *IEEE Trans. Geosci. Remote Sens.* 36.4, pp. 1088–1100. DOI: [10.1109/36.700993](https://doi.org/10.1109/36.700993).
- Barthel, R. (2006). "Common problematic aspects of coupling hydrological models with groundwater flow models on the river catchment scale". In: *Adv. Geosci.* 9, pp. 63–71. ISSN: 1680-7359. DOI: [10.5194/adgeo-9-63-2006](https://doi.org/10.5194/adgeo-9-63-2006).
- Bastiaanssen, W.G.M. et al. (1998). "A remote sensing surface energy balance algorithm for land (SEBAL)." In: *J. Hydrol.* 212-213.JANUARY, pp. 213–229. ISSN: 00221694. DOI: [10.1016/S0022-1694\(98\)00254-6](https://doi.org/10.1016/S0022-1694(98)00254-6).
- Batelaan, O. and F. De Smedt (2007). "GIS-based recharge estimation by coupling surface-subsurface water balances". In: *J. Hydrol.* 337.3-4, pp. 337–355. ISSN: 00221694. DOI: [10.1016/j.jhydrol.2007.02.001](https://doi.org/10.1016/j.jhydrol.2007.02.001).
- Bennett, S. Ji, T. F.A. Bishop, and R. W. Vervoort (2013). "Using SWAP to quantify space and time related uncertainty in deep drainage model estimates: A case study from northern NSW, Australia". In: *Agric. Water Manag.* 130, pp. 142–153. DOI: [10.1016/j.agwat.2013.08.020](https://doi.org/10.1016/j.agwat.2013.08.020).
- Benyon, R. G. and T. M. Doody (2004). *Water Use by Tree Plantations in South East South Australia*. CSIRO Forestry and Forest Products. Tech. rep.

- Benyon, R. G. and T. M. Doody (2015). "Comparison of interception, forest floor evaporation and transpiration in *Pinus radiata* and *Eucalyptus globulus* plantations". In: *Hydrol. Process.* 29.6, pp. 1173–1187. ISSN: 08856087. DOI: [10.1002/hyp.10237](https://doi.org/10.1002/hyp.10237). arXiv: [hyp.10237 \[10.1002\]](https://arxiv.org/abs/10.1002/hyp.10237).
- Benyon, R. G., S. Theiveyanathan, and T. M. Doody (2006). "Impacts of tree plantations on groundwater in south-eastern Australia". In: *Aust. J. Bot.* 54.2, p. 181. ISSN: 0067-1924. DOI: [10.1071/BT05046](https://doi.org/10.1071/BT05046).
- Benyon, R. G. et al. (2008). *Plantation forest water use in southwest Victoria*. Tech. rep. CSIRO: Water for a Healthy Country National Research Flagship.
- Besbes, M. and G. De Marsily (1984). "From infiltration to recharge: use of a parametric transfer function". In: *J. Hydrol.* 74.3-4, pp. 271–293. ISSN: 00221694. DOI: [10.1016/0022-1694\(84\)90019-2](https://doi.org/10.1016/0022-1694(84)90019-2).
- Beven, K. and A. Binley (1992). "The future of distributed models: Model calibration and uncertainty prediction". In: *Hydrol. Process.* 6.3, pp. 279–298. ISSN: 10991085. DOI: [10.1002/hyp.3360060305](https://doi.org/10.1002/hyp.3360060305).
- Beven, K. J. and M. J. Kirkby (1979). "A physically based, variable contributing area model of basin hydrology". In: *Hydrol. Sci. Bull.* 24.1, pp. 43–69. ISSN: 03036936. DOI: [10.1080/02626667909491834](https://doi.org/10.1080/02626667909491834).
- Bindlish, R., W. T. Crow, and T. J. Jackson (2009). "Role of passive microwave remote sensing in improving flood forecasts". In: *IEEE Geosci. Remote Sens. Lett.* 6.1, pp. 112–116. ISSN: 1545598X. DOI: [10.1109/LGRS.2008.2002754](https://doi.org/10.1109/LGRS.2008.2002754).
- Brunner, P. et al. (2007). "How can remote sensing contribute in groundwater modeling?" In: *Hydrogeol. J.* 15.1, pp. 5–18. ISSN: 14312174. DOI: [10.1007/s10040-006-0127-z](https://doi.org/10.1007/s10040-006-0127-z).
- Campbell, Gaylon S (1974). "A simple method for determining unsaturated conductivity from moisture retention data". In: *Soil science* 117.6, pp. 311–314.
- Camporese, M. et al. (2009). "Ensemble Kalman filter data assimilation for a process-based catchment scale model of surface and subsurface flow". In: *Water Resour. Res.* 45.10, pp. 1–14. ISSN: 00431397. DOI: [10.1029/2008WR007031](https://doi.org/10.1029/2008WR007031).
- Camporese, M. et al. (2010). "Surface-subsurface flow modeling with path-based runoff routing, boundary condition-based coupling, and assimilation of multi-source observation data". In: *Water Resour. Res.* 46.2. ISSN: 00431397. DOI: [10.1029/2008WR007536](https://doi.org/10.1029/2008WR007536).
- Carroll, R. W. H. et al. (2015). "Calibrating a Basin-Scale Groundwater Model to Remotely Sensed Estimates of Groundwater Evapotranspiration". In: *J. Am. Water Resour. Assoc.* ISSN: 17521688. DOI: [10.1111/jawr.12285](https://doi.org/10.1111/jawr.12285).
- Charney, J.G., M. Halem, and R. Jastrow (1969). "Use of incomplete historical data to infer the present state of the atmosphere." In: *J. Atmos. Sci* 26, pp. 1160–1163.
- Chemin, Y., K. Honda, and A. V. M. Ines (2004). "Genetic algorithm for assimilating remotely sensed evapotranspiration data using a soil-water-atmosphere-plant model—implementation issues". In: *FOSS/GRASS User Conf. Bangkok, Thailand*. September, pp. 88–92.

- Cheng, W.-C. et al. (2011). "A real-time groundwater management model using data assimilation". In: *Water Resour. Res.* 47.6. ISSN: 00431397. DOI: [10.1029/2010WR009770](https://doi.org/10.1029/2010WR009770).
- Clapp, R. B. and G. M. Hornberger (1978). "Empirical equations for some soil hydraulic properties". In: *Water Resour. Res.* 14.4, pp. 601–604. ISSN: 19447973. DOI: [10.1029/WR014i004p00601](https://doi.org/10.1029/WR014i004p00601). arXiv: [2014WR016527](https://arxiv.org/abs/2014WR016527) [[10.1002](https://doi.org/10.1002)].
- Coelho, V. H. R. et al. (2017). "Alluvial groundwater recharge estimation in semi-arid environment using remotely sensed data". In: *J. Hydrol.* 548, pp. 1–15. ISSN: 00221694. DOI: [10.1016/j.jhydrol.2017.02.054](https://doi.org/10.1016/j.jhydrol.2017.02.054).
- Crosbie, R. S. et al. (2015). "Ground truthing groundwater-recharge estimates derived from remotely sensed evapotranspiration: a case in South Australia". In: *Hydrogeol. J.* 23.2, pp. 335–350. ISSN: 1431-2174. DOI: [10.1007/s10040-014-1200-7](https://doi.org/10.1007/s10040-014-1200-7).
- Crosbie, R. S. et al. (2017). "Estimating groundwater recharge and its associated uncertainty : Use of regression kriging and the chloride mass balance method". In: *J. Hydrol.* ISSN: 0022-1694. DOI: [10.1016/j.jhydrol.2017.08.003](https://doi.org/10.1016/j.jhydrol.2017.08.003).
- Daley, R. (1991). "Atmospheric data analysis". In: *Cambridge Univ. Press*, 460 pp.
- Daneshmand, H. et al. (2019). "Water and salt balance modelling of intermittent catchments using a physically-based integrated model". In: *J. Hydrol.* 568. November 2018, pp. 1017–1030. ISSN: 00221694. DOI: [10.1016/j.jhydrol.2018.11.035](https://doi.org/10.1016/j.jhydrol.2018.11.035).
- De Lannoy, G. J.M. et al. (2006). "Assessment of model uncertainty for soil moisture through ensemble verification". In: *J. Geophys. Res. Atmos.* 111.10. ISSN: 01480227. DOI: [10.1029/2005JD006367](https://doi.org/10.1029/2005JD006367).
- De Lathauwer, E. et al. (2011). "Estimation of the Spatially Distributed Surface Energy Budget for AgriSAR 2006, Part II: Integration of Remote Sensing and Hydrologic Modeling". In: *IEEE J. Sel. Top. Appl. Earth Obs. Remote Sens.* 4.2, pp. 482–493. ISSN: 21511535. DOI: [10.1109/JSTARS.2010.2094997](https://doi.org/10.1109/JSTARS.2010.2094997).
- Diersch, H.-J.G. and O. Kolditz (1998). "Coupled groundwater flow and transport: 2. Thermohaline and 3D convection systems". In: *Adv. Water Resour.* 21.5, pp. 401–425. ISSN: 03091708. DOI: [10.1016/S0309-1708\(97\)00003-1](https://doi.org/10.1016/S0309-1708(97)00003-1).
- Doble, R. C. and R. S. Crosbie (2017). "Review: Current and emerging methods for catchment-scale modelling of recharge and evapotranspiration from shallow groundwater". In: *Hydrogeol. J.* 25.1, pp. 3–23. ISSN: 1431-2174. DOI: [10.1007/s10040-016-1470-3](https://doi.org/10.1007/s10040-016-1470-3).
- Doble, R. C. et al. (2015). *Goyder South East Project A new approach for modelling groundwater recharge in the South East of South Australia using MODFLOW*. Tech. rep. 33 King William Street Adelaide SA: Goyder Institute for water research.
- Doble, R. C. et al. (2017). "Emulation of recharge and evapotranspiration processes in shallow groundwater systems". In: *J. Hydrol.* 555, pp. 894–908. ISSN: 00221694. DOI: [10.1016/j.jhydrol.2017.10.065](https://doi.org/10.1016/j.jhydrol.2017.10.065).

- Donohue, R. J., T. R. McVicar, and M. L. Roderick (2010). "Assessing the ability of potential evaporation formulations to capture the dynamics in evaporative demand within a changing climate". In: *J. Hydrol.* 386.1-4, pp. 186–197. ISSN: 00221694. DOI: [10.1016/j.jhydrol.2010.03.020](https://doi.org/10.1016/j.jhydrol.2010.03.020).
- Donohue, R. J., M. L. Roderick, and T. R. McVicar (2007). "On the importance of including vegetation dynamics in Budyko's hydrological model". In: *Hydrol. Earth Syst. Sci.* 11.2, pp. 983–995. ISSN: 16077938. DOI: [10.5194/hess-11-983-2007](https://doi.org/10.5194/hess-11-983-2007).
- Dripps, W. R. and K. R. Bradbury (2007). "A simple daily soil-water balance model for estimating the spatial and temporal distribution of groundwater recharge in temperate humid areas". In: *Hydrogeol. J.* 15.3, pp. 433–444. ISSN: 14312174. DOI: [10.1007/s10040-007-0160-6](https://doi.org/10.1007/s10040-007-0160-6).
- Droogers, P., W. W. Immerzeel, and I. J. Lorite (2010). "Estimating actual irrigation application by remotely sensed evapotranspiration observations". In: *Agric. Water Manag.* 97.9, pp. 1351–1359. ISSN: 03783774. DOI: [10.1016/j.agwat.2010.03.017](https://doi.org/10.1016/j.agwat.2010.03.017).
- Droogers, P., A. van Loon, and W. W. Immerzeel (2008). "Quantifying the impact of model inaccuracy in climate change impact assessment studies using an agro-hydrological model". In: *Hydrol. Earth Syst. Sci.* 12, pp. 669–678. DOI: <https://doi.org/10.5194/hess-12-669-2008>.
- Droogers, P. et al. (2000). "Distributed agro-hydrological modeling of an irrigation system in western Turkey". In: *Agric. Water Manag.* 43.2, pp. 183–202. ISSN: 03783774. DOI: [10.1016/S0378-3774\(99\)00055-4](https://doi.org/10.1016/S0378-3774(99)00055-4).
- Dye, P. and D. Versfeld (2007). "Managing the hydrological impacts of South African plantation forests: An overview". In: *For. Ecol. Manage.* 251.1-2, pp. 121–128. ISSN: 03781127. DOI: [10.1016/j.foreco.2007.06.013](https://doi.org/10.1016/j.foreco.2007.06.013).
- Entekhabi, D. and M. Moghaddam (2007). "Mapping recharge from space: Roadmap to meeting the grand challenge". In: *Hydrogeol. J.* ISSN: 14312174. DOI: [10.1007/s10040-006-0120-6](https://doi.org/10.1007/s10040-006-0120-6).
- Entekhabi, D., H. Nakamura, and E.G. Njoku (1994). "Solving the inverse problem for soil moisture and temperature profiles by sequential assimilation of multifrequency remotely sensed observations". In: *IEEE Trans. Geosci. Remote Sens.* 32.2, pp. 438–448. ISSN: 0196-2892. DOI: [10.1109/36.295058](https://doi.org/10.1109/36.295058).
- Entekhabi, D. et al. (2010). "Performance Metrics for Soil Moisture Retrievals and Application Requirements". In: *J. Hydrometeorol.* 11.3, pp. 832–840. ISSN: 1525-755X. DOI: [10.1175/2010jhm1223.1](https://doi.org/10.1175/2010jhm1223.1).
- Evensen, G. (1994). "Sequential data assimilation with a nonlinear quasi-geostrophic model using Monte Carlo methods to forecast error statistics". In: *J. Geophys. Res.* 99.C5, p. 10143. ISSN: 0148-0227. DOI: [10.1029/94JC00572](https://doi.org/10.1029/94JC00572).
- Facchi, A et al. (2004). "Coupled SVAT-groundwater model for water resources simulation in irrigated alluvial plains". In: *Environ. Model. Softw.* 19.11, pp. 1053–1063. ISSN: 13648152. DOI: [10.1016/j.envsoft.2003.11.008](https://doi.org/10.1016/j.envsoft.2003.11.008).

- Farkas, C. et al. (2014). "Impact of expected climate change on soil water regime under different vegetation conditions". In: *Biol.* 69.11, pp. 1510–1519. ISSN: 13369563. DOI: [10.2478/s11756-014-0463-8](https://doi.org/10.2478/s11756-014-0463-8).
- Fatichi, S. et al. (2016). "An overview of current applications, challenges, and future trends in distributed process-based models in hydrology". In: *J. Hydrol.* 537, pp. 45–60. ISSN: 00221694. DOI: [10.1016/j.jhydro1.2016.03.026](https://doi.org/10.1016/j.jhydro1.2016.03.026).
- Feddes, R. A. et al. (1976). "Simulation of field water uptake by plants using a soil water dependent root extraction function". In: *J. Hydrol.* 31.1-2, pp. 13–26. ISSN: 00221694. DOI: [10.1016/0022-1694\(76\)90017-2](https://doi.org/10.1016/0022-1694(76)90017-2).
- Gelsinari, S. et al. (2020). "Feasibility of improving groundwater modeling by assimilating evapotranspiration rates." In: *Water Resour. Res.* ISSN: 0043-1397. DOI: [10.1029/2019WR025983](https://doi.org/10.1029/2019WR025983).
- Giroto, M. and M. Rodell (2019). *Terrestrial water storage*. Elsevier Inc., pp. 41–64. ISBN: 9780128148990. DOI: [10.1016/b978-0-12-814899-0.00002-x](https://doi.org/10.1016/b978-0-12-814899-0.00002-x).
- Giroto, M. et al. (2019). "Multi-sensor assimilation of SMOS brightness temperature and GRACE terrestrial water storage observations for soil moisture and shallow groundwater estimation". In: *Remote Sens. Environ.* 227. April, pp. 12–27. ISSN: 00344257. DOI: [10.1016/j.rse.2019.04.001](https://doi.org/10.1016/j.rse.2019.04.001).
- Gleeson, T. and A. H. Manning (2008). "Regional groundwater flow in mountainous terrain: Three-dimensional simulations of topographic and hydrogeologic controls". In: *Water Resour. Res.* 44.10. ISSN: 00431397. DOI: [10.1029/2008WR006848](https://doi.org/10.1029/2008WR006848).
- Glenn, E. P., P. L. Nagler, and A. R. Huete (2010). "Vegetation Index Methods for Estimating Evapotranspiration by Remote Sensing". In: *Surv. Geophys.* 31.6, pp. 531–555. ISSN: 0169-3298. DOI: [10.1007/s10712-010-9102-2](https://doi.org/10.1007/s10712-010-9102-2).
- Glenn, E. P. et al. (2011). "Actual evapotranspiration estimation by ground and remote sensing methods: the Australian experience". In: *Hydrol. Process.* 25.26, pp. 4103–4116. DOI: [10.1002/hyp.8391](https://doi.org/10.1002/hyp.8391).
- Gokmen, M. et al. (2013). "Assessing Groundwater Storage Changes Using Remote Sensing–Based Evapotranspiration and Precipitation at a Large Semiarid Basin Scale". In: *J. Hydrometeorol.* 14.6, pp. 1733–1753. DOI: [10.1175/JHM-D-12-0156.1](https://doi.org/10.1175/JHM-D-12-0156.1).
- Grinevskii, S. O. (2011). "Modeling root water uptake when calculating unsaturated flow in the vadose zone and groundwater recharge". In: *Moscow Univ. Geol. Bull.* 66.3, pp. 189–201. ISSN: 0145-8752. DOI: [10.3103/s0145875211030057](https://doi.org/10.3103/s0145875211030057).
- GSA (2009). *Managing the water resource impacts of plantation forests*. Tech. rep. Adelaide: Government of South Australia, pp. 1–44.
- Guerschman, J. P. et al. (2009). "Scaling of potential evapotranspiration with MODIS data reproduces flux observations and catchment water balance observations across Australia". In: *J. Hydrol.* 369.1-2, pp. 107–119. ISSN: 00221694. DOI: [10.1016/j.jhydro1.2009.02.013](https://doi.org/10.1016/j.jhydro1.2009.02.013).

- Güntner, A. (2008). "Improvement of global hydrological models using GRACE data". In: *Surv. Geophys.* 29.4-5, pp. 375–397. ISSN: 01693298. DOI: [10.1007/s10712-008-9038-y](https://doi.org/10.1007/s10712-008-9038-y). arXiv: [arXiv:1011.1669v3](https://arxiv.org/abs/1011.1669v3).
- Harbaugh, Arlen, W. (2005). "MODFLOW-2005, The U.S. Geological Survey Modular Ground-Water Model — the Ground-Water Flow Process". In: *U.S. Geol. Surv. Tech. Methods*, p. 253. ISSN: 6-A16.
- Hartanto, I. M. et al. (2017). "Data assimilation of satellite-based actual evapotranspiration in a distributed hydrological model of a controlled water system". In: *Int. J. Appl. Earth Obs. Geoinf.* 57, pp. 123–135. ISSN: 1872826X. DOI: [10.1016/j.jag.2016.12.015](https://doi.org/10.1016/j.jag.2016.12.015).
- He, X. et al. (2019). "Real-time simulation of surface water and groundwater with data assimilation". In: *Adv. Water Resour.* 127. September 2018, pp. 13–25. ISSN: 03091708. DOI: [10.1016/j.advwatres.2019.03.004](https://doi.org/10.1016/j.advwatres.2019.03.004).
- Hendricks Franssen, H. J. et al. (2011). "Operational real-time modeling with ensemble Kalman filter of variably saturated subsurface flow including stream-aquifer interaction and parameter updating". In: *Water Resour. Res.* ISSN: 00431397. DOI: [10.1029/2010WR009480](https://doi.org/10.1029/2010WR009480).
- Hendrickx, J. M.H. et al. (2016). "Benchmarking Optical/Thermal Satellite Imagery for Estimating Evapotranspiration and Soil Moisture in Decision Support Tools". In: *J. Am. Water Resour. Assoc.* 52.1, pp. 89–119. ISSN: 17521688. DOI: [10.1111/1752-1688.12371](https://doi.org/10.1111/1752-1688.12371).
- Hersbach, H. (2000). "Decomposition of the continuous ranked probability score for ensemble prediction systems". In: *Weather Forecast.* 15.5, pp. 559–570. ISSN: 08828156. DOI: [10.1175/1520-0434\(2000\)015<0559:DOTCRP>2.0.CO;2](https://doi.org/10.1175/1520-0434(2000)015<0559:DOTCRP>2.0.CO;2).
- Hopmans, J.W. and J.N.M. Stricker (1989). "Stochastic Description of Field-Measured Infiltration Data". In: *Trans. ASAE* 32.6, p. 1987. ISSN: 2151-0059. DOI: [10.13031/2013.31252](https://doi.org/10.13031/2013.31252). arXiv: [89/03.50](https://arxiv.org/abs/8903.50) [0022.1694].
- Houborg, R. et al. (2012). "Drought indicators based on model-assimilated Gravity Recovery and Climate Experiment (GRACE) terrestrial water storage observations". In: *Water Resour. Res.* ISSN: 00431397. DOI: [10.1029/2011WR011291](https://doi.org/10.1029/2011WR011291).
- Houser, P.R., G.J. M. De Lannoy, and J.P. Walker (2012). "Hydrologic Data Assimilation". In: *Approaches to Manag. Disaster - Assess. Hazards, Emergencies Disaster Impacts*, pp. 42–64. ISBN: 978-953-51-0294-6.
- Hughes, J. D. and J. Liu (2008). "MIKE SHE: Software for integrated surface water/ground water modeling". In: *Ground Water* 46.6, pp. 797–802. ISSN: 0017467X. DOI: [10.1111/j.1745-6584.2008.00500.x](https://doi.org/10.1111/j.1745-6584.2008.00500.x).
- Irmak, A. and B. Kamble (2009). "Evapotranspiration data assimilation with genetic algorithms and SWAP model for on-demand irrigation". In: *Irrig. Sci.* 28.1, pp. 101–112. ISSN: 0342-7188. DOI: [10.1007/s00271-009-0193-9](https://doi.org/10.1007/s00271-009-0193-9).
- Jackson, R. B., E. G. Jobbágy, and M. D. Noretto (2009). "Ecohydrology in a human-dominated landscape". In: *Ecohydrology* 2.3, pp. 383–389. ISSN: 19360584. DOI: [10.1002/eco.81](https://doi.org/10.1002/eco.81).

- Jiang, X. W. et al. (2009). "Effect of exponential decay in hydraulic conductivity with depth on regional groundwater flow". In: *Geophys. Res. Lett.* ISSN: 00948276. DOI: [10.1029/2009GL041251](https://doi.org/10.1029/2009GL041251).
- Jones, J.E. and C.S. Woodward (2001). "Newton-Krylov-multigrid solvers for large-scale, highly heterogeneous, variably saturated flow problems". In: *Adv. Water Resour.* 24.7, pp. 763–774. ISSN: 03091708. DOI: [10.1016/S0309-1708\(00\)00075-0](https://doi.org/10.1016/S0309-1708(00)00075-0).
- Kalman, R. E. (1960). "A New Approach to Linear Filtering and Prediction Problems". In: *J. Basic Eng.* 82.1, p. 35. DOI: [10.1115/1.3662552](https://doi.org/10.1115/1.3662552).
- Kennedy, J. and R. Eberhart (1995). "Particle Swarm Optimization". In: *Proc. 1995 IEEE Int. Conf. Neural Networks. Part 1 (of 6)* 4, pp. 1942–1948. ISSN: 1935-3812. DOI: [10.1007/s11721-007-0002-0](https://doi.org/10.1007/s11721-007-0002-0).
- Khatami, S. et al. (2019). "Equifinality and Flux Mapping: A New Approach to Model Evaluation and Process Representation Under Uncertainty". In: *Water Resour. Res.*, pp. 1–20. ISSN: 19447973. DOI: [10.1029/2018WR023750](https://doi.org/10.1029/2018WR023750).
- Kim, C. P. and J. N.M. Stricker (1996). "Influence of spatially variable soil hydraulic properties and rainfall intensity on the water budget". In: *Water Resour. Res.* 32.6, pp. 1699–1712. ISSN: 00431397. DOI: [10.1029/96WR00603](https://doi.org/10.1029/96WR00603).
- King, E A et al. (2011). "Actual evapotranspiration datasets for inter-comparison and evaluation". In: *Water a Heal. Ctry. Flagsh. Rep. Ser.* ISSN 1835-095X April.
- Kroes, J.G. et al. (2017). *SWAP version 4*. Tech. rep. Wageningen University & Recharge. DOI: [10.18174/416321](https://doi.org/10.18174/416321).
- Krysanova, V. and J.G. Arnold (2008). "Advances in ecohydrological modelling with SWAT - A review". In: *Hydrol. Sci. J.* 53.5, pp. 939–947. ISSN: 02626667. DOI: [10.1623/hysj.53.5.939](https://doi.org/10.1623/hysj.53.5.939).
- Kustas, W. P. and J. M. Norman (1996). "Use of remote sensing for evapotranspiration monitoring over land surfaces". In: *Hydrol. Sci. J.* 41.4, pp. 495–516. ISSN: 0262-6667. DOI: [10.1080/02626669609491522](https://doi.org/10.1080/02626669609491522).
- Laio, F. et al. (2001). "Plants in water-controlled ecosystems: Active role in hydrologic processes and response to water stress IV. Discussion of real cases". In: *Adv. Water Resour.* 24.7, pp. 745–762. ISSN: 03091708. DOI: [10.1016/S0309-1708\(01\)00007-0](https://doi.org/10.1016/S0309-1708(01)00007-0).
- Lamontagne S. and Leaney, F. W. and A.L. Herczeg (2005). "Groundwater-surface water interactions in a large semi-arid floodplain: Implications for salinity management". In: *Hydrol. Process.* 19.16, pp. 3063–3080. ISSN: 08856087. DOI: [10.1002/hyp.5832](https://doi.org/10.1002/hyp.5832).
- Leblanc, M. et al. (2012). "A review of historic and future hydrological changes in the Murray-Darling Basin". In: *Glob. Planet. Change* 80-81, pp. 226–246. DOI: [10.1016/j.gloplacha.2011.10.012](https://doi.org/10.1016/j.gloplacha.2011.10.012).
- Levy, G. et al. (2010). "Model Development Physically-based data assimilation". In: *Geosci. Model Dev.* 3, pp. 669–677. DOI: [10.5194/gmd-3-669-2010](https://doi.org/10.5194/gmd-3-669-2010).

- Li, P. and L. Ren (2019). "Evaluating the effects of limited irrigation on crop water productivity and reducing deep groundwater exploitation in the North China Plain using an agro-hydrological model: I. Parameter sensitivity analysis, calibration and model validation". In: *J. Hydrol.* 574.2, pp. 497–516. ISSN: 00221694. DOI: [10.1016/j.jhydrol.2019.04.053](https://doi.org/10.1016/j.jhydrol.2019.04.053). URL: <https://doi.org/10.1016/j.jhydrol.2019.04.053>.
- Li, Y. et al. (2016). *Application of remote sensing data to constrain operational rainfall-driven flood forecasting: A review*. DOI: [10.3390/rs8060456](https://doi.org/10.3390/rs8060456).
- Liu, Y. et al. (2012). "Advancing data assimilation in operational hydrologic forecasting: Progresses, challenges, and emerging opportunities". In: *Hydrol. Earth Syst. Sci.* 16.10, pp. 3863–3887. ISSN: 10275606. DOI: [10.5194/hess-16-3863-2012](https://doi.org/10.5194/hess-16-3863-2012).
- Long, D., L. Longuevergne, and B.R. Scanlon (2014). "Uncertainty in evapotranspiration from land surface modeling, remote sensing, and GRACE satellites." In: *Water Resour. Res.* 50, pp. 1131–1151. DOI: [10.1002/2013WR014581](https://doi.org/10.1002/2013WR014581).
- Lu, Y., S. C. Steele-Dunne, and G. J.M. De Lannoy (2020). "Improving soil moisture and surface turbulent heat flux estimates by assimilation of SMAP brightness temperatures or soil moisture retrievals and GOES land surface temperature retrievals". In: *J. Hydrometeorol.* 21.2, pp. 183–203. ISSN: 15257541. DOI: [10.1175/JHM-D-19-0130.1](https://doi.org/10.1175/JHM-D-19-0130.1).
- Lucas, M. et al. (2015). "Evaluation of remotely sensed data for estimating recharge to an outcrop zone of the Guarani Aquifer System (South America)". In: *Hydrogeol. J.* 23.5, pp. 961–969. ISSN: 1431-2174. DOI: [10.1007/s10040-015-1246-1](https://doi.org/10.1007/s10040-015-1246-1).
- Madry, S., J. Pelton, and A. Bukley (2010). "Satellites in the service to humanity, in The Farthest Shore: A 21st Century Guide to Space 2." In: *Apogee Press. Burlingt.*, p. 1. ISSN: 1098-6596. DOI: [10.1007/978-1-4419-7671-0](https://doi.org/10.1007/978-1-4419-7671-0). arXiv: [arXiv:1011.1669v3](https://arxiv.org/abs/1011.1669v3).
- Markstrom, S.L. et al. (2008). "GSFLOW—Coupled Ground-Water and Surface-Water Flow Model Based on the Integration of the Precipitation-Runoff Modeling System (PRMS) and the Modular Ground-Water Flow Model (MODFLOW-2005)". In: *U.S. Geol. Surv. Techniques and Methods 6-D1*, p. 240. DOI: [10.13140/2.1.2741.9202](https://doi.org/10.13140/2.1.2741.9202).
- Mccabe, M F, J D Kalma, and S W Franks (2005). "Spatial and temporal patterns of land surface fluxes from remotely sensed surface temperatures within an uncertainty modelling framework". In: *Hydrol. Earth Syst. Sci.* 9, pp. 467–480.
- McCabe, M. F. et al. (2017). "The future of Earth observation in hydrology". In: *Hydrol. Earth Syst. Sci.* 21.7, pp. 3879–3914. ISSN: 16077938. DOI: [10.5194/hess-21-3879-2017](https://doi.org/10.5194/hess-21-3879-2017).
- Melsen, L. et al. (2018). "Mapping (dis)agreement in hydrologic projections". In: *Hydrol. Earth Syst. Sci.* 22, pp. 1775–1791. DOI: [10.5194/hess-22-1775-2018](https://doi.org/10.5194/hess-22-1775-2018).

- Mensforth, L.J. et al. (1994). "Sources of water used by riparian *Eucalyptus camaldulensis* overlying highly saline groundwater". In: *Oecologia* 100.1-2, pp. 21–28. ISSN: 00298549. DOI: [10.1007/BF00317126](https://doi.org/10.1007/BF00317126).
- Miller, J. (2019). *La Niña and the Making of Climate Optimism*. Cham: Springer International Publishing. ISBN: 978-3-319-76140-4. DOI: [10.1007/978-3-319-76141-1](https://doi.org/10.1007/978-3-319-76141-1).
- Miller, R. N., M. Ghil, and F. Gauthiez (1994). *Advanced Data Assimilation in Strongly Nonlinear Dynamical-Systems*. DOI: [Doi10.1175/1520-0469\(1994\)051<1037:Adaisn>2.0.Co;2](https://doi.org/10.1175/1520-0469(1994)051<1037:Adaisn>2.0.Co;2).
- Mitchell, H. L., P. L. Houtekamer, and G. Pellerin (2002). "Ensemble Size, Balance, and Model-Error Representation in an Ensemble Kalman Filter*". In: *Mon. Weather Rev.* 130.11, pp. 2791–2808. ISSN: 0027-0644. DOI: [10.1175/1520-0493\(2002\)130<2791:ESBAME>2.0.CO;2](https://doi.org/10.1175/1520-0493(2002)130<2791:ESBAME>2.0.CO;2).
- Mohanty, B. P. et al. (2013). "Remote Sensing for Vadose Zone Hydrology—A Synthesis from the Vantage Point". In: *Vadose Zo. J.* 12.3, pp. 1–6. ISSN: 1539-1663. DOI: [10.2136/vzj2013.07.0128](https://doi.org/10.2136/vzj2013.07.0128).
- Montzka, C. et al. (2011). "Hydraulic parameter estimation by remotely-sensed top soil moisture observations with the particle filter". In: *J. Hydrol.* 399.3-4, pp. 410–421. ISSN: 00221694. DOI: [10.1016/j.jhydrol.2011.01.020](https://doi.org/10.1016/j.jhydrol.2011.01.020).
- Montzka, C. et al. (2012). *Multivariate and multiscale data assimilation in terrestrial systems: A review*. DOI: [10.3390/s121216291](https://doi.org/10.3390/s121216291).
- Múnch, Z. et al. (2013). "Satellite earth observation as a tool to conceptualize hydrogeological fluxes in the Sandveld, South Africa". In: *Hydrogeol. J.* 21.5, pp. 1053–1070. DOI: [10.1007/s10040-013-1004-1](https://doi.org/10.1007/s10040-013-1004-1).
- Nearing, G. et al. (2018). "The Efficiency of Data Assimilation". In: *Water Resour. Res.* ISSN: 00431397. DOI: [10.1029/2017WR020991](https://doi.org/10.1029/2017WR020991).
- Nejadi, S., J. J. Trivedi, and J. Leung (2012). "Ensemble Kalman Filter predictor bias correction method for non-Gaussian geological facies detection". In: *IFAC Proc. Vol.* ISBN: 9783902661999. DOI: [10.3182/20120531-2-NO-4020.00023](https://doi.org/10.3182/20120531-2-NO-4020.00023).
- Neumann, R. B. and Z. G. Cardon (2012). "The magnitude of hydraulic redistribution by plant roots: a review and synthesis of empirical and modeling studies." In: *New Phytol.* 194.2, pp. 337–52. ISSN: 1469-8137. DOI: [10.1111/j.1469-8137.2012.04088.x](https://doi.org/10.1111/j.1469-8137.2012.04088.x).
- Ng, G.H.C. et al. (2009). "Using data assimilation to identify diffuse recharge mechanisms from chemical and physical data in the unsaturated zone". In: *Water Resour. Res.* 45.9. ISSN: 00431397. DOI: [10.1029/2009WR007831](https://doi.org/10.1029/2009WR007831).
- O'Reilly, A. M. (2004). "A Method for Simulating Transient Ground-Water Recharge in Deep Water-Table Settings in Central Florida by Using a Simple Water-Balance / Transfer-Function Model". In: *U.S. Geol. Surv. Sci. Investig. Rep.* 2004-5195, p. 49.

- Orellana, F. et al. (2012). "Monitoring and modeling water-vegetation interactions in groundwater-dependent ecosystems". In: *Rev. Geophys.* 50.3. DOI: [10.1029/2011RG000383](https://doi.org/10.1029/2011RG000383).
- Oreskes, N., K. Shrader-Frechette, and K. Belitz (1994). "Verification, validation, and confirmation of numerical models in the earth sciences". In: *Science* (80-.). 263.5147, pp. 641–646. ISSN: 00368075. DOI: [10.1126/science.263.5147.641](https://doi.org/10.1126/science.263.5147.641).
- Paniconi, C. et al. (2003). "Newtonian nudging for a Richards equation-based distributed hydrological model". In: *Adv. Water Resour.* 26.2, pp. 161–178. ISSN: 03091708. DOI: [10.1016/S0309-1708\(02\)00099-4](https://doi.org/10.1016/S0309-1708(02)00099-4).
- Pauwels, V. R. N. and G. J. M. De Lannoy (2009). "Ensemble-based assimilation of discharge into rainfall-runoff models: A comparison of approaches to mapping observational information to state space". In: *Water Resour. Res.* ISSN: 00431397. DOI: [10.1029/2008WR007590](https://doi.org/10.1029/2008WR007590).
- Pauwels, V. R. N. et al. (2001). "The importance of the spatial patterns of remotely sensed soil moisture in the improvement of discharge predictions for small-scale basins through data assimilation". In: *J. Hydrol.* 251.1-2, pp. 88–102. ISSN: 00221694. DOI: [10.1016/S0022-1694\(01\)00440-1](https://doi.org/10.1016/S0022-1694(01)00440-1).
- Pauwels, V. R. N. et al. (2013). "Simultaneous estimation of model state variables and observation and forecast biases using a two-stage hybrid Kalman filter". In: *Hydrol. Earth Syst. Sci.* 17.9, pp. 3499–3521. ISSN: 1607-7938. DOI: [10.5194/hess-17-3499-2013](https://doi.org/10.5194/hess-17-3499-2013).
- Pelton, Joseph N., Scott Madry, and Sergio Camacho-Lara (2017). *Handbook of Satellite Applications*. Ed. by J. N. Pelton, S. Madry, and S. Camacho-Lara. Cham: Springer International Publishing. ISBN: 978-3-319-23385-7. DOI: [10.1007/978-3-319-23386-4](https://doi.org/10.1007/978-3-319-23386-4).
- Peterson, T. J. and A. W. Western (2014). "Multiple hydrological attractors under stochastic daily forcing: 2. Can multiple attractors exist?" In: *Water Resour. Res.* 50.4, pp. 2993–3009. ISSN: 00431397. DOI: [10.1002/2012WR013003](https://doi.org/10.1002/2012WR013003).
- Pinheiro, E. A. R., Q. de Jong van Lier, and J. Šimůnek (2019). "The role of soil hydraulic properties in crop water use efficiency: A process-based analysis for some Brazilian scenarios". In: *Agric. Syst.* 173. December 2018, pp. 364–377. ISSN: 0308521X. DOI: [10.1016/j.agsy.2019.03.019](https://doi.org/10.1016/j.agsy.2019.03.019).
- Pipunic, R. C., D. Ryu, and J. P. Walker (2014). "Assessing Near-Surface Soil Moisture Assimilation Impacts on Modeled Root-Zone Moisture for an Australian Agricultural Landscape". In: *Remote Sens. Terr. Water Cycle* 9781118872, pp. 305–317. DOI: [10.1002/9781118872086.ch18](https://doi.org/10.1002/9781118872086.ch18).
- Pipunic, R. C., J. P. Walker, and A. W. Western (2008). "Assimilation of remotely sensed data for improved latent and sensible heat flux prediction: A comparative synthetic study". In: *Remote Sens. Environ.* 112.4, pp. 1295–1305. ISSN: 00344257. DOI: [10.1016/j.rse.2007.02.038](https://doi.org/10.1016/j.rse.2007.02.038).

- Rajabi, M. M., B. Ataie-Ashtiani, and C. T. Simmons (2018). "Model-data interaction in groundwater studies: Review of methods, applications and future directions". In: *J. Hydrol.* 567, September, pp. 457–477. ISSN: 00221694. DOI: [10.1016/j.jhydrol.2018.09.053](https://doi.org/10.1016/j.jhydrol.2018.09.053).
- Reichle, R., D.B. McLaughlin, and D. Entekhabi (2002). "Hydrologic data assimilation with the ensemble Kalman filter." In: *Mon. Weather Rev.* 130.1, pp. 103–114. DOI: [10.1175/1520-0493\(2002\)130<0103:HDAWTE>2.0.CO;2](https://doi.org/10.1175/1520-0493(2002)130<0103:HDAWTE>2.0.CO;2).
- Reichle, R. H. (2008). "Data assimilation methods in the Earth sciences". In: *Adv. Water Resour.* 31.11, pp. 1411–1418. ISSN: 03091708. DOI: [10.1016/j.advwatres.2008.01.001](https://doi.org/10.1016/j.advwatres.2008.01.001).
- Renard, B. et al. (2010). "Understanding predictive uncertainty in hydrologic modeling: The challenge of identifying input and structural errors". In: *Water Resour. Res.* 46.5, pp. 1–22. ISSN: 00431397. DOI: [10.1029/2009WR008328](https://doi.org/10.1029/2009WR008328).
- Scanlon, B. R., R. W. Healy, and P. G. Cook (2002). "Choosing appropriate techniques for quantifying groundwater recharge". In: *Hydrogeol. J.* 10.1, pp. 18–39. ISSN: 14312174. DOI: [10.1007/s10040-001-0176-2](https://doi.org/10.1007/s10040-001-0176-2).
- Scheerlinck, K. et al. (2009). "Calibration of a water and energy balance model: Recursive parameter estimation versus particle swarm optimization". In: *Water Resour. Res.* 45.10. ISSN: 00431397. DOI: [10.1029/2009WR008051](https://doi.org/10.1029/2009WR008051).
- Schneider, R., H. J. Henriksen, and S. Stisen (2020). "A robust objective function for calibration of groundwater models in light of deficiencies of model structure and observations". In: *Hydrol. Earth Syst. Sci. Discuss.* January, pp. 1–26. ISSN: 1027-5606. DOI: [10.5194/hess-2019-685](https://doi.org/10.5194/hess-2019-685).
- Schumann, A. H. and M. Antl (2001). "Probabilistic characterization of uncertainties of climate change impact assessments". In: *IAHS-AISH Publ.* 268, pp. 247–254. ISSN: 01447815.
- Schuermans, J.M. et al. (2003). "Assimilation of remotely sensed latent heat flux in a distributed hydrological model". In: *Adv. Water Resour.* 26.2, pp. 151–159. ISSN: 03091708. DOI: [10.1016/S0309-1708\(02\)00089-1](https://doi.org/10.1016/S0309-1708(02)00089-1).
- Shi, Y. and R. Eberhart (1998). "A modified particle swarm optimizer". In: *1998 IEEE Int. Conf. Evol. Comput. Proceedings. IEEE World Congr. Comput. Intell. (Cat. No.98TH8360)*. IEEE, pp. 69–73. ISBN: 0-7803-4869-9. DOI: [10.1109/ICEC.1998.699146](https://doi.org/10.1109/ICEC.1998.699146). arXiv: [0-7803-4869-9198](https://arxiv.org/abs/0-7803-4869-9198){\}\$}10.0001998EEE.
- Shrestha, A., R. Sada, and L. Melsen (2014). "Adapting to Peri-urban Water Insecurity Induced by Urbanization and Climate Change". In: *Hydro Nepal J. Water, Energy Environ.* 14, pp. 43–48. ISSN: 1998-5452. DOI: [10.3126/hn.v14i0.11259](https://doi.org/10.3126/hn.v14i0.11259).
- Shuttleworth, W. J. (1992). "Evaporation". In: *Handb. Hydrol.* Ed. by D. R. Maidment. Trelea. New York.: McGraw-Hill, pp. 4.1–4.53.
- Silberstein, R. et al. (2009). *A vertical flux model for the Perth groundwater region (PRAMS)*. Tech. rep. June. DOI: [978-1-921675-57-7](https://doi.org/10.1016/j.advwatres.2008.01.001).

- Simmons, C. S. and P. D. Meyer (2000). "A simplified model for the transient water budget of a shallow unsaturated zone". In: *Water Resour. Res.* 36.10, pp. 2835–2844. ISSN: 00431397. DOI: [10.1029/2000WR900202](https://doi.org/10.1029/2000WR900202).
- Swaffer, B. A. et al. (2020). "Applying satellite-derived evapotranspiration rates to estimate the impact of vegetation on regional groundwater flux". In: *Ecohydrology* 13.1, pp. 1–14. ISSN: 19360592. DOI: [10.1002/eco.2172](https://doi.org/10.1002/eco.2172).
- Szilagyi, J., V. A. Zlotnik, and J. Jozsa (2013). "Net recharge vs. depth to groundwater relationship in the platte river Valley of Nebraska, United States". In: *Groundwater* 51.6, pp. 945–951. ISSN: 0017467X. DOI: [10.1111/gwat.12007](https://doi.org/10.1111/gwat.12007).
- Szilagyi, J. et al. (2011). "Mapping mean annual groundwater recharge in the Nebraska Sand Hills, USA". In: *Hydrogeol. J.* ISSN: 14312174. DOI: [10.1007/s10040-011-0769-3](https://doi.org/10.1007/s10040-011-0769-3).
- Talagrand, O., R. Vautard, and B. Strauss (1997). *Evaluation of Probabilistic Prediction Systems*. Tech. rep. Illkirch, France: Meteo-France.
- Taufik, M., B. I. Setiawan, and H.A.J. van Lanen (2019). "Increased fire hazard in human-modified wetlands in Southeast Asia". In: *Ambio* 48.4, pp. 363–373. ISSN: 16547209. DOI: [10.1007/s13280-018-1082-3](https://doi.org/10.1007/s13280-018-1082-3).
- Taylor, R. G. et al. (2013). "Ground water and climate change". In: *Nat. Clim. Chang.* 3.4, pp. 322–329. ISSN: 1758678X. DOI: [10.1038/nclimate1744](https://doi.org/10.1038/nclimate1744).
- Therrien, R. et al. (2006). *Hydrosphere—a three-dimensional numerical model describing fully-integrated subsurface and surface flow and solute transport*. Tech. rep. Waterloo, Ont., Canada.: Groundwater Simul. Group., 275pp.
- Usman, M., R. Liedl, and A. Kavousi (2015). "Estimation of distributed seasonal net recharge by modern satellite data in irrigated agricultural regions of Pakistan". In: *Environ. Earth Sci.* 74.2, pp. 1463–1486. ISSN: 18666299. DOI: [10.1007/s12665-015-4139-7](https://doi.org/10.1007/s12665-015-4139-7).
- van Dam, J. C. et al. (2008). "Advances of modeling water flow in variably saturated soils with SWAP". In: *Vadose Zo. J.* 7.2, p. 640. ISSN: 1539-1663. DOI: [10.2136/vzj2007.0060](https://doi.org/10.2136/vzj2007.0060).
- van Der Salm, C. et al. (2006). "The effect of afforestation on water recharge and nitrogen leaching in The Netherlands". In: *For. Ecol. Manage.* 221.1-3, pp. 170–182. ISSN: 03781127. DOI: [10.1016/j.foreco.2005.09.027](https://doi.org/10.1016/j.foreco.2005.09.027).
- van Dijk, A. I. J. M. et al. (2013). "The Millennium Drought in southeast Australia (2001-2009): Natural and human causes and implications for water resources, ecosystems, economy, and society". In: *Water Resour. Res.* 49.2, pp. 1040–1057. ISSN: 00431397. DOI: [10.1002/wrcr.20123](https://doi.org/10.1002/wrcr.20123).
- van Genuchten, M. Th. (1980). "A closed-form equation for predicting the Hydraulic conductivity of unsaturated zone". In: *Soil Sci. Soc. Am. J.* 44, pp. 892–898.
- van Walsum, P. E. V. and A. A. Veldhuizen (2011). "Integration of models using shared state variables: Implementation in the regional hydrologic modelling

- system SIMGRO". In: *J. Hydrol.* 409.1-2, pp. 363–370. ISSN: 00221694. DOI: [10.1016/j.jhydro1.2011.08.036](https://doi.org/10.1016/j.jhydro1.2011.08.036).
- Vazifiedoust, M. et al. (2009). "Assimilation of satellite data into agrohydrological models to improve crop yield forecasts". In: *Int. J. Remote Sens.* May. DOI: [01431160802552769](https://doi.org/10.10431160802552769).
- Vervoort, R. W. and S. E.A.T.M. van der Zee (2012). "On stochastic modelling of groundwater uptake in semi-arid water-limited systems: Root density and seasonality effects". In: *Ecohydrology* 5.5, pp. 580–595. ISSN: 19360584. DOI: [10.1002/eco.1288](https://doi.org/10.1002/eco.1288).
- Vrugt, J. A. and K. J. Beven (2018). "Embracing equifinality with efficiency: Limits of Acceptability sampling using the DREAM(LOA) algorithm". In: *J. Hydrol.* 559.May, pp. 954–971. ISSN: 00221694. DOI: [10.1016/j.jhydro1.2018.02.026](https://doi.org/10.1016/j.jhydro1.2018.02.026).
- Vrugt, J. A. and M. Sadegh (2013). "Toward diagnostic model calibration and evaluation: Approximate Bayesian computation". In: *Water Resources Research* 49.7, pp. 4335–4345. DOI: [10.1002/wrcr.20354](https://doi.org/10.1002/wrcr.20354).
- Vrugt, J. A. et al. (2001). "One-, two-, and three-dimensional root water uptake functions for transient modeling". In: *Water Resour. Res.* 37.10, pp. 2457–2470. ISSN: 00431397. DOI: [10.1029/2000WR000027](https://doi.org/10.1029/2000WR000027).
- Walker, G. R. and L. Zhang (2002). *Plot-Scale Models and Their Application to Recharge Studies*. Collinivood VIC 3066 Australia Telephone: CSIRO Publishing. ISBN: 0 643 06297 1 (set).
- Walker, J. P., G. R. Willgoose, and J. D. Kalma (2001). "One-dimensional soil moisture profile retrieval by assimilation of near-surface observations: a comparison of retrieval algorithms". In: DOI: [0309-1708/01](https://doi.org/10.1029/2000WR000027).
- Wang, J., T. A. Endreny, and J. M. Hassett (2006). "Power function decay of hydraulic conductivity for a TOPMODEL-based infiltration routine". In: *Hydrol. Process.* ISSN: 08856087. DOI: [10.1002/hyp.6159](https://doi.org/10.1002/hyp.6159).
- Welch, G. and G. Bishop (2006). *An introduction to the Kalman Filter*. Tech. rep. UNC-Chapel Hill.
- Xu, X. et al. (2012). "Integration of SWAP and MODFLOW-2000 for modeling groundwater dynamics in shallow water table areas". In: *J. Hydrol.* 412-413, pp. 170–181. ISSN: 00221694. DOI: [10.1016/j.jhydro1.2011.07.002](https://doi.org/10.1016/j.jhydro1.2011.07.002).
- Xue, L. (2015). "Application of the Multimodel Ensemble Kalman Filter Method in Groundwater System". In: *Water* 7.2, pp. 528–545. ISSN: 2073-4441. DOI: [10.3390/w7020528](https://doi.org/10.3390/w7020528).
- Zeng, J. et al. (2019). "Capturing soil-water and groundwater interactions with an iterative feedback coupling scheme : new HYDRUS package for MODFLOW". In: pp. 637–655.
- Zhu, Y. et al. (2011). "Method of coupling 1-D unsaturated flow with 3-D saturated flow on large scale". In: *Water Sci. Eng.* 4.4, pp. 357–373. ISSN: 16742370. DOI: [10.3882/j.issn.1674-2370.2011.04.001](https://doi.org/10.3882/j.issn.1674-2370.2011.04.001).

- Zhu, Y. et al. (2012). "A fully coupled numerical modeling for regional unsaturated-saturated water flow". In: *J. Hydrol.* 475, pp. 188–203. ISSN: 00221694. DOI: [10.1016/j.jhydrol.2012.09.048](https://doi.org/10.1016/j.jhydrol.2012.09.048).
- Zou, L. et al. (2017). "Implementation of evapotranspiration data assimilation with catchment scale distributed hydrological model via an ensemble Kalman Filter". In: *J. Hydrol.* 549, pp. 685–702. ISSN: 00221694. DOI: [10.1016/j.jhydrol.2017.04.036](https://doi.org/10.1016/j.jhydrol.2017.04.036).